Office of Academic Resources
Ubon Ratchathani University

UBON RATCHATHANI UNIVERSITY

DEVELOPMENT OF ORGANIC MATERIALS FOR HIGHLY EFFICIENT DYE-SENSITIZED SOLAR CELLS BASED ON THEORETICAL INVESTIGATIONS

RUANGCHAI TARSANG

A THESIS SUBMITTED IN PARTIAL FULFILLMENT OF THE
REQUIREMENTS FOR THE DEGREE OF DOCTOR OF
PHILOSOPHY
MAJOR IN CHEMISTRY
FACULTY OF SCIENCE
UBON RATCHATHANI UNIVERSITY
ACADEMIC YEAR 2014

COPYRIGHT OF UBON RATCHATHANI UNIVERSITY

UBON RATCHATHANI UNIVERSITY

UBON RATCHATHANI UNIVERSITY
THESIS APPROVAL
DOCTOR OF PHILOSOPHY
IN CHEMISTRY FACULTY OF SCIENCE

TITLE DEVELOPMENT OF ORGANIC MATERIALS FOR HIGHLY EFFICIENT DYE-SENSITIZED SOLAR CELLS BASED ON THEORETICAL INVESTIGATIONS

AUTHOR MR. RUANGCHAI TARSANG

EXAMINATION COMMITTEE

ASSOC. PROF. DR. VINICH PROMARAK	CHAIRPERSON
ASSOC. PROF. DR. SIRIPORN JUNGSUTTIWONG	MEMBER
ASSOC. PROF. DR. SAYANT SAENGSUWAN	MEMBER
DR. SUPAWADEE NAMUANGRUK	MEMBER

ADVISOR

Siriporn Jungsuttiwong

(ASSOC. PROF. DR. SIRIPORN JUNGSUTTIWONG)

Utith Inprasit

(ASSOC. PROF. DR. UTITH INPRASIT)
DEAN, FACULTY OF SCIENCE

(ASSOC. PROF. DR. ARIYAPORN PONGRAT)
VICE PRESIDENT
FOR ACADEMIC AFFAIRS

COPYRIGHT OF UBON RATCHATHANI UNIVERSITY

ACADEMIC YEAR 2014

ACKNOWLEDGMENTS

I would like to deeply express my appreciation to Assoc. Prof. Dr. Siriporn Jungsuttiwong, my advisor, for her excellent suggestions, supervision, and understanding throughout my study. I would like to give a special thanks to Assoc. Prof. Dr. Vinich Promarak, for his committee and valuable suggestions. I also would like to thank Assoc. Prof. Dr. Sayant Seangsuwan and Dr. Supawadee Namuangruk for constructive comments for this thesis.

My appreciation is extended to all the lecturer of the Department of Chemistry. Furthermore, I feel thankful to my friends, sisters, brothers here in Center for Organic Electronic and Alternative Energy. I am especially grateful to Human Resource Development in Science Project (Science Achievement Scholarship of Thailand, SAST) program for financial support.

Lastly, and most importantly, I feel appreciate and grateful to my beloved family for their supporting and encouragement on my education.

Ruangchai T.

Ruangchai Tarsang

Researcher

บทคัดย่อ

เรื่อง : การพัฒนาวัสดุอินทรีย์สำหรับเซลล์แสงอาทิตย์ชนิดสีย้อมไวแสงประสิทธิภาพสูงโดยวิธีทางทฤษฎี
ผู้วิจัย : เรืองชัย ตาแสง
ชื่อปริญญา : ปรัชญาดุษฎีบัณฑิต
สาขาวิชา : เคมี
อาจารย์ที่ปรึกษา: รองศาสตราจารย์ ดร. ศิริพร จึงสุทธิวงษ์

คำสำคัญ : หมู่ให้, หมู่รับ, ไพ-คอนจูเกต, เซลล์แสงอาทิตย์ชนิดสีย้อมไวแสง, ทฤษฎีเด็นซิตี้ฟังก์ชันแนล

ในงานวิจัยนี้รายงานการออกแบบและศึกษาสารสีย้อมไวแสงอินทรีย์ชนิดใหม่สำหรับใช้ในเซลล์แสงอาทิตย์ชนิดสีย้อมไวแสงที่มีประสิทธิภาพสูง โดยสีย้อมชนิดไตรฟีนิลเอมีนทำหน้าที่เป็นหมู่ให้อิเล็กตรอนถูกเติมด้วยหมู่คาร์บาโซล และไดเอริลเอมีนซึ่งทำหน้าที่เป็นหมู่ให้อิเล็กตรอนเพิ่มเติมจำนวนหนึ่งและสองหมู่แทนที่ เรียกว่าสีย้อมในระบบ D-D-π-A และ 2D-D-π-A ตามลำดับ เพื่อทำการเปรียบเทียบกับสีย้อมระบบ D-π-A ผลการศึกษาพบว่าสีย้อมในระบบ 2D-D-π-A มีช่วงการดูดกลืนแสงกว้างที่สุด นอกจากนี้ยังพบว่าการเปลี่ยนชนิดของหมู่ให้อิเล็กตรอนเพิ่มเติม ส่งผลให้ได้ค่าความสามารถในการดูดกลืนแสงแตกต่างกัน โดยหมู่ไดเอริลเอมีนให้ค่าการดูดกลืนแสงเลื่อนไปทางความยาวคลื่นมากขึ้นหรือเรดชิฟท์มากที่สุด และเมื่อพิจารณาโครงสร้างที่เสถียรพบว่าการเติมหมู่ไดเอริลเอมีน จะมีมุมไดฮีดรัลระหว่างหมู่ไตรฟีนิลเอมีนและหมู่ไดเอริลเอมีนน้อย ส่งผลให้สามารถปรับปรุงสมบัติการดูดกลืนแสงและการส่งผ่านอิเล็กตรอนได้ดี

ในสีย้อมชนิดไตรฟีนิลเอมีนยังได้ทำการศึกษาผลของการเติมหมู่เบนโซไธอะไดอาโซล (BTD) ซึ่งทำหน้าที่เป็นหมู่รับอิเล็กตรอนเพิ่มเติม ในสีย้อมระบบ D-A-π-A ผลการศึกษาพบว่าการเติม BTD ส่งผลต่อสมบัติการดูดกลืนแสง โดยตำแหน่งของการเติมยิ่งไกลจากหมู่ไตรฟีนิลเอมีนจะยิ่งทำให้สามารถปรับปรุงสมบัติการดูดกลืนแสงให้ดีโดยมีช่วงการดูดกลืนแสงที่กว้างมากขึ้น อย่างไรก็ตามการเติม BTD ติดกับหมู่รับอิเล็กตรอนโดยตรงจะส่งผลให้เกิดการรวมตัวแบบย้อนกลับ ซึ่งสามารถแก้ไขได้โดยการคั่น BTD กับหมู่รับอิเล็กตรอนด้วยหมู่ไธโอฟีน

ทำการศึกษาสีย้อมชนิดแอนทราซีนถูกเติมด้วยพันธะสาม ทำหน้าที่เป็นไพ-คอนจูเกตคั่นระหว่างหมู่ให้อิเล็กตรอนและหมู่รับอิเล็กตรอน ผลการศึกษาพบว่าการเติมพันธะสามช่วยลดมุมไดฮีดรัลระหว่างแอนทราซีนกับหมู่ที่อยู่ติดกัน ทำให้ได้โครงสร้างที่แบนราบ ซึ่งส่งผลดีต่อการส่งผ่านอิเล็กตรอนได้ดีขึ้น รวมถึงทำให้การฉีดอิเล็กตรอนจากสีย้อมไปยังสารกึ่งตัวนำเกิดได้ดีขึ้นด้วย

นอกจากนี้ยังได้ทำการศึกษาผลของการเปลี่ยนชนิดหมู่ให้อิเล็กตรอนรวมไปถึงชนิดของหมู่เชื่อมต่อ ผลการศึกษาหมู่ให้อิเล็กตรอนที่แตกต่างกันระหว่าง ฟลูออรีน คาร์บาโซล และฟีโนไทเอซีนพบว่าได้โครงสร้างที่ต่างกัน โดยโครงสร้างแบนราบได้จากหมู่ฟลูออรีน และคาร์บาโซล ส่วนหมู่ฟีโนไทเอซีนให้โครงสร้างไม่แบนราบลักษณะคล้ายปีกผีเสื้อ แต่ทั้งสองโครงสร้างให้สมบัติทางแสงไม่แตกต่างอย่างมีนัยสำคัญ ส่วนผลของหมู่เชื่อมต่อที่แตกต่างกันพบว่าเมื่อทำการเพิ่มจำนวนหมู่ไธโอฟีนมากขึ้น ส่งผลให้ลดค่าระดับพลังงาน LUMO และทำให้ช่วงการดูดกลืนแสงกว้างขึ้น จากผลการศึกษา

แสดงให้เห็นว่าสามารถปรับปรุงคุณสมบัติต่างๆ ของสีย้อมได้โดยการปรับปรุงโครงสร้างสีย้อมในรูปแบบต่างๆ ซึ่งคาดว่าสีย้อมเหล่านี้จะสามารถนำไปใช้เป็นเซลล์แสงอาทิตย์ได้อย่างมีประสิทธิภาพ และหวังว่าการศึกษาทางทฤษฎีจะช่วยแนะแนวทางการในออกแบบสีย้อมชนิดใหม่ ๆ สำหรับการศึกษาในอนาคตได้

ABSTRACT

TITLE : DEVELOPMENT OF ORGANIC MATERIALS FOR HIGHLY EFFICIENT DYE-SENSITIZED SOLAR CELLS BASED ON THEORETICAL INVESTIGATIONS
AUTHOR : RUANGCHAI TARSANG
DEGREE : DOCTOR OF PHILOSOPHY
MAJOR : CHEMISTRY
ADVISOR : ASSOC. PROF. SIRIPORN JUNGSUTTIWONG, Ph.D.
KEYWORDS : DONOR, ACCEPTOR, π-CONJUGATE LINKER, DYE-SENSITIZED SOLAR CELLS, DENSITY FUNCTIONAL THEORY

This thesis deals with the design and theoretical investigation of a new series of organic dye sensitizers to develop newly the high power conversion efficiency. The starburst triphenylamine dyes were introduced by using carbazole and diphenylamine moieties acting as auxiliary donor groups. The starburst triphenylamine dyes acting as electron donor groups capped with mono- and di-substituted auxiliary donors coded as D-D-π-A and 2D-D-π-A, respectively, were studied for the propose of comparison with only one triphenylamine moiety as donor in the D-π-A system. Among these architectures, the results suggested that the 2D-D-π-A system showed the largest absorption range. We found that different types of auxiliary donors provided different light-harvesting ability; the diphenylamine auxiliary donor can improve properties of the better light harvesting ability. In addition, the optimized geometries showed that adding of diphenylamine auxiliary donor provided smaller external dihedral angles (EDA) leading to wider absorption range with strong charge-transfer character compared to other dyes.

A series of newly designed triphenylamine-based sensitizers incorporating a benzo-thiadiazole (BTD) unit as an additional electron-withdrawing group in a specific donor–acceptor–π-acceptor (D-A-π-A) architecture has been investigated. We found that different positions of the BTD unit provided significantly different responses for light absorption. Among these, it was established that the further the BTD unit is away from the donor part, the broader the absorption spectra, which is an observation that can be applied to improve light-harvesting ability. However, when the BTD unit is connected to the anchoring group a faster, unfavorable charge recombination takes place; therefore, a thiophene unit was inserted between these two acceptors, providing red-shifted absorption spectra as well as blocking unfavorable charge recombination.

We performed a theoretical investigation on a series of organic dyes incorporating an anthracene moiety between a carbazole donor group and a cyanoacrylic acid acceptor, in which a triple bond (TB)-modified moiety acts as a π-conjugated linker. We found that optimized anthracene structures lay almost perpendicular to the plane of the adjacent substituents. The introduction of a modified TB moiety significantly decreases the dihedral angle and results in a planar structure, which extends the length of the π-conjugated system to provide a broader absorption spectrum. Introduction of a TB moiety into the dye structure facilitates electron transfer from the donor and acceptor. The TB-modified dye structure has a significant effect on electron injection from the dye sensitizer to the TiO_2 surface.

The effect of different electron donors and conjugate bridges on the structural, optical, and electron transfer properties of new designed dyes were studied. The different electron donor of fluorene, carbazole, and phenothiazine showed different structural conformation. Fluorene and carbazole acting as electron donors provided the planar conformation, while phenothiazine acting as electron donor provided the butterfly conformation was found. However, these two different conformations are not significant effect on energy level, intramolecular charge transfer property and optical property. For the effect of conjugated-bridge, the LUMO energy level can be significantly decreased when increased the thiophene units. In addition, the red shift of absorption spectra was found when the conjugated bridge was extended. Our results are suggested to be the possible reasons for the enhancement of conversion efficiency in dye-sensitized solar cells. We hope our work could provide a theoretical guidance for the future research of dye-sensitized solar cells.

CONTENTS

	PAGE
ACKNOWLEDGMENTS	I
THAI ABSTRACT	II
ENGLISH ABSTRACT	IV
CONTENTS	VI
LIST OF TABLES	VIII
LIST OF FIGURES	XI
LIST OF ABBREVIATIONS	XVI
CHAPTER 1 INTRODUCTION	
1.1 Introduction to dye-sensitized solar cells (DSSCs)	1
1.2 Molecular properties	3
1.3 Computational chemistry	5
1.4 Aims and scope of thesis	18
CHAPTER 2 LITERATURE REVIEWS	
2.1 Triphenylanine (TPA) based dyes	21
2.2 Organic dyes in D-A-π-A configuration	25
2.3 Anthracene based dyes	27
2.4 Phenothiazine based dyes	29
2.5 Dye adsorption on TiO_2 surface	30
CHAPTER 3 TUNING THE ELECTRON DONATING ABILITY IN THE TRIPHYLAMINE- BASED D-π-A CHITECTURE FOR HIGHLY EFFICIENT DYE- SENSITIZED SOLAR CELLS	
3.1 Introduction	32
3.2 Computational details	34
3.3 Results and discussion	36
3.4. Conclusions	49
CHAPTER 4 MODIFICATION ON D-A-π-A CONFIGURATION TOWARD HIGH- PERFORMANCE STARBRURT TRIPHENYLAMINE-BASED SENSITIZER FOR DYE	

CONTENTS (CONTINUED)

PAGE

SENSITIZED SOLAR CELLS: A THEORETICAL INVESTIGATION
4.1 Introduction 51
4.2 Computational details 54
4.3 Results and discussion 55
4.4 Conclusions 71
CHAPTER 5 TRIPLE BOND-MODIFIED ANTHRACENE SENSITIZERS FOR DYE-SENSITIZED SOLAR CELLS: A COMPUTATIONAL STUDY
5.1 Introduction 73
5.2 Computational details 76
5.3 Results and discussion 78
5.4 Conclusions 93
CHAPTER 6 THEORETICAL INVESTIGATION ON INFLUENCE OF DIFFERENT ELECTRON DONORS AND CONJUGATE BRIEGES IN ORGANIC DYES FOR DYE-SENSITIZED SOLAR CELLS
6.1 Introduction 95
6.2 Computational details 97
6.3 Results and discussion 98
6.4 Methods validation with the Performance of DSSCs 112
6.5 Conclusions 114
CHAPTER 7 SUMMARY 115
REFFERENCES 117
APPENDIX 126
CURRICULUM VITAE 128

LIST OF TABLES

TABLE		PAGE
3.1	Selected dihedral angle (in degrees) of the triphenylamine-based dyes added the carbazole, diphenylamine and fluorene-connected carbazole (or diphenylamine) moieties as the secondary electron donor	39
3.2	Maximal absorption wavelength (λ_{max}), excitation energy (E_g), oscillator strength (f), electronic transition configurations of triphenylamine dyes obtained by TD-CAM-B3LYP/6-31G(d,p) level	43
3.3	The excitation energies, oscillator strengths, and molecular compositions for the three lowest states of dyes adsorbed on $(TiO_2)_{38}$ surfaces calculated by TD-CAM-B3LYP/6-31(d) level of theory	49
4.1	Calculated excitation energies (E), oscillator strengths (f), and compositions in terms of molecular orbital contributions of **TPA1** – **TPA8** dyes obtained under TD-CAM-B3LYP/6-31G(d,p) level in CH_2Cl_2	58
4.2	The calculated adsorption energy (E_{ads}) and molecular dipole moment (Debye) in perpendical direction to the TiO_2 surface of **TPA1-**, **TPA2-**, **TPA4-** and **TPA6-TiO_2** adsorption complexes by Dmol^3 calculation	61
4.3	The calculated excitation energy (E), oscillator strengths (f) and corresponding transition natures of **TPA1**- and **TPA2-TiO_2** adsorption complexes obtained under TD-CAM-B3LYP/6-31G(d,p) level in CH_2Cl_2	63
5.1	Selected bond lengths (r, Å) and dihedral angles (ϕ, degree) for optimized structures of dyes **An1–An4** calculated at the B3LYP/6-31G(d,p) level of theory	81

LIST OF TABLES (CONTINUED)

TABLE PAGE

5.2 The maximum absorption wavelength (λ_{abs}), oscillator strength (*f*), light harvesting efficiency (*LHE*), electron injection driving force (ΔG^{inject}) and transition compositions of **An1- An4** dyes, calculated by TD-CAM-B3LYP/6-31G(d,p) in CH_2Cl_2 solution (C-PCM model) 84

5.3 The calculated adsorption energy (E_{ads}) obtained using the DMoL^3 computer program. Excitation energies (E_{ex}), oscillator strengths (*f*), and the transition compositions for **An1-**, **An2-**, **An3-**, and **An4-TiO$_2$** adsorption complexes, calculated by the TD-CAM-B3LYP/3-21G(d,p) level of theory 91

6.1 The optimized geometrical parameters, dihedral angle (in degree), of the studied organic dyesby using B3LYP/6-31G(d,p) method 99

6.2 The optimized geometrical parameters, dihedral angle (in degree), of the new designed phenothiazine-based dyesby using B3LYP/ 6-31G(d,p) method 102

6.3 Calculated charge distribution oneach group of the donor, π spacer and acceptor of the studied organic dyesunder B3LYP/6-31G(d,p) method. 103

6.4 Calculated charge distribution on each group of the donor, π spacer and acceptor of the new designed phenothiazine-based dyes under B3LYP/6-31G(d,p) method. 105

6.5 Maximal absorption wavelength (λ_{max}), excitation energy (E_g), oscillator strength (*f*), and electronic transition configurations of the studied organic dyes obtained by TD-CAM-B3LYP/6-31G (d,p) level in dichloromethane 109

LIST OF TABLES (CONTINUED)

TABLE		PAGE
6.6	Maximal absorption wavelength (λ_{max}), excitation energy (E_g), oscillator strength (f), and electronic transition configurations of the new designed phenothiazine-based dyes obtained by TD-CAM-B3LYP/6-31G(d,p) level in dichloromethane	111
6.7	Photovoltaic performance of DSSCs based on phenothaiazine dyes	114

LIST OF FIGURES

FIGURE		PAGE
1.1	The components and working principle of DSSCs	1
1.2	The diagram showing the various kinds of electronic excitation	3
1.3	Diagram of absorption and emission process	4
1.4	The chart for absorption, emission and stokes shift	5
1.5	Simplified flowchart of the self-consistent field procedure	6
1.6	Chemical structure of newly designed dyes	19
2.1	Chemical structures of the triphenylamine dyes **TPA1-TPA3**	22
2.2	The triphenylamine dyes connected by carbazole forming D-D-π-A structure	22
2.3	Molecular structures of **D1**, **D2**, and **D3**	23
2.4	Molecular structures, optimized geometries, and molecular orbital distribution of **D2**	24
2.5	Molecular structures, optimized geometries, and molecular orbital distribution of **PTZ-1**	24
2.6	Molecular structures and molecular orbital distribution of **WD-2** and **WD-3**	25
2.7	Chemical structure of D-A-π-A sensitizer **WS-9**	26
2.8	Chemical structures of D-A-π-A organic sensitizers **WS-1** (indoline donor) and **WS-3** (triphenylamine donor)	26
2.9	Molecular structures of anthracene	27
2.10	Structures of the anthracene-based dyes **5**, **7** and **9**	28
2.11	Structures of the anthracene-based dyes **13**	28
2.12	Molecular structures of metal-Free organic dyes (**TC201-203**, **TC401-403**) bridged by anthracene-containing π-conjugations	29
2.13	Structures of dyes PT-Cn (n = 2, 6, 8, 12)	29
2.14	(a) Molecular structure of the **CS1A** dyes, and (b) optimized structures of the dyes	30

LIST OF FIGURES (CONTINUED)

FIGURE		PAGE
2.15	Optimized geometrical structures **1** and **2** adsorbed onto the $(TiO_2)_{38}$ model, and their molecular orbitals	31
2.16	Relative probability density at dye's anchor and titania interface. The larger arrow reflects the experimentally observed increase in J_{sc} with the increase in the charge density	31
3.1	The typical procedure to add more donor groups	34
3.2	Molecular structures of the triphenylamine based **TPA** dye and its derivatives **TPA1-TPA6** dyes added more auxiliary donor	34
3.3	The optimized ground-state geometries of **TPA1-TPA6** dyes	38
3.4	Energy diagram of HOMO and LUMO for the triphenylamine dyes, TiO_2, and the electrolyte	41
3.5	Isodensity plotted of HOMO and LUMO for the triphenylamine dyes (**TPA**, **TPA2**, **TPA5**) by B3LYP/6-31G(d,p) level	42
3.6	Simulated absorption spectra of the triphenylamine dyes (**TPA**, **TPA2**, **TPA5**) at the CAM-B3LYP/6-31g(d,p) level in dichloromethane solution	44
3.7	The charge density difference between the ground- and first excited-state of **TPA**, **TPA2** and **TPA5** dyes	45
3.8	Relaxed structures of triphenylamine based dyes, (a) **TPA2**; (b) **TPA5**, adsorbed on $(TiO_2)_{38}$ surfaces by DMoL^3 calculation	47
3.9	MOs of **TPA5** adsorbed on $(TiO_2)_{38}$ surface related to the transitions calculated by TD-CAM-B3LYP/6-31G(d)	47
3.10	MOs of **TPA2** adsorbed on $(TiO_2)_{38}$ surface related to the transitions calculated by TD-CAM-B3LYP/6-31G(d)	48
4.1	Chemical structures of studied organic dyes: simple D-π-A and D-A-π-A dye architectures of (a) the triphenylamine-based dyes with different electron donating ability and (b) the dyes with different BTD unit positions	53

LIST OF FIGURES (CONTINUED)

FIGURE **PAGE**

4.2 Calculated HOMO-LUMO levels of **TPA1** and **TPA2** dyes using B3LYP/6-31G(d,p) calculation 55

4.3 Simulated absorption spectra of **TPA1** and **TPA2** dyes containing with additional electron withdrawing group of benzothiadiazole (BTD) obtained by TD-CAM-B3LYP/6-31G(d,p) calculation in CH_2Cl_2 57

4.4 Optimized structures of **TPA1**- and **TPA2-TiO_2** adsorption complexes calculated by PBE/DNP in DMoL^3 61

4.5 Electronic transitions of **TPA1**- and **TPA2-TiO_2** adsorption complexes calculated by TD-CAM-B3LYP/6-31G(d,p) in CH_2Cl_2 63

4.6 Simulated UV-vis absorption spectra of **TPA2 – TPA4** dyes calculated by TD-CAM-B3LYP/6-31G(d,p) calculation in CH_2Cl_2 66

4.7 Simulated UV-vis absorption spectra of **TPA4 - TPA6** dyes calculated by TD-CAM-B3LYP/6-31G(d,p) calculation in CH_2Cl_2 67

4.8 Optimized structures of **TPA4**- and **TPA6-TiO_2** adsorption complexes calculated by PBE/DNP in DMoL^3 69

4.9 Simulated UV-vis absorption spectra of **TPA6- TPA8** dyes calculated by TD-CAM-B3LYP/6-31G(d,p) calculation in CH_2Cl_2 70

4.10 Comparison of optimized ground-state structures of **TPA7** and **TPA8** dyes 71

4.11 Comparison of calculated energy level of HOMO and LUMO for **TPA7** and **TPA8** dyes compared with **TPA6** dye 71

5.1 Sketch map of the studied dyes **An1-An4** 76

5.2 (a) The molecular structures were categorized into three parts of donor, linker, and acceptor, (b) Optimized structures of the studied dyes **An1 - An4** calculated by B3LYP/6-31G(d,p) level of theory 80

LIST OF FIGURES (CONTINUED)

FIGURE **PAGE**

5.3 The frontier molecular orbitals of HOMO (left) and LUMO (middle), and the charge density difference between the ground- and excited-state (right) of the studied dyes calculated under TD-CAM-B3LYP/6-31G(d,p). The purple represent where the electrons are decreased and the yellow represents where the electrons are increased 83

5.4 Computed HOMO-LUMO energy levels for the studied dyes **An-An4** at the TD-CAM-B3LYP/6-31G(d,p), together with the TiO_2 conduction band edge and the I^-/I_3^- redox potential. 85

5.5 The simulated UV-Vis spectra of **An1-An4** dyes using TD-CAM-B3LYP/6-31G(d,p) model in CH_2Cl_2 solution 87

5.6 LHE curve of **An21-An4** dyes along with photon flux spectrum at ASTM-G173 AM1.5 88

5.7 Schematic of free energy change (ΔG^{inject}) producing from the energy difference between E_{LUMO} and E_{CB} 89

5.8 Optimized structures of **An1-**, **An2-**, **An3-** and **An4-TiO₂** adsorption complexes calculated by PBE/DNP in the $DMoL^3$ 90

5.9 Schematic energy diagram of isolated **An3** and **An4** dyes, isolated TiO_2, and interacting **An3@TiO₂** and **An4@TiO₂** 92

5.10 Electronic transitions of a) **An1-**, b) **An2-**, c) **An3-** and d) **An4-TiO₂** adsorption complexes calculated by TD-CAM-B3LYP/6-31G(d,p). 94

6.1 Chemical structure of newly designed dyes 97

6.2 Optimized ground-state geometries of **CFTPA**, **CCTPA** and **CPTPA**dyes by B3LYP/6-31G(d,p) calculation 99

6.3 Optimized ground-state geometries of **CPPA**, **CPTPA**, **CPT2PA**, and **CPT3A** dyes by B3LYP/6-31G(d,p) calculation 101

LIST OF FIGURES (CONTINUED)

FIGURE		PAGE
6.4	The frontier molecular orbitals of **CFTPA**, **CCTPA** and **CPTPA** dyes	102
6.5	The different density between ground- and the first excited-state of **CFTPA**, **CCTPA** and **CPTPA** dyes	104
6.6	The frontier molecular orbitals of **CPPA**, **CPTPA**, **CPT2PA**, and **CPT3A** dyes, and the different density between ground- and the first excited-state of **CPPA**, **CPTPA**, **CPT2PA**, and **CPT3A** dyes	104
6.7	LUMO and HOMO energy level diagram of **CFTPA**, **CCTPA**, and **CPTPA** dyes	106
6.8	LUMO and HOMO energy level diagram of **CPPA**, **CPTPA**, **CPT2PA** and **CPT3A** dyes	107
6.9	Simulated absorption spectra of **CFTPA**, **CCTPA**, and **CPTPA** dyes	108
6.10	Simulated absorption spectra of **CPPA**, **CPTPA**, **CPT2PA**, and **CPT3A** using the hybrid functional CAM-B3LYP at 6-31G(d,p) level in dichloromethane	110
6.11	The absorption spectra of PhCPdye, PhCT1Pdye, PhCT2Pdye, and PhCT3dye	113

LIST OF ABBREVIATIONS

ABBREVIATION	**DEFINITION**
B3LYP	Becke's three-parameter hybrid functional and Lee-Yang-parr's gradient-corrected correlation functional
CAM-B3LYP	coulomb-attenuating method of B3LYP
CB	conduction band
CPCM	conductor-like polarizable continuum model
DSSCs	dye-sensitized solar cell
DBP	dipyrenyl benzene
D-D-π-A	donor-donor-π-conjugated-acceptor
D-π-A	donor-π -conjugated-acceptor
DFT	density functional theory
EA	electron affinity
EL	electroluminescence
E_g	excitation energy
E_{flu}	fluorescence energies
GGA	gradient approximation
GTO	Gaussian type orbital
HF	Hartree-Fock
HOMO	highest occupied molecular orbitals
IP	ionization potential
I^-/I^-_3	iodide/triiodide redox couple
KS	Kohn-Sham
LCD	liquid-crystal displays
LDA	local density approximation
LUMO	lowest unoccupied molecular orbitals
nm	nanometer
PCM	polarizable continuum model
Ru	ruthenium
SCF	self-consistent field

LIST OF ABBREVIATIONS (CONTINUED)

ABBREVIATION	**DEFINITION**
STO	Slater type orbital
TD-DFT	time- dependent density functional theory
TiO_2	titanium dioxide
TPA	triphenylamine
η	conversion efficiency
Ψ	wave function
E	energy
$\hat{H}$	Hamiltonian operator
ρ	electron density
T	kinetic energy
v	exchange-correlation potential
f	oscillator strengths
λ_{onset}	wavelength onset
λ_{max}	wavelength maxima

CHAPTER 1

INTRODUCTION

1.1 Introduction to dye-sensitized solar cells (DSSCs)

1.1.1 What is dye-sensitized solar cells?

The dye-sensitized solar cells (DSSCs) is an alternative solar cell technology which has attracted considerable attention due to their high light-to-electricity conversion efficiency and low production cost, since they are built from cheaper materials than the silicon-based solar cells. Moreover, DSSCs show distinguished advantages such as their high optical absorption extinction coefficient, adjustable spectral wavelength response, low cost materials, and their environmental friendly. [1] The DSSCs is a complex system composed of three main different components of the semiconductor material often used titanium dioxide (TiO_2), the dye molecules and the electrolyte. The components of DSSCs are shown in Figure 1.1. Based on this structure, a dye-sensitized photoanode often uses a dye-sensitized coating with semiconductor such as TiO_2 and it acts as a working electrode. An electrolyte solution, usually is organic solvent containing iodide/triiodide (I^-/I^-_3), and a counter electrode is a platinized conductive glass substrate.

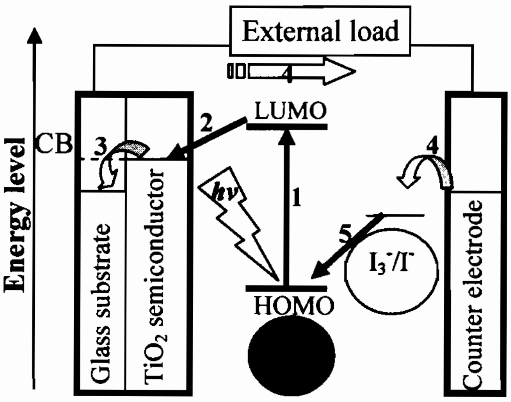

Figure 1.1 The components and working principle of DSSCs [2]

1.1.2 The working principle of DSSCs operations

Solar energy is converted to electric energy in the DSSCs process by first the dye molecule absorbs a photon and gives its energy to the electron located on the highest occupied molecular orbital (HOMO). The electron is subsequently shifted to the lowest unoccupied molecular orbital (LUMO) called photon excitation (Process 1). Then, the electron is injected from the LUMO to the conduction band (CB) of TiO_2 via anchoring group in quickly time called electron injection (Process 2). These electrons were collected called electron collection (Process 3) and flow through the external load to the counter electrode called electron transportation (Process 4), at the same time the oxidized dyes are neutralized to ground state via I^-/I^-_3 system called charge recombination (Process 5). The molecule is then restored to the ground state, which completes the circuit. The principle operations of DSSCs are also shown in Figure 1.1. [2]

As presented in the DSSCs process, practical DSSCs should have the following properties; (i) organic dyes used for efficient DSSCs are required to broaden spectral absorption with high intensity to get most of sunlight in first step, (ii) the highest occupied molecular orbital (HOMO) energy level of the dye must be below that of the redox couple of the I^-/I^-_3 electrolyte, and (iii) the lowest unoccupied molecular orbital (LUMO) energy level of the dye must be above the conduction band of the semiconductor material. [3]

1.1.3 The research for DSSCs application

After the electron has been excited to the LUMO state it is instantaneously injected to the porous semiconductor, assuming that the rate of the injection process is fast enough. The efficiency of DSSCs is based on the injection of electrons from dye molecules into the conduction band of TiO_2. To develop highly efficiency of DSSCs, it has possible to do in various ways such as the development on nanoporous semiconductor materials, or the development on the electrolyte system. [4] In addition, the development on the research of suitable sensitizer for increasing DSSCs efficiency has the most considerable attention. The majority of this work has centered on ruthenium polypyridyl complex [5], where the greatest performance attained in solar-to-electronic conversion efficiency has been 11%. However, the Ru dyes are limited with the problem of manufacturing cost and toxicity issues. Therefore, many research teams have attempted to increase the performance of organic dyes not only in the synthesis laboratory, but also in the field of theoretical investigation based on computational study for understanding mechanism of electron transfer, which is the main target of this study.

1.2 Molecular properties

1.2.1 UV-Visible absorption process

When light is absorbed by molecules, energy from the light is used to promote an electron from a bonding or non-bonding orbital into one of the empty anti-bonding orbitals. The possible electron jumps that light might cause is shown in Figure 1.2.

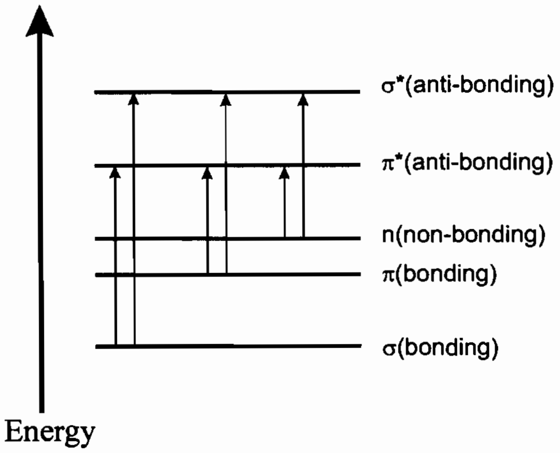

Figure 1.2 The diagram showing the various kinds of electronic excitation [6]

In each possible case, an electron is excited from a full orbital into an empty anti-bonding orbital. Each jump takes energy from the light, and a big jump obviously needs more energy than a small one. Each wavelength of light has a particular energy associated with it. If that particular amount of energy is just right for making one of these energy jumps, then that wavelength will be absorbed which its energy will have been used in promoting an electron. UV-visible absorption spectra are always given using wavelengths of light rather than frequency. That means that you need to know the relationship between wavelength and frequency by following equation. [6]

$$v = \frac{c}{\lambda}$$

where ν is the frequency, c is the speed of light and λ is the wavelength.

1.2.2 Fluorescence emission process

Emission is the process by which a higher energy quantum mechanical state of a particle becomes converted to a lower one through the emission of a photon, resulting in the production of light. [7] The frequency of light emitted is a function of the energy of the transition. Since energy must be conserved, the energy difference between the two states equals the energy carried off by the photon. The energy states of the transitions can lead to emissions over a very large range of frequencies. When the electrons in the atom are excited, for example by being heated, the additional energy pushes the electrons to higher energy orbitals. When the electrons fall back down and leave the excited state, energy is re-emitted in the form of a photon. The wavelength (or frequency) of the photon is determined by the difference in energy between the two states. These emitted photons form the element's emission spectrum. The frequencies of light that an atom can emit are dependent on states the electrons can be in. When excited, an electron moves to a higher energy level/orbital. When the electron falls back to its ground level the light is emitted. Figure 1.3 shows a number of possible routes by which an excited molecule can return to its ground or room temperature state via unstable triplet states. The difference between positions of the band maxima of the absorption and emission spectra of the same electronic transition is call Stokes shift as showed in Figure 1.4.

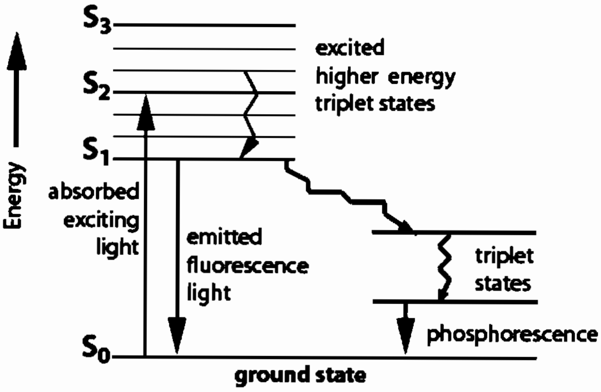

Figure 1.3 Diagram of absorption and emission process [8]

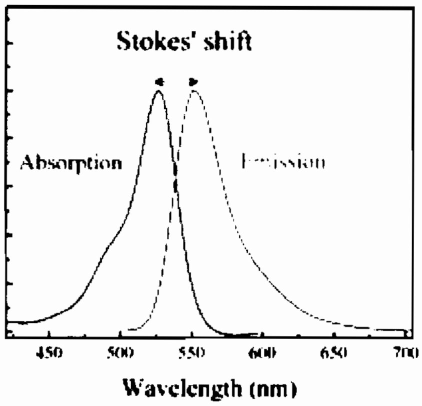

Figure 1.4 The chart for absorption, emission and stokes shift [9]

1.3 Computational chemistry

1.3.1 Electronic structure theory

The heart of quantum chemistry is the famous Schrödinger equation,

$$\hat{H}_{tot}\,\Psi_{tot} = E_{tot}\,\Psi_{tot} \tag{1.1}$$

here expressed in a time-independent non-relativistic form. Ψ_{tot} is the total wave function which depends on the electronic and nuclear coordinates, E_{tot} is the total energy, $\hat{H}_{\mathrm{tot}}$ is the Hamiltonian of the system, containing the kinetic and potential energy operators for all particles. In most quantum chemical calculations the Born-Oppenheimer approximation is invoked, which separates the motions of nuclei and electrons, so that an electronic Schrödinger equation for fixed nuclei is obtained,

$$\hat{H}_{elec}\,\Psi_{elec} = E_{elec}\,\Psi_{elec} \tag{1.2}$$

which only depends parametrically on the nuclear positions. Historically, most quantum chemical calculations have been based on the Hartree-Fock (HF) approximation to solve the electronic Schrödinger equation. In HF theory, each electron is described by a spin-specific one-electron function, a spin orbital constructed as a product of a spatial orbital and a spin function, and Ψ_{elec} is expressed in the form of a single Slater determinant of spin orbitals. A set of one-electron equations known as the Hartree-Fock equations is obtained by minimizing the energy of the HF trial wave function based on the variational principle, which states that a trial wave function has an energy that is higher than or equal to the exact energy. These equations have to be solved iteratively until self-consistency using the self-consistent field (SCF) procedure shown in Figure 1.5, because the operators in these equations depend on the orbitals that one is seeking.

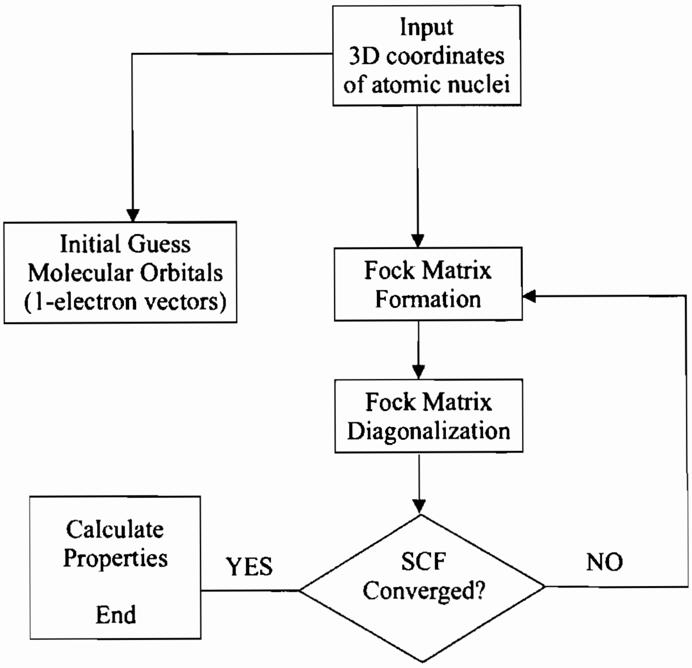
Input
3D coordinates
of atomic nuclei
Initial Guess
Molecular Orbitals
(1-electron vectors)
Fock Matrix
Formation
Fock Matrix
Diagonalization
Calculate
Properties
End
YES
SCF
Converged?
NO

Figure 1.5 Simplified flowchart of the self-consistent field procedure

In practical calculations, the Hartree-Fock orbitals can be defined as restricted, where electrons of different spin are, pair wise, described by a common spatial orbital, or as unrestricted where each electron has its own spatial distribution. The HF method generates solutions to the electronic Schrödinger equation, where the real electron-electron interaction is replaced by an average interaction. The consequence of this replacement is that the correlation of electrons' motion is not described properly. The correlation of electrons having the same spin is partially accounted for via an exchange interaction, but the correlation of electrons having opposite spins is not described. The exchange interaction is a non-classical interaction between two electrons with the same spin. A good description of electron correlation is important when calculating molecular properties. Hence, it is usually required to improve the HF description in order to obtain results that compare quantitatively, or even qualitatively, with experimental results. There are several approaches to systematically improve the HF approximation by including varying amounts of electron correlation, such as Møller-Plesset perturbation theory, configuration interaction, coupled-cluster theory, and multiconfiguration self-consistent field theory. For a detailed description of HF theory and electronic structure methods that go beyond this approximation, the reader is referred to the books of Szabo and Ostlund or Hehre, Radom, Schleyer and Pople. [10]

1.3.2 Born-Oppenheimer approximation

The atom nuclei are massive compared to the electrons. In the Born-Oppenheimer approximation it is assumed that the electrons react instantaneously to the movement of the nuclei. In other words, for any given atom configuration the electrons are always located in the energetically lowest possible configuration. Another way to explain this approximation is that since the movement of the electrons is rapid compared to the movement of the nuclei, they "see" the change of the locations of the nuclei as an adiabatic change in the system. With these approximations the total energy of the system is,

$$E_{total} = \sum_i \frac{1}{2} m_i \dot{\vec{r}}_i^{\,2} + \sum_i \sum_{j>i} \frac{Z_i Z_j}{|r_i - r_j|} + E_{elec}\left(\{\vec{r}_i^{\,2}\}\right) \tag{1.3}$$

where $\dot{\vec{r}}_i$ is the position, $\vec{r}_i$ is the velocity, m_i the mass and Z_i the charge of i:th ion. The first term describes the classical kinetic energy of the ions and the second the Coulombic interaction of the ions. The index of summation at second term is $i > j$ to count each ion-ion interaction only once and to exclude self-interaction. The third term is the total energy of the electron gas in current ion configuration (the {r} stands for a list of all positions of the ions).

The first and the second terms are more or less easy to calculate. The total energy of the electron gas is calculated via the density functional theory (DFT). [11]

1.3.3 Density functional theory

Traditional methods for calculating the energy of the electron gas are based on using many-electron wave functions. For N electrons, one has 3N variables to work out.

The main drawback with the HF based electronic structure methods that include electron correlation is that they become too time-consuming for most realistic molecular systems. This fact is the main motivation for using density functional theory (DFT) which has the inherent capability of treating electron correlation at a much lower computational cost. In DFT the basic variables, the wave-function Ψ_{elec} , is replaced by the electron density, ρ (r) , which is a function of only 3 spatial coordinates. The energy as well as other observables of the molecular system are obtained from ρ (r) by so-called functionals. As a consequence of the two theorems of Hohenberg and Kohn, the electron density may be considered the fundamental variable of multi-electron theory. [12, 13]

1.3.3.1 Kohn-Sham method

Soon after the paper from Hohenberg and Kohn a practical way to solve the density of the electron gas for the ground state was introduced by Kohn and Sham which is briefly described in the following.

The Kohn-Sham (KS) scheme is a computational strategy for approaching the true electron density and energy of an arbitrary atomic or molecular system. The KS method is the basis of the majority of DFT calculations performed today and has been employed in the present thesis. The idea behind the KS scheme was to make use of a hypothetical reference system composed of *N* non-interacting electrons in *N* orbitals, Ψ_i, moving in an effective potential, v_S. For this type of system, a single Slater determinant describes the exact ground state wave function. The optimal orbitals for the non-interacting system are obtained by solving the following one-electron equations

$$\left\{-\frac{1}{2}\nabla^2 + v_s\right\} \Psi_i = \varepsilon_i \Psi_i \tag{1.4}$$

with a Hamiltonian consisting of a kinetic energy term and an effective onebody potential. The total electron density is the sum of the orbital densities

$$\rho_r(\bar{r}) = \sum_i^n |\Psi_i(\bar{r})|^2 \tag{1.5}$$

The connection of the non-interacting electron system to a system of fully interacting electrons is established by choosing the effective one-body potential such that the electron distribution exactly equals the total ground state electron density of the real fully interacting system. Even though the actual form of the exact energy functional, $E[\rho]$, is unknown, its ingredients can be expressed as

$$E[\rho] = T_s[\rho] + E_{ne}[\rho] + J[\rho] + E_{xc}[\rho] \tag{1.6}$$

Here, ρ is the density of the fully interacting system, and the functional forms of the first three terms are known. The first term in equation 1.6 is the kinetic energy of a system composed of non-interacting electrons, the second term is the potential energy from coulombic attraction between electrons and nuclei, and the third term is the classical electrostatic electron-electron repulsion energy. All contributions to the total energy not accounted for by the first three terms are collected in one term, $E_{XC}[\rho]$, called the exchange correlation functional. $E_{XC}[\rho]$ formally includes all non-classical effects of exchange and correlation, but also the portion of the kinetic energy not cove red by $T_S[\rho]$. The exchange-correlation functional is also constructed to correct for the self-interaction error of $J[\rho]$, which stems from the fact that the functional form of $J[\rho]$ allows for an unphysical interaction of an electron with itself. Minimizing this energy with respect to independent variations in the orbitals (with orthonormality constraints), results in a set of one-electron equations, the KS equations,

$$\hat{h}_{KS}\Psi_i = \varepsilon_i \Psi_i \qquad i = 1, 2, \ldots, N \tag{1.7}$$

The one-electron operator, $\hat{h}_{KS}$, contains the kinetic energy, the potential due to the nuclei, the classical Coulomb potential and the potential generated by $E_{XC}[\rho]$:

$$\hat{h}_{KS} = -\frac{1}{2}\nabla^2 - \sum_A \frac{Z_A}{|R_A - \bar{r}|} + \int \frac{\rho(\vec{r})}{|\bar{r} - \acute{\bar{r}}|} d\acute{\bar{r}} + v_{XC}(\bar{r}) = -\frac{1}{2}\nabla^2 + v_{eff}(\bar{r}) \tag{1.8}$$

The exchange-correlation potential, v_{XC}, is defined as the functional derivative of the exchange-correlation energy with respect to ρ,

$$v_{XC}(\bar{r}) = \frac{\partial E_{XC[\rho]}}{\partial \rho(\bar{r})} \tag{1.9}$$

Now, by comparing equation 1.4 with equation 1.7 and equation 1.8 it becomes clear that if the one-body potential, v_S, in equation 4 is defined as v_{eff} (r) in equation 1.8, the system with N non-interacting electrons is transformed to a system of fully interacting electrons. The KS equations are thus defined by setting $v_S = v_{eff}$ (r) in equation 4 and the orbitals obtained from these equations are termed KS orbitals. Since v_{eff} (r) depends on the electron density, and hence on the KS orbitals, equation 1.8 has to be solved iteratively in a self-consistent manner, just as in HF theory. The energy of the system is then obtained by inserting the electron density constructed from the KS orbitals according to equation 1.5 into equation 1.6. [12]

1.3.3.2 Density functional methods

Recently, a third class of electronic structure methods have come into wide use: density functional methods (DFT). These DFT methods are similar to ab initio methods in many ways. DFT calculations require about the same amount of computation resource as Hartree-Fock theory, the least expensive ab initio methods. DFT methods are attractive because they include the effect of electron correlation the fact that electrons in molecular system react to one another's motion and attempt to keep out of one another's way in their model. Hartree-Fock calculations consider this effect only in an average sense each electron sees and reacts to an averaged electron density while methods including electron correlation account for the instantaneous interactions of pairs of electrons with opposite spin. This approximation causes

Hartree-Fock results to be accurate for some type of systems. Thus, DFT methods can provide the benefits of some more expensive ab initio methods at essentially Hartree-Fock coast.

1.3.4 Functionals

1.3.4.1 The local density approximation

The exchange-correlation (XC) functional contains all the errors that are made when calculating the properties of the real system using the noninteracting one. Kohn and Sham used the local density approximation (LDA) in their derivation,

$$E_{XC}^{LDA}[n] = \int n(\vec{r}) \in_{XC} [n](\vec{r}) d\vec{r} \qquad (1.10)$$

where the ϵ_{XC}[n] is the exchange-correlation energy density of uniform electron gas. The ϵ_{XC}[n](r) has been constructed from Monte Carlo simulations. In principle the LDA should only work when the density of the electron gas is almost homogeneous. It has been, however, found to give very good results even when the density of electron gas varies rapidly. [14]

1.3.4.2 Generalized gradient approximation

To take into account the changes in the density of the electron gas the gradient of the density must be included somehow to the XC energy. In that case the approximation is called the generalized gradient approximation (GGA). It has the general form

$$E_{XC}^{GGA}[n] = \int f(n(\vec{r}), \ \nabla n(\vec{r}) d^3\vec{r} \qquad (1.11)$$

Many different kinds of functional have been developed, and there is no easy way to tell which the best is. Some work well in some situations and fail in others. Some rely on fitted parameters to experimental data while others have been derived purely from the theoretical basis. [14]

1.3.4.3 Hybrid exchange and correlation functional

The explicit forms of the exact exchange-correlation functional and the exchange-correlation potential are not known. If they were, solving the KS equations would result in the exact ground state energy and DFT would be an exact theory. The quality of the density functional approach thus depends on the accuracy of the chosen approximation to E_{XC}. The exchange correlation functional is usually divided into two parts:

$$E_{XC} = E_X + E_C \tag{1.12}$$

where E_X and E_C are functionals for the exchange part and for the correlation part of the energy, respectively. The exchange part contains only same spin interactions while the correlation part contains both same-spin and opposite- spin interactions. The existing approximate exchange- correlation functionals can be subdivided according to how the electron density is treated in the calculation of the energy. In the simplest approximation, the local density approximation (LDA), the electron density is treated as an uniform electron gas, and E_{XC}^{LDA} is computed from

$$E_{XC}^{LDA}[\rho] = \int \rho(\bar{r})\, \varepsilon_{XC}[\rho(\bar{r})]d\bar{r} \tag{1.13}$$

where the integrand, ε_{XC} , is a functional depending only on the local density at a specific point, $\bar{r}$, in space. The exchange part of LDA is known as the α_X functional and the correlation part is called VWN, and these functional are most useful for systems where the real density is slowly varying (i.e. for densities resembling a uniform electron gas), such as in large metal surfaces. In the generalized gradient approximation (GGA), which is the main approximation for all DFT methods used in this thesis, the exchange correlation functional has the following general form

$$E_{XC}^{GGA}[\rho] = \int f\,[\rho, \nabla\rho]d\bar{r} \tag{1.14}$$

In GGA functionals, the integrand is a functional depending not only on the local density, but also on the gradient of the electron density. These functional are more useful than LDA functionals for calculations on molecules since such systems have regions where the density is far from slowly varying. Another type of DFT methods includes a fraction of exact HF exchange energy (computed from the KS orbitals) in addition to exchange and correlation from pure DFT functionals. These methods are referred to as hybrid functionals, and have the general form

$$E_{XC}^{Hybrid} = cE_X^{HF} + (1-c)E_X^{DFT} + E_C^{DFT} \qquad (1.15)$$

where c determines the amount of HF exchange included. In this thesis, the popular B3LYP hybrid functional has been used for most calculations. This functional includes 20% exact HF exchange and is expressed as:

$$E_{XC}^{B3LYP} = (1-a)E_X^{LDA} + aE_X^{HF} + bE_X^{B88} + cE_C^{LYP} + (1-c)E_C^{LDA} \qquad (1.16)$$

Here the components of the exchange part are LDA exchange (E_X^{LDA}), HF exchange (E_X^{HF}), and the GGA exchange functional Becke88 (E_X^{B88}). The correlation part of the B3LYP functional has contributions from LDA (E_C^{LDA}), and from GGA in the correlation functional of Lee, Yang, and Parr (E_C^{LYP}).The three parameters *a*, *b*, and c (0.20, 0.72 and 0.81, respectively) in equation 16 were determined by fitting to experimental data including atomization energies, ionization potentials, and electron affinities on a large set of molecules, using the correlation functional of Perdew and Wang instead of E_C^{LDA} and E_C^{LYP}. In addition to B3LYP, four other exchange-correlation functionals have been employed in this thesis. These are the PBE1PBE hybrid functional which incorporates 25% exact HF exchange, the pure BLYP and HCTH GGA functionals and a pure GGA functional composed of exchange from PW86 and correlation from PW91, a combination which in the following is referred to as PW [14].

1.3.5 Basis sets

The individual orbitals Ψ_i, molecular or atomic depending on the investigated system, are expanded in terms of a set of basis functions $\{\varphi_V\}$, centered on the nucleus or nuclei,

$$\Psi_i = \sum_v c_{iv}\varphi_v \tag{1.17}$$

where the orbital expansion coefficients, c_{iv}, are optimized during the calculation. The set of basis functions available for an expansion is called the basis set. These basis functions can be Slater type orbital (STO) functions which are similar to the orbitals obtained by the analytical solution of the Schrödinger equation for the hydrogen atom. However, a more efficient computation of two-electron integrals is achieved with Gaussian type orbital (GTO) functions. It is therefore more common to use so-called contracted Gaussian functions, in which several primitive GTO functions are combined in a fixed, predefined linear combination.

The smallest possible basis set representation is termed a minimal or single zeta basis set and comprises only the number of functions required to accommodate all the electrons of the atoms of the system. Doubling the number of functions, a double zeta basis set, provides a more flexible description since there are two sets of functions for each occupied shell of the atoms. So-called split-valence basis sets, where the description is split into an inner component describing the core electrons with one level of representation, e.g. minimal basis, and an outer component describing the valence electrons with another level of representations, e.g. a double zeta basis.

This splitting is motivated by the fact that chemistry is mainly dependent on the valence electrons, and core electrons have little influence on chemical processes. Additional improvements of the basis set can be achieved by adding polarization functions and/or diffuse functions. In this thesis, the majority of calculations were performed using either Dunning's D95V basis set or the Pople family of basis sets.

The choice of basis set is very important for the quality of the computational results. A sufficiently flexible and well-balanced basis set must be used to obtain accurate results, but accuracy and computational cost has to be weighted against each other. This trade-off becomes increasingly important to consider when large systems are investigated [15].

1.3.5.1 Minimal basis sets

Minimal basis sets contain the minimum number of basis functions needs for each atom, as these examples:

H: 1s

C: 1s, 2s, $2p_x$, $2p_y$, $2p_z$

Minimal basis sets use fixed-size atomic-type orbitals. The STO-3G basis set is a minimal basis set. It use three gaussian primitives per basis function, which accounts for the "3G" in its name. "STO" stands for "Slater-type orbitals," and the STO-3G basis set approximates Slater orbitals with guassian functions.

1.3.5.2 Split valence basis sets

The first way that a basis can be made larger is to increase the number of basis functions per atom. Split valence basis sets, such as 3-21G, have two sizes of basis function for each valence orbital. For example, hydrogen and carbon are represented as:

H: 1s, 1s′

C: 1s, 2s, 2s′, $2p_x$, $2p_y$, $2p_z$, $2p_x'$, $2p_y'$, $2p_z'$

where the primed and unprimed orbitals differ in size. The triple split valence basis sets, like 6-311G, use three sizes of contracted functions for each orbital-type.

1.3.5.3 Polarized basis sets

Split valence basis sets allow orbitals to change size, but not to change shape. Polarized basis sets remove this limitation by adding orbitals with angular momentum beyond what is required for the ground state to the description of each atom. For example, Polarized basis sets add d functions to carbon atoms and f functions to transition metals, and some of them add p functions to hydrogen atoms. So far, the only polarized basis sets we've used is 6-31G(d). Its name indicates that it is the 6-31G basis sets with d functions added to heavy atoms. This basis sets is becoming very common for calculations involving up to medium-sized systems. This basis sets also know as 6-31G*. Another popular polarized basis set is 6-31G(d,p), also know as 6-31G**, which add p functions to hydrogen atoms in addition to the d functions on heavy atoms.

Office of Academic Resources Ubon Ratchathani University

1.3.5.4 Diffuse functions

Diffuse functions are large-size versions of s- and p-type functions. They allow orbitals to occupy a larger region of space. Basis sets with diffuse functions are important for systems where electrons are relatively far from the nucleus: molecules with lone pairs, anions, and other systems with significant negative charge, systems in their excited state, systems with low ionization potentials, descriptions of absolute acidities, and so on. The 6-31+G(d) basis set is the 6-31G(d) basis set with diffuse functions added to heavy atoms. The double plus version, 6-31G++(d), adds diffuse functions to the hydrogen atoms as well. Diffuse functions on hydrogen atoms seldom make a significant difference in accuracy. [16]

1.3.6 Time-dependent density functional theory

There is also other method to calculate the excited state properties. One method to calculate the excited state of the system is called the time dependent density-functional theory (TD-DFT). Time-dependent density functional theory (TD-DFT) is an extension of DFT to time dependent problems, such as a molecular system's interaction with a time-dependent external field. In the case of a spectroscopic measurement of an optical absorption spectrum the external field is an electromagnetic wave. Under these conditions, the effect on the system by the external field is sufficiently small to allow that the system's response is described by time dependent perturbation theory. Within this approach, the excitations are expressed in terms of ground state properties and excited states are not evaluated explicitly. [17]

The simplest form of the interaction of the system and the electromagnetic wave is the electric dipolar interaction, giving the time dependent perturbation needed to be considered, for example, the following form:

$$H^{(1)}(t) = -\vec{\mu} \cdot \vec{E}(t) \tag{1.18}$$

where μ is the dipole moment operator of the electrons, and the electric field, E is oscillating with frequency ω in the simple case of monochromatic light. The linear response of the system to such a perturbation is described by the dynamic polarizability $\alpha(\omega)$. Since the molecules are randomly oriented in for example solution and gas phase, the interesting quantity for comparisons with experiments is the mean dynamic polarizability, $\bar{\alpha}(\omega)$, a property that has the following form:

$$\bar{\alpha}(\omega) = \sum_{I}^{excited\ state} \frac{f_I}{\omega_I^2 - \omega^2} \tag{1.19}$$

where $\omega_I = E_I - E_0$ are the excitation energies and f_I are the oscillator strengths, which contain the transition dipole moments

$$f_I = \frac{2}{3}(E_I - E_0)|\langle \Psi_0|\vec{\mu}|\Psi_I\rangle|^2 \tag{1.20}$$

The dynamic polarizability has poles (diverges) at frequencies corresponding to excitation energies. Hence, the absorption spectrum of a system can in principle be obtained as the poles and residues (numerator at the poles) of the mean dynamic polarizability.

It appears to be generally accepted that TD-DFT provides fairly accurate excitation energies as long as low-energy transitions involving valence states are investigated. Hybrid functionals, such as B3LYP, seem to yield slightly more accurate results than simple GGA functionals especially for charge transfer states. [18]

1.3.7 Koopmans' Theorem

Given an N-electron Hartree-Fock single determinant $|^N\Psi_0\rangle$ with occupied and virtual spin orbital energies ε_a and ε_r, then the ionization potential to produce an (N - 1)-electron single determinant $|^{N-1}\Psi_a\rangle$ with identical spin orbitals, obtained by removing an electron from spin orbitals χ_a, and the electron affinity to produce an (N + 1)-electron electron single determinant $|^{N+1}\Psi^r\rangle$ with identical spin orbitals, obtained by adding an electron to spin orbitals χ_r, are just $-\varepsilon_a$ and $-\varepsilon_r$, respectively.

Koopmans' Therorem thus give us away of calculating approximate ionization potentials and electron affinities. This "frozen orbitals" approximation assumes that the spin orbitals in the (N ± 1)-electron state, i.e., the positive and negative ions if $|^N\Psi_0\rangle$ is a neutral species, are identical with those of the N-electron state. This approximation neglect relaxation of the spin orbitals in the (N ± 1)-electron state, i.e., the spin orbitals of $|^{N}\Psi_0\rangle$ are not the optimum spin orbitals for $|^{N+1}\Psi_0\rangle$ or $|^{N-1}\Psi_0\rangle$. Optimizing the spin orbitals in the (N ± 1)-electron single determinant by performing a separate Hartree-Fock calculation on these state would lower the energies $^{N+1}E_a$ and $^{N-1}E_a$ thus the neglect of relaxation in Koopmans' Therorem calculations tends to produce too positive an ionization potential and too negative an electron affinity. In addition, of course, the approximation of a single determinant wave function leads to error, and the correlation effects, which one obtains in going beyond the Hartree-Fock approximation, will produce further corrections to Koopmans' Therorem results. In particular, correlation energies are largest for the system with the highest number of electrons. Therefore, correlation effects tend to cancel the relaxation error for electron affinities. N general, Koopmans' ionization potentials are reasonable first approximations to experimental ionization potentials. Koopmans' electron affinities are unfortunately often bad. Many neutral molecules will add an electron to form a stable negative ion [19].

1.4 Aims and scope of thesis

1.4.1 To study the structural and energetic properties of newly designed dyes (as shown in Figure 1.6) using the computational calculations.

1.4.2 To study the effect of different hybrid functional such as B3LYP, PBE1PBE, BHandHLYP and CAM-B3LYP on the calculated absorption spectra of newly designed dyes.

1.4.3 To calculate and analysis the important key parameter, such as the density of state (DOS), natural bond orbitals (NBO), free energies of injection (ΔG^{inject}), and light-harvesting efficiencies (LHE).

1.4.4 To calculate the adsorption energies of newly designed dyes using the DMol^3 program in Material Studio 5.5 software suite.

1.4.5 To model the adsorption behavior of newly designed dyes on the TiO_2 cluster surface cell and calculate the single point energy to determine the electron injection phenomena.

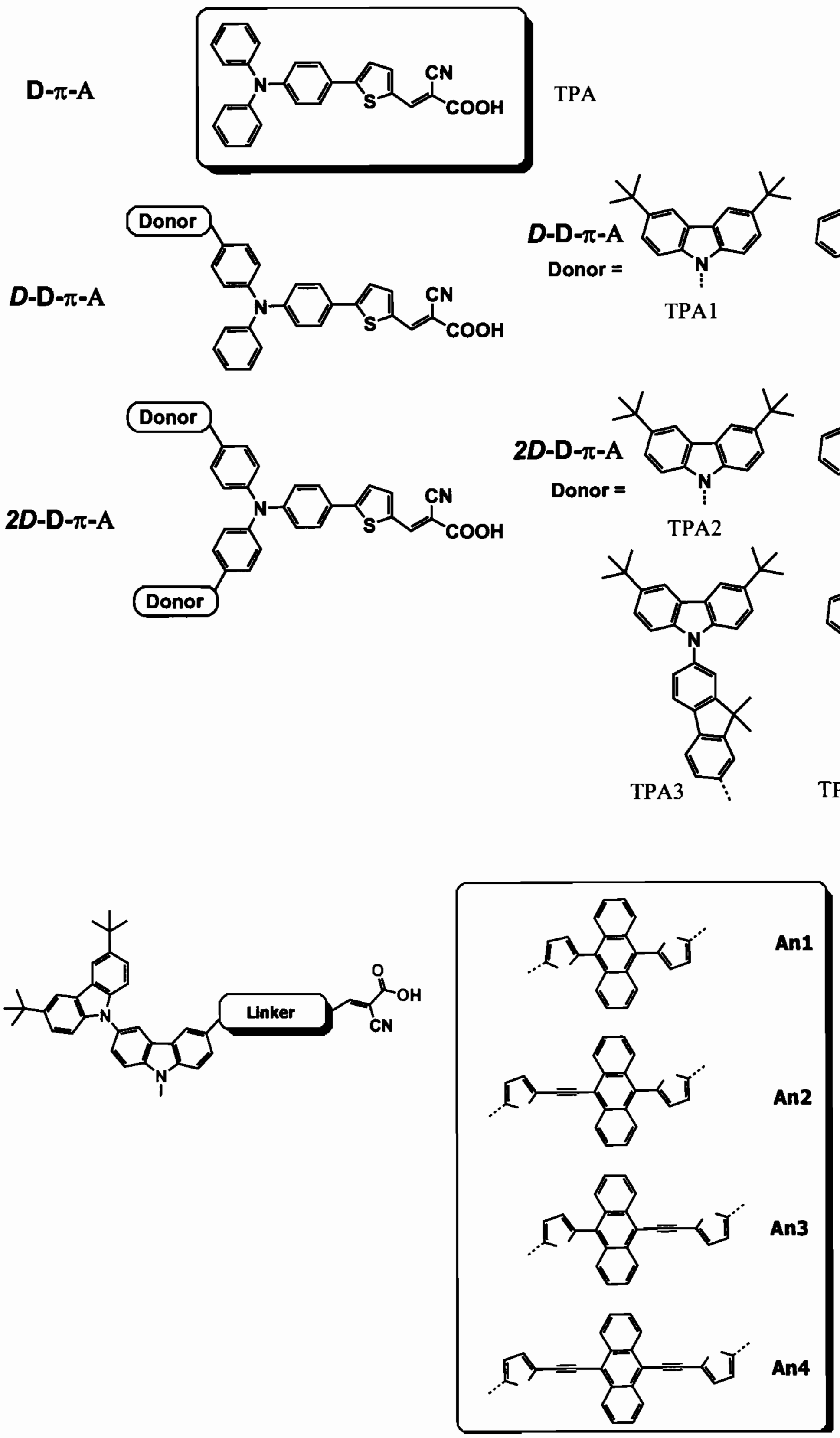
D-π-A
N
S
CN
COOH
TPA
Donor
D-D-π-A
Donor =
N
TPA1
TPA4
2D-D-π-A
TPA2
TPA5
TPA3
TPA6
Linker
O
OH
CN
An1
An2
An3
An4

Figure 1.6 Chemical structures of newly designed dyes

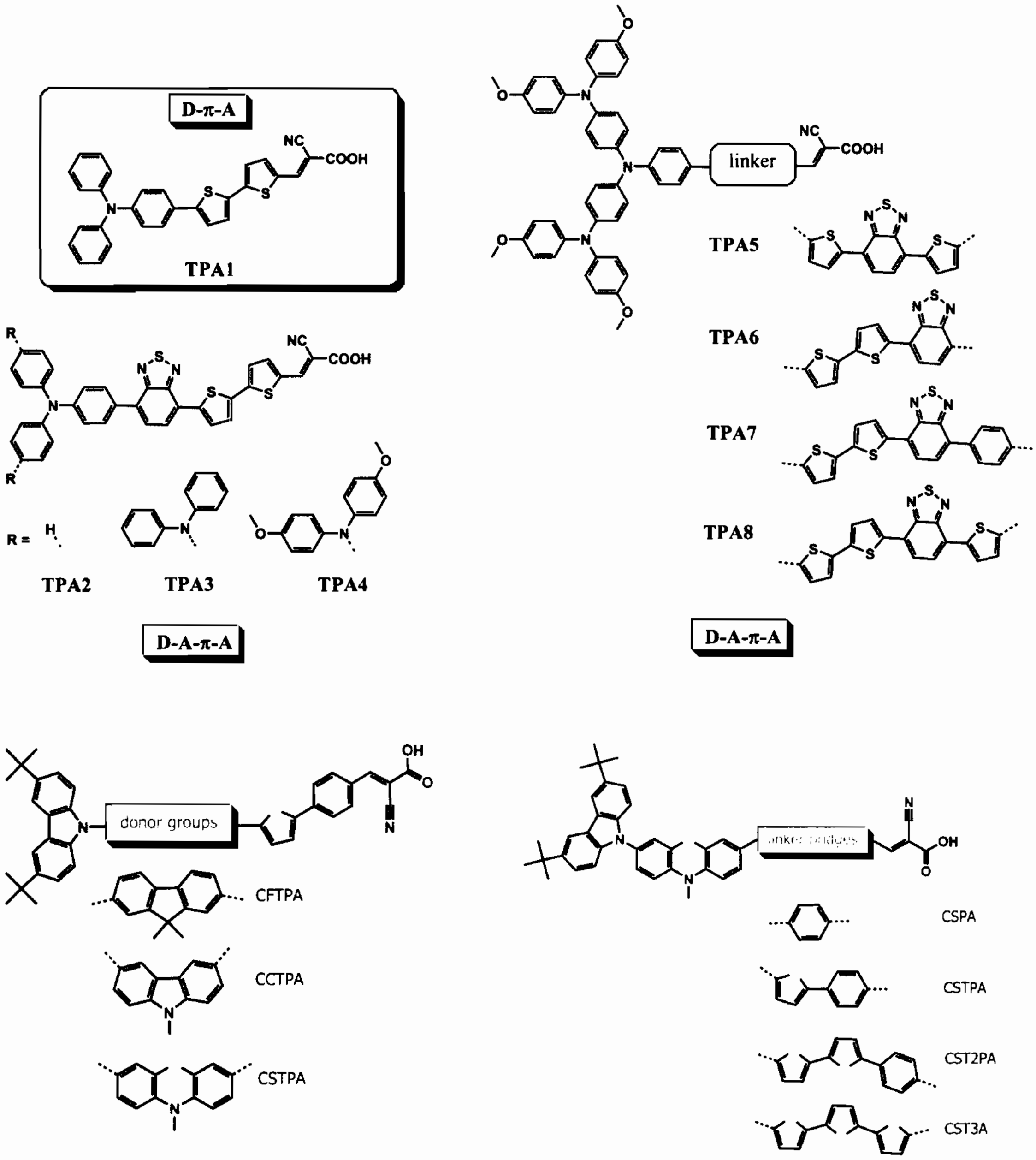
D-π-A
NC
COOH
N
S
S
TPA1
R
N
N
S
N
R = H
TPA2
TPA3
TPA4
O
D-A-π-A
linker
TPA5
TPA6
TPA7
TPA8
D-A-π-A
OH
O
donor groups
CFTPA
CCTPA
CSTPA
CSPA
CSTPA
CST2PA
CST3A

Figure 1.6 Chemical structures of newly designed dyes (Continued)

CHAPTER 2

LITERATURE REVIEW

A large amount of research has been made to organic dyes for using in dye-sensitized solar cells (DSSCs). Several research groups have developed organic dyes and to date some of them have obtained efficiencies in the range of 5–9%. We classify such organic dyes into 4 groups based on the role of our target molecules.

2.1 Triphenylanine (TPA) based dyes

The electron donors in organic sensitizers play a vital role in determining the overall conversion efficiency studied by many research teams. Triarylamine was used as an electron donor for metal-free organic sensitizers because of its excellent electron donating capability and aggregation resistant nonplanar molecular configuration. Employing triarylamine as electron donor, sensitizers with various conjugating units and acceptors were investigated. J. Xu et al. [20] reported that TPA dyes with more conjugated thiophene units (as shown in Figure 2.1) can effect on red-shifted of absorption spectra due to the increase of the π-conjugation system, which is one of the approaches to improve performance of organic dyes. W. Lei et al. [21] had also studied to describe the π-spacer effect of these various units of thiophene on the geometrical, electronic structures, and the electronic absorption spectra using density functional theory calculations. They found that the introduction of more thiophene units (TPA3) provides broader absorption bands and larger extinction coefficients of dye, but it is also enlarged the distance between electron donor group and semiconductor surface, reduced the electronic coupling, decreased the electron injection rate and then gave rise to lower overall conversion efficiency.

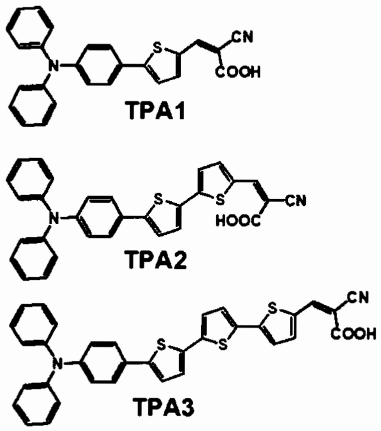
N
S
CN
COOH
TPA1
N
S
S
HOOC
CN
TPA2
N
S
S
S
CN
COOH
TPA3

Figure 2.1 Chemical structures of the triphenylamine dyes TPA1–TPA3

Z. Ning et al. [22] reported a novel starburst triarylamine based dyes introduced carbazole molecules into the molecule to form the D-D-π-A structure (as shown in Figure 2.2). They found that the absorption region can be extended to a broader which is an advantageous spectral property for light harvesting of the solar spectrum, and the molar extinction coefficient can be enhanced comparing with the D-π-A structure. The HOMO and LUMO energy levels of this dye are an efficient transporting material system in terms of balance between photovoltage and driving forces for future preparation of highly efficient dyes by matching suitable donor-linker-acceptor components.

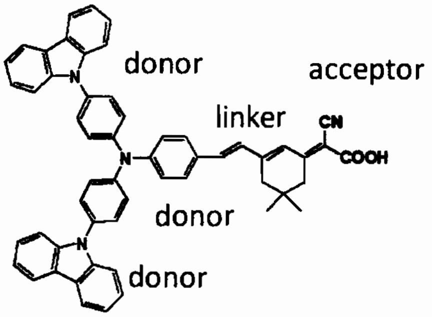
N
donor
acceptor
linker
CN
N
COOH
donor
N
donor

Figure 2.2 The triphenylamine dyes connected by carbazole forming D-D-π-A structure

C. Jia et al. also [23] studied on the carbazole–triphenylamine-based dyes for dye-sensitized solar cells using the theoretical study (as shown in Figure 2.3). They reported the effect of different acceptors on the geometries, electronic structures, and electronic absorption spectra ofthese dyes. The calculated results showed that these dyes can be used as potential sensitizers for TiO_2 nanocrystalline solar cells together with I^-/I_3^- electrolyte. But taking the geometries, electronic structures, frontier molecular orbital energies and electronic absorption spectra of these dyes into account **D2** should favor the best performance for DSSCs.

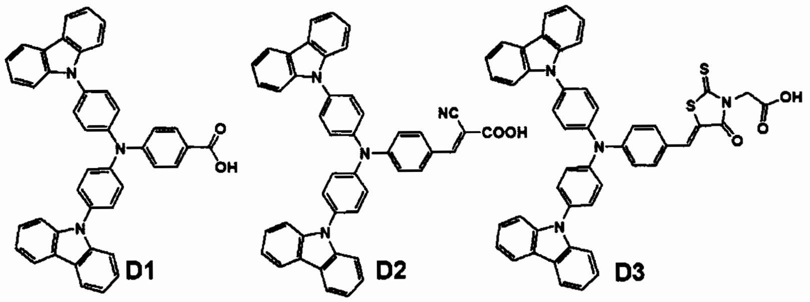

Figure 2.3 Molecular structures of D1, D2, and D3

For theoretical study, C. Jia et al. [23] reported that carbazole group was used as secondary electron donor for triphenylamine-based dyes (as shown in Figure 2.4). The dihedral angles formed between carbazole and benzene plane are 56.15° which can help to inhibit the close intermolecular aggregation effectively. The calculated TDDFT-B3LYP/6-31G(d,p) absorption peak of D2 is 475.8 nm.

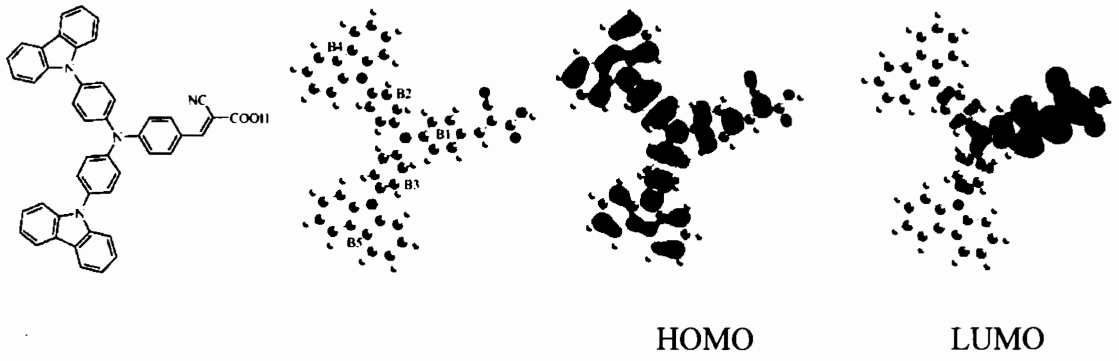

Figure 2.4 Molecular structures, optimized geometries, and molecular orbital distribution of D2

Z. Wan et al. [24] reported that phenothiazine group was also used as secondary electron donor for triphenylamine-based dyes (as shown in Figure 2.5). The dihedral angles between phenothiazine and benzene are all noncoplanar, which can help to inhibit the close π-π aggregation effectively between the starburst structures. The electron distributions of the HOMOs are homogeneously distributed on phenothiazine ring. The absorption spectrum of the **PTZ-1** has one intense visible absorption band centered at 433 nm.

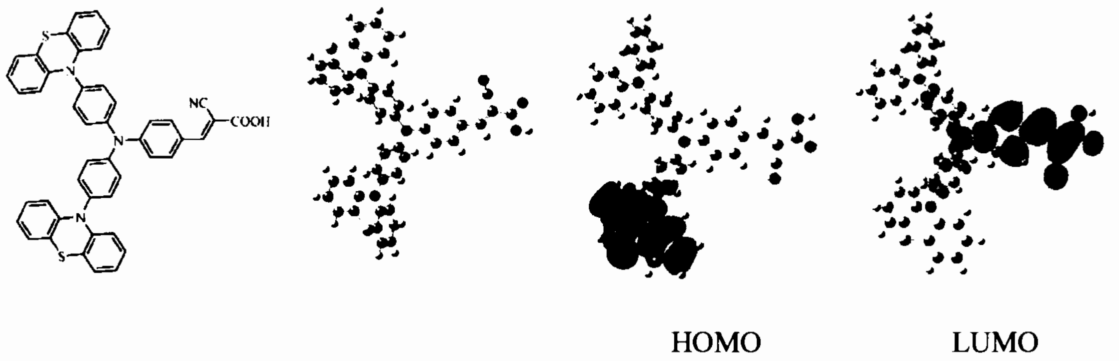

Figure 2.5 Molecular structures, optimized geometries, and molecular orbital distribution of PTZ-1

Z. Wan et al. also [25] reported that carbazole and phenothiazine groups are used as secondary electron donor (as shown in Figure 2.6). The UV-vis absorption spectra of the two dyes in CH_2Cl_2 are 473 and 468 nm for carbazole and phenothiazine respectively which may be due to the introduction of phenothiazine unit brings the decrease of co-planarity between the electron donor and the electron acceptor in the ground-state, but the molar extinction coefficient of phenothiazine is higher, which is an advantageous spectral property for harvesting the light. The excited state oxidation potentials of two dyes are far more negative than the band edge energy of the nanocrystalline TiO_2 electrode. Carbazole sensitized cell gives an overall conversion efficiency of 3.1%, while phenothiazine sensitized cell gives an overall conversion efficiency of 2.1%. The research results show that the inefficient electron injection from the excited dyes into the conduction band of TiO_2 results in the low efficiencies of DSSCs based on the two dyes.

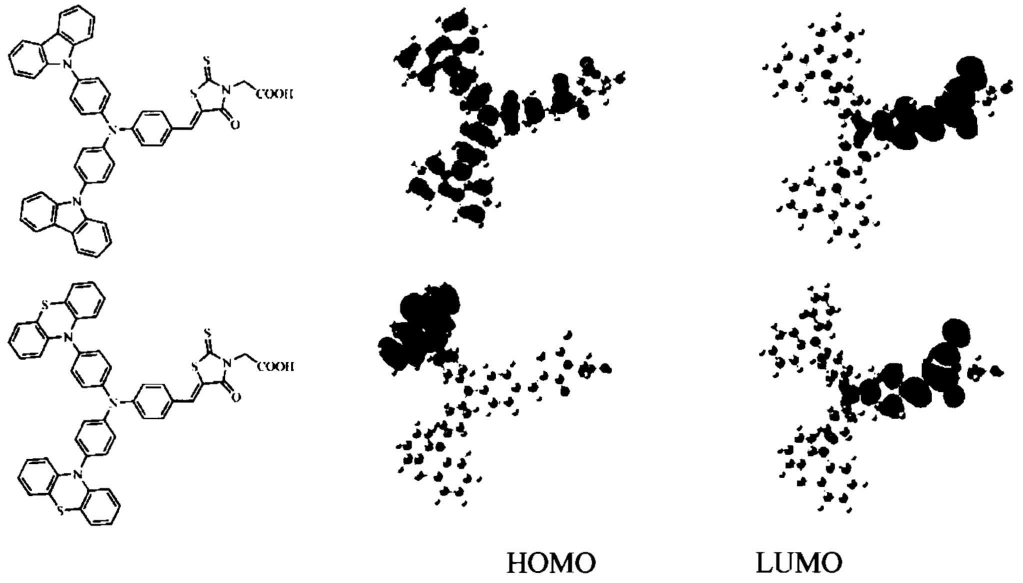

Figure 2.6 Molecular structures and molecular orbital distribution of WD-2 and WD-3

2.2 Organic dyes in D-A-π-A configuration

During the past two decades, thousands of organic sensitizers have been developed with the D-π-A configuration, exhibiting a promising photo-to-electricity conversion efficiency. As is well known, the π-linker segment has influences on the photophysical and electrochemical properties to a large extent which also greatly affects the photovoltaic performance of sensitizers. A D-A-π-A configuration was proposed with an auxiliary acceptor between the donor and conjugation bridge to expand the light-harvesting capability of the sensitizer for an increase in photocurrent.

Recently, a high photovoltaic performance of **WS-9** dye (as shown in Figure 2.7) nearly 9% based on a D-A-π-A configuration was reported by Y. Wu et al. [26], and then the dyes in D-A-π-A system was received increasing attention as promising efficient sensitizers for dye-sensitized solar cells (DSSCs).

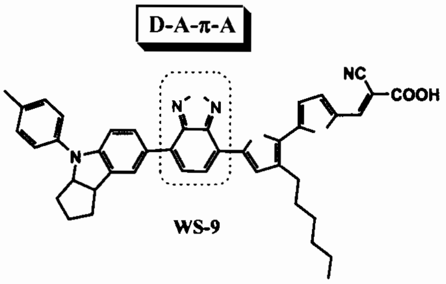

Figure 2.7 Chemical structure of D–A–π–A sensitizer WS-9

The D-A-π-A configuration can significantly reduce the HOMO-LUMO energy gap along with an improved light stability, highly desirable in photovoltatic optimization of sensitizers. The auxiliary electron-donating effect between indoline and triphenylamine (as shown in Figure 2.8) was also studied by Y. Wu et al. [27] They reported that sensitizers bearing indoline as the electron-donating group, a promising electron donor with priority in optimizing the absorption spectra of sensitizers.

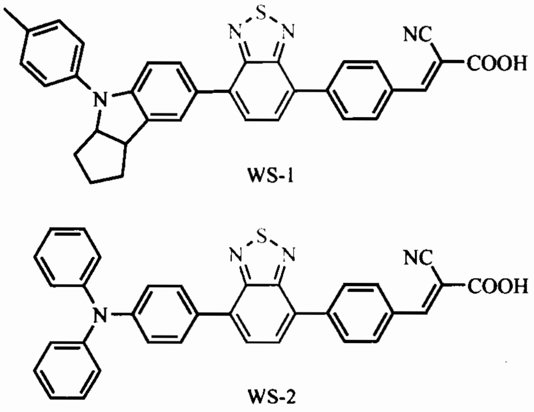

Figure 2.8 Chemical structures of D–A–π–A organic sensitizers WS-1 (indoline donor) and WS-3 (triphenylamine donor)

2.3 Anthracene based dyes

Anthracene derivatives, being among the most frequently used and most promising chromophores, have been extensively investigated in many fields, including organic photovoltaic devices. This is due mainly to characteristics such as intense luminescence, their planar conjugated backbone and their linear ring system. Moreover, many structural variations are possible in anthracene derivatives especially in relation to the variety of substituents in reactive positions 9 and 10 of their basic structure (as shown in Figure 2.9), which can influence their optical properties.

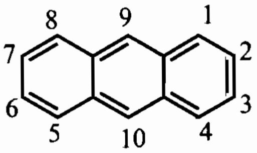

Figure 2.9 Molecular structures of anthracene

K.R.J. Thomas et al. [28] reported anthracene-based triarylamine donor and cyanoacrylic acid acceptor (as shown in Figure 2.10). The optical spectra of the dyes are dominated by a charge transfer transition. This band is red-shifted and increased in intensity on elongation of conjugation by the introduction of bithiophene or dithienylbenzothiadiazole moiety. Theoretical calculations revealed the charge transfer to occur between anthracene and triarylamine moieties. However, in the benzothiadiazole containing dye the charge transfer is observed between the amine and the acceptor segment. Dye-sensitized solar cells fabricated using these dyes showed moderate efficiency which is highly dependent on the nature of the conjugation bridge.

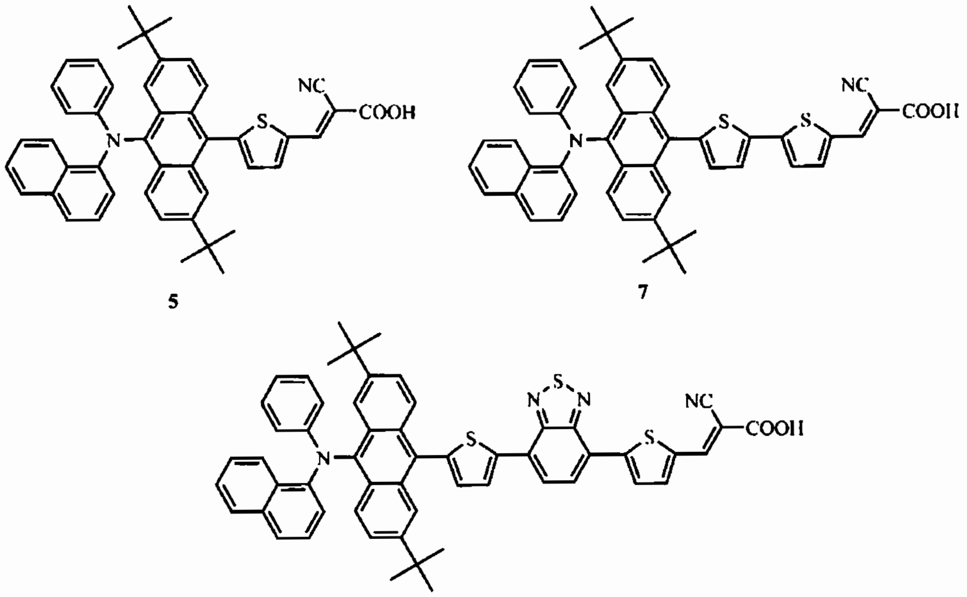

5 7 9

Figure 2.10 Structures of the anthracene-based dyes 5, 7 and 9

D. Heo et al. [29] reported metal-free organic dyes bridged by anthracene-mediated π-conjugated moieties (as shown in Figure 2.11). By introducing an anthracene moiety into the dye structure, together with a triple bond and thiophene moieties for fine-tuning of molecular configurations and for broadening the absorption spectra, the short-circuit photocurrent densities (J_{sc}), and open-circuit photovoltages (V_{oc}) of DSSCs were improved.

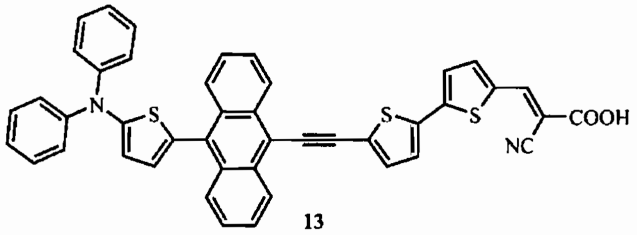

13

Figure 2.11 Structures of the anthracene-based dyes 13

The donor-(π-conjugation)-acceptor (D-π-A) system is the basic feature for most metal-free organic dyes due to the effective photoinduced intramolecular charge transfer property. C. Teng et al. [30] reported appropriate π-conjugation between an electron donor and an electron acceptor (as shown in Figure 2.12) to be beneficial to red shift the charge-transfer transition. Fused aromatic compounds such as anthracene have big π-conjugations and are available as fine chemicals.

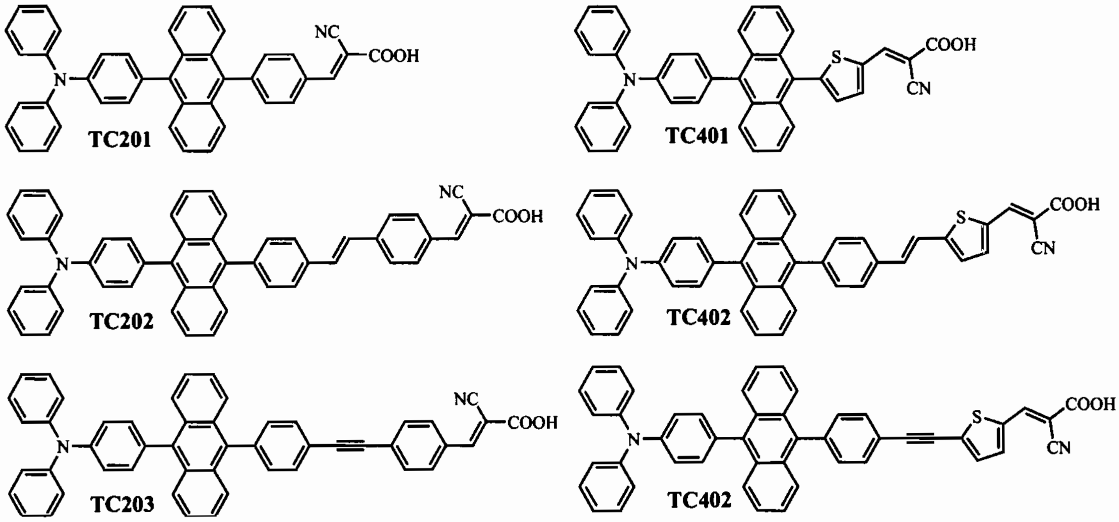

Figure 2.12 Molecular structures of metal-Free organic dyes (TC201-203, TC401-403) bridged by anthracene-containing π-conjugations

2.4 Phenothiazine based dyes

The electron rich nature of a phenothiazine moiety provides a good relay for the electron migration from D to A. It is worth noting that a phenothiazine-based dye contains electron-rich nitrogen and sulfur heteroatoms in a heterocyclic structure with high electron-donating ability, and its nonplanar butterfly conformation can sufficiently inhibit molecular aggregation and the formation of intermolecular excimers. Y. Hua et al. [31] reported a series of simple phenothiazine-based dyes (as shown in Figure 2.13) that represents the highest photovoltaic conversion efficiency value (8.18%) when compared with other reported phenothiazine-derived dyes, and exceeds the reference N719 (7.73%) under identical fabrication conditions.

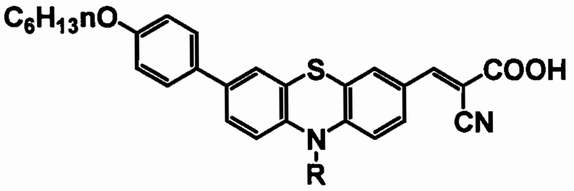

PT-C_2 R = Ethyl
PT-C_6 R = 1-Hexyl
PT-C_8 R = 1-Octyl
PT-C_{12} R = 1-Docedyl

Figure 2.13 Structures of dyes PT-Cn (n = 2, 6, 8, 12)

S. Agrawal et al. [32] investigated the phenothiazine-based organic solar cell sensitizers (as shown in Figure 2.14) with the computational modeling to understand the individual effects of solvation and aggregation on the dyes optical properties. They showed that DFT/TDDFT calculations can quantify propensity of PTZ-based dyes to form the dye aggregation on the TiO_2 surface.

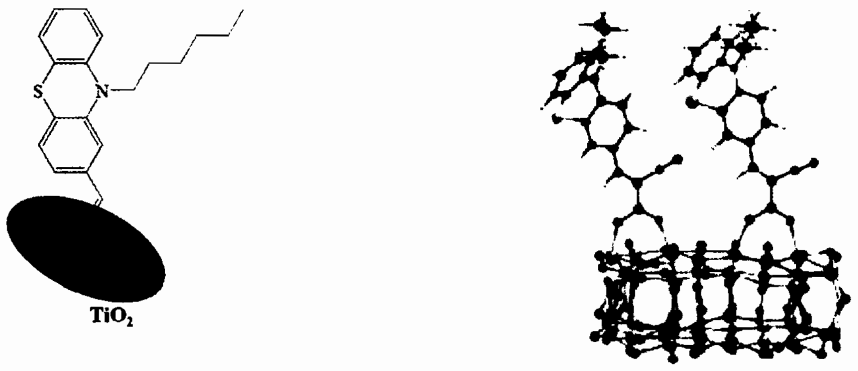

(a) (b)

Figure 2.14 (a) Molecular structure of the CS1A dyes, and (b) optimized structures of the dyes

2.5 Dye adsorption on TiO_2 surface

A key process in the operation of dye-sensitized photovoltaic solar cell devices is the charge injection from the dye molecule at the surface of the semiconductor nanoparticle to the conduction band states. The generally accepted injection mechanism involves photoexcitation to a dye excited state, from which an electron is subsequently transferred to the semiconductor, typically TiO_2 anatase, conduction band states called as "indirect injection". By contrast, a mechanism involving a direct photoexcitation from the dye to an empty state of the nanoparticle called as "direct injection". [33]

F. De Angeli [34] successfully studied the direct and indirect injection mechanisms in perylene dye-sensitized solar cells using large-scale excited state Time-Dependent DFT (TDDFT) calculations. The electron transfer accompanying photoexcitation have clearly shown in Figure 2.15, a purely indirect injection mechanism in **1** to a partially direct injection regime in **2**.

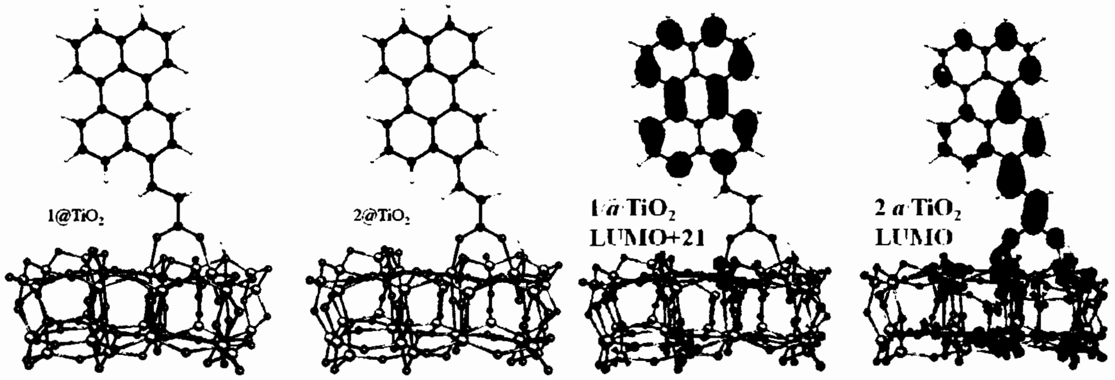

Figure 2.15 Optimized geometrical structures 1 and 2 adsorbed onto the $(TiO_2)_{38}$ model, and their molecular orbitals

S. Agrawal et al. [35] successfully investigated the optical properties of dye-sensitized solar cells (DSSCs) comprised of TiO_2 nanoparticle sensitized with two coumarins (as shown in Figure 2.16) using Time-Dependent Density Functional Theory (TD-DFT). The TD-DFT results suggest that both dyes exhibit direct charge transfer to titania due to excitation.

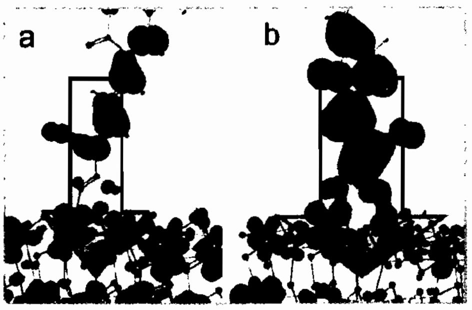

Figure 2.16 Relative probability density at dye's anchor and titania interface. The larger arrow reflects the experimentally observed increase in J_{sc} with the increase in the charge density

CHAPTER 3

TUNING THE ELECTRON DONATING ABILITY IN THE TRIPHYLAMINE-BASED D-π-A ARCHITECTURE FOR HIGHLY EFFICIENT DYE-SENSITIZED SOLAR CELLS

3.1 Introduction

Dye-sensitized solar cells (DSSCs) have been attracting wide interest after O'Regan and Gratzel presented their high efficiency solar cell in 1991, [4] and been considered as major topic of research with over 1000 articles being published by the end of year 2010. [36] As reported, the DSSCs based on the organic materials acting as a sensitizer molecule appear to be a highly promising and cost-effective candidate for the solar cell technology because of its application of high solar-to-electricity conversion efficiency, low costs, and the straightforward manufacturing procedures. [2,37] Up to now, DSSCs performance has reached power conversion efficiencies exceeding 12%, such as **N3**, **N719** and Black dye using ruthenium sensitizers, [38] but has limited efficiencies exceeding 10% for metal-free organic dyes. [39]

Recently, developments of higher power conversion efficiency of metal-free organic dyes have been considered in active research projects relating to the key component of dye sensitizer in DSSCs. The novel designed dyes with the donor-π conjugated-acceptor (D-π-A) system can usually achieve an efficient photovoltaic performance. [40,41] The properties of D-π-A dyes can be easily tuned by varying donor, [25,42,43] spacer, [44-46] and acceptor moieties.[47,48] From this perspective, the dyes play an important role in gaining higher solar-to-electricity conversion efficiency because the performance of DSSCs strongly depends on the following factors which are the criteria for a good dye sensitizer: (i) Wide absorption wavelength in visible to near infrared (IR) region; (ii) Easy electron injection from the excited state of the dyes to the the conduction band of TiO_2 and (iii) Good electron transfer from the donor to acceptor. [49] All these factors are closely associated with the ground and excited electronic states of the dye sensitizer. However, only few research groups have studied the electronic structures and photophysical properties of dye sensitizer. [50-52]

The design for new dyes based on synthesis is usually time consuming and expensive. As a result, combined experimental and theoretical investigations are very important to understand the relationship between the structure, properties, and performance of dye-sensitizers in order to design new dye molecules. Density functional theory (DFT) is a reliable standard tool for the theoretical treatment of molecular structures and electronic structures. [53] In addition, its time-dependent (called time-dependent DFT or TD-DFT) can give reliable values for valence excitation energies and absorption spectra. [54-56]

In this work, theoretical study of the electronic structures and the optical properties of metal-free organic dyes, were carried out. The structural modification of organic dye molecules by investigation of the effect of different donors architectures were mainly focused to obtain high efficient dye sensitizer for DSSC applications. We have investigated the effect of introducing more electron donor, thereby forming *D*-D-π-A and *2D*-D-π-A structures. [58-60] The typical procedure to add more donor groups by introductions of more electron donors on a simple D-π-A dye system both of mono- and di-substituted to form *D*-D-π-A and *2D*-D-π-A dye system were designed as can be seen in Figure 3.1. The chemical structures of the triphenylamine based TPA dye and its derivatives are shown in Figure 3.2. In addition, the adsorption of dyes on TiO_2 surface under theoretical prediction was performed. The excitation energies were investigated with CAM-B3LYP DFT functional. Attempts to design different number and types of auxiliary donor effecting the electronic structures and photophysical properties of the dyes have been made.

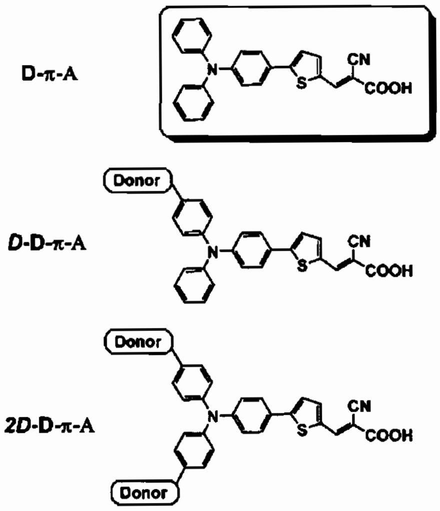
D-π-A
CN
COOH
Donor
D-D-π-A
2*D*-D-π-A

Figure 3.1 The typical procedure to add more donor groups

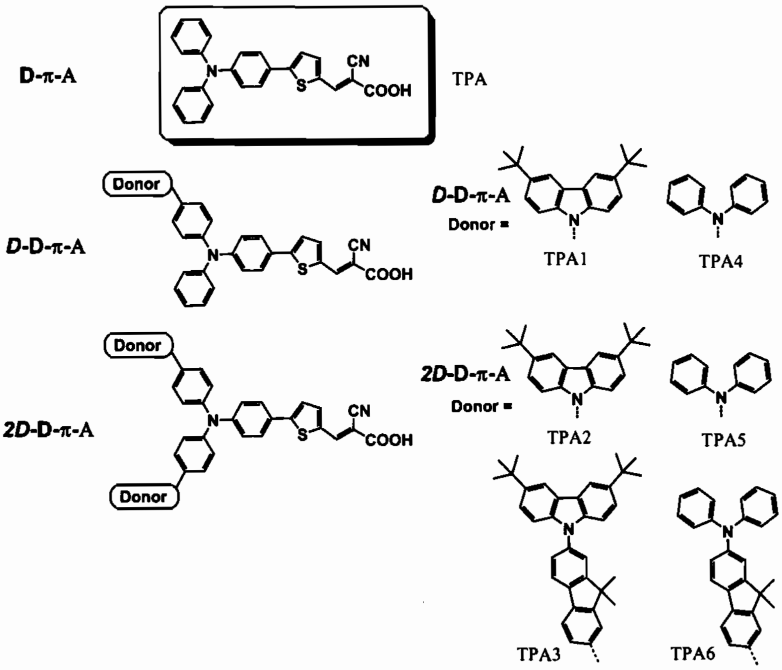
D-π-A
TPA
Donor
D-D-π-A
Donor =
TPA1
TPA4
2*D*-D-π-A
TPA2
TPA5
TPA3
TPA6
CN
COOH

Figure 3.2 Molecular structures of the triphenylamine based TPA dye and its derivatives TPA1-TPA6 dyes added more auxiliary donor

3.2 Computational details

We used the GAUSSIAN 09 software suite for all of our calculations. All organic dyes coded **TPA1-TPA6** represented by *D*-D-π-A and *2D*-D-π-A dye systems were computed in comparison with the **TPA** dye represented by the D-π-A dye system. The ground-state geometries were fully optimized using the Density

Functional Theory (DFT) method combined with Becke's three-parameter hybrid functional and Lee-Yang-Parr's gradient-corrected correlation functional (B3LYP) [60] at 6-31G(d,p) level. All calculations were performed without symmetry constraints and only in a gas phase. These optimized structures were calculated for the first excitation energy (E_g), maximal absorption wavelength (λ_{max}) and oscillator strengths (f) for the 10 states by using Time-Dependent Density Functional Theory (TD-DFT) with CAM-B3LYP [61] at 6-31G(d,p) level in dichloromethane. Subsequently, the TD-DFT results were entered into the SWizard program [62] for the simulation of absorption spectra of these dyes.

Furthermore, electronic transition and its character related to the absorption wavelength is discussed in relation to the results. To gain insight into the electron injection capability of dyes, the adsorption of dyes on the $(TiO_2)_{38}$ cluster was performed with DFT calculations using DMoL^3 [63] program in Materials Studio version 5.5. The structure of $(TiO_2)_{38}$ was comprised of 38 TiO_2 units which modeled a TiO_2 nanoparticle, as discussed in a previous report. [59] The $(TiO_2)_{38}$ configurations were fully optimized using the generalized gradient-corrected approximation (GGA) method. The Perdew–Burke–Ernzerhof (PBE) functional was used to account for exchange–correlation effects with the DNP basis set. The core electron was treated with DFT-semicore Pseudopotentials (DSPPs). After optimization, the adsorption energies (E_{ads}) of dyes on the $(TiO_2)_{38}$ cluster were obtained using the following equation:

$$E_{ads} = E_{dye} + E_{TiO_2} - E_{dye+TiO_2} \tag{3.1}$$

where E_{dye} is the total energy of isolated dye, E_{TiO_2} is the total energy of $(TiO_2)_{38}$ cluster, and $E_{dye+TiO_2}$ is the total energy of dye-$(TiO_2)_{38}$ complexes. After applying the above expression equation, the results of the positive value of E_{ads} indicated a stable adsorption.

3.3 Results and discussion

The derivatives of triphenylamine-based dye in the present study, namely **TPA1-TPA6**, were theoretically investigated. These dyes composed of an electron-accepting cyanoacrylic acid group and a π-conjugated bridge of one thiophene moiety while there were on different electron donor groups. We aimed to see the sensitizer donor effects on both the geometrical structures and the optical properties of the derivatives of triphenylamine-based dye. Therefore, the introductions of more electron donors on a simple D-π-A dye system both of mono- and di-substituted to form *D*-D-π-A and *2D*-D-π-A dye system were designed as can be seen in Figure 3.1. The variations of auxiliary donor are categorized into four types: (i) mono- and di-substituted of carbazole moiety at para position of TPA core forming **TPA1** and **TPA2**, respectively, (ii) fluorene-connected carbazole moity forming **TPA3**, (iii) mono- and di-substituted of diphenylamine moiety at para position of TPA core forming **TPA4** and **TPA5**, respectively, and (iv) fluorene-connected diphenylamine moiety forming **TPA6**. Figure 3.2 shows the molecular structures of **TPA1-TPA6** which were studied for the purpose of comparison with a simple triphenylamines-based **TPA** dye. The calculated results are presented and were based on the variation and architecture of the auxiliary donor.

3.3.1 The optimized ground-state structures

The optimized ground-state geometries of **TPA1-TPA6** dyes are shown in Figure 3.3, and the selected dihedral angles are listed in Table 3.1. As shown, each dye molecule was grouped into four fragments; triphenylamine (TPA) core acting as primary electron donor (denoted as D), secondary electron donor (denoted as *D* or *2D*) adding to para-position of TPA core, thiophene moiety acting as π-conjugated linker (denotes as π) and cyano acrylic acid acting as electron acceptor (denoted as A). Furthermore, the three units of the phenyl rings on TPA donor were labeled as 1-3 as internal rings of TPA donor for the purpose of comparison. Considering the dihedral angles between linker bridge and electron acceptor, the optimized structures of **TPA1-TPA6** dyes in the ground electronic state showed that these dihedral angles in column π-A as shown in Table 3.1 were calculated as less than 1 degree, indicating that the π-conjugated thiophene bridge was located to be coplanar with cyano acrylic acid group acting as both the acceptor and the anchoring group on the TiO_2 surface. These coplanar structures between the linker bridge and electron acceptor led to a strong conjugation effect as well as being effectively injected into the conduction band of TiO_2 through the cyano acrylic acid group. It can be seen that the molecular coplanarity of the linker bridge and electron acceptor was not affected by the auxiliary donor being added at the para-position of the TPA group.

In Table 3.1, the dihedral angles of between auxiliary donor and primary donor *(D(2D)*-D) were named as external dihedral angle (EDA) while the dihedral angles between phenyl rings on the triphenylamine core (1-2 and 1-3) were named as internal dihedral angles (IDA) to aid comparison. It is interesting to note that introducing carbazole auxiliary donor (**TPA1-TPA2**), EDAs were calculated to be about 53 degrees whereas adding diphenylamine auxiliary donor **(TPA4-TPA5)**, EDA were calculated to be only 38 degrees. These results indicated that diphenylamine auxiliary donor tends to be slightly twisted to the TPA core while carbazole auxiliary donor was significantly more twisted to the TPA core.

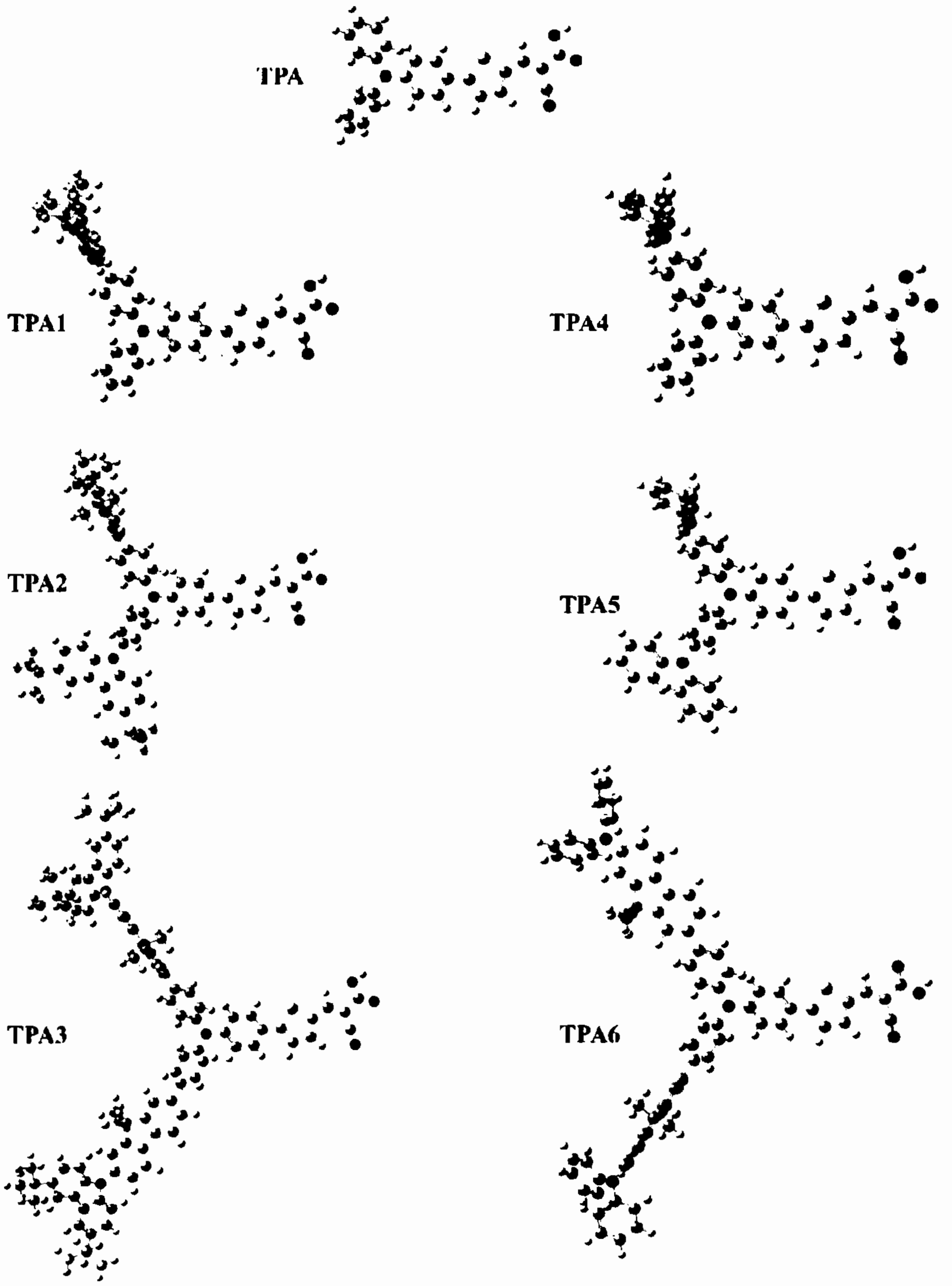
TPA
TPA1
TPA4
TPA2
TPA5
TPA3
TPA6

Figure 3.3 The optimized ground-state geometries of TPA1-TPA6 dyes

Table 3.1 Selected dihedral angle (in degrees) of the triphenylamine-based dyes added the carbazole, diphenylamine and fluorene-connected carbazole (or diphenylamine) moieties as the secondary electron donor

Dye	Dihedral angle (°)				
				TPA donor	
	D(2*D*)-D	D-π	π-A	1 - 2	1 - 3
Triphenylamine based dye:					
TPA		-20.76	0.93	46.80	45.62
Modified by added carbazole:					
TPA1	52.88	-21.59	1.00	44.43	47.06
TPA2	53.07 (-52.09)	-22.13	0.63	45.65	45.40
Modified by added fluorene-connected carbazole:					
TPA3	36.97(-36.34)	-21.28	0.69	46.52	43.93
Modified by added diphenylamine:					
TPA4	38.64	-20.64	0.97	49.51	45.03
TPA5	38.80 (-39.18)	-19.91	0.99	48.55	47.94
Modified by added fluorene-connecteddiphenylamine:					
TPA6	36.75(-35.64)	-20.86	1.00	46.58	45.82

D(2D) represented to mono- and di-substituted of auxiliary electron donor
D represented to primary electron donor
π represented to linker bridge
A represented to electron acceptor

In the case of the **TPA1** and **TPA2** dyes, the EDAs were calculated as approximately 52-53 degrees while calculated IDAs were about 44-47 degrees. The larger EDAs over the IDAs in **TPA1-TPA2** may significantly lead to difficulty of electron delocalization in the π-conjugated bridge and can effectively suppress the increase of conjugation length. In contrast, for **TPA4** and **TPA5** dyes, the EDAs were calculated as 38-39 degrees while IDAs were 47-49 degrees, it was found that the EDAs were lower than the IDAs. These smaller EDAs could provide the smooth electron delocalization in the π-conjugated bridge resulting in an extended π-conjugated system.

One way to reduce the large EDA of **TPA2** dyes is the insertion of fluorene connected between carbazole and the TPA donor forming **TPA3** dye. This optimized structure revealed that the external dihedral angle of **TPA3** was considerably changed from approximately 53 degrees to about 36 degrees. This indicated that the insertion of fluorene between secondary and primary donor is an appropriate approach to the rational design of dyes. As discussed above, if our designed dye showed lower EDAs than the IDA, it may virtually affect the extension of electron delocalization in the π-conjugation of the dyes. However, the insertion of fluorene connected between diphenylamine and the TPA donor in **TPA6** dye, the EDA was slightly decreased. According to their structural properties, we may conclude that diphenylamine can enhance the extent of electron delocalization of the sensitizer which may be used as the efficient secondary electron donor for the dye in the *D*-D-π-A and *2D*-D-π-A systems.

3.3.2 HOMO, LUMO levels and the energies diagram

The additional electron donor group's effect on HOMO and LUMO levels were also discussed. The appropriated dyes require suitable energy levels. The LUMO level must be sufficiently negative with respect to the conduction band of TiO_2 to inject electrons effectively and the HOMO level should be more positive than the redox potential of I^-/I_3^- for efficient dye regeneration. To evaluate the possibility of electron injection to the conduction band of the TiO_2 and electron regeneration from the electrolyte system, the HOMO and LUMO levels of the dyes were calculated. The energies diagram is shown in Figure 3.4.

As shown, the HOMO levels of triphenylamine derivative **TPA1-TPA6** dyes were systematically increased when adding more donor ability approaching the redox potential of the electrolyte system. Compared with electrolyte redox potential, these HOMO levels were below the iodine/iodide redox potential. These results show the suitability for accepting electron efficiency from the electrolyte system to the oxidized dye molecules. For LUMO levels, the results show that adding both carbazole and diphenylamine moieties slightly affected the LUMO level. However, the

LUMO levels of all dyes were above the conduction band of TiO_2 which is suitable for electron injection into the CB of TiO_2.

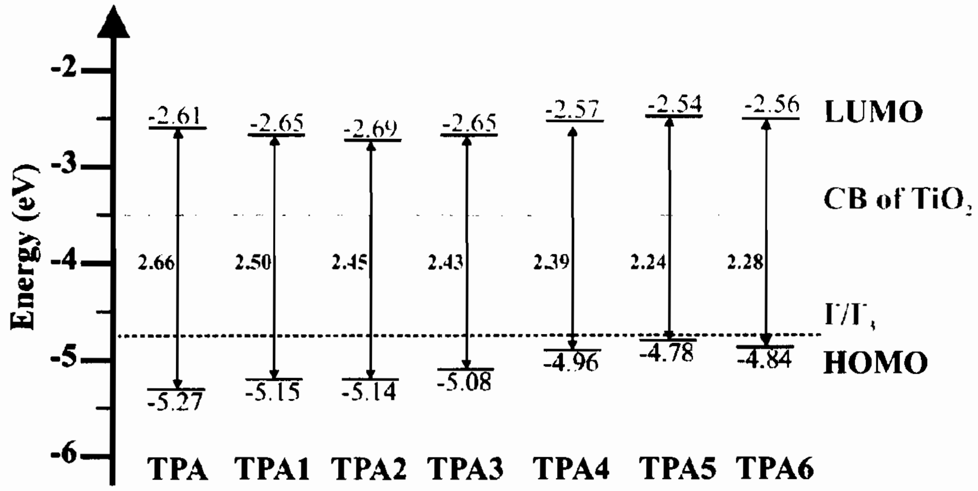

Figure 3.4 Energy diagram of HOMO and LUMO for the triphenylamine dyes, TiO_2, and the electrolyte

In addition, comparison between the energy gap of carbazole and diphenylamine moiety acting as auxiliary electron donor revealed that the energy gaps of diphenylamine auxiliary donor were narrower than that of carbazole auxiliary donor. Therefore, triphenylamine dyes with diphenylamine auxiliary donor would be an efficient auxiliary donor to extend the absorption wavelengths of triphenylamine dyes.

Furthermore, the isodensity plot of HOMO and LUMO levels of **TPA**, **TPA2** and **TPA5** are shown in Figure 3.5. The HOMO plot of **TPA** dye presents the electron density on the triphenylamine donor. When adding more electron donor for carbazole and diphenylamine moieties as **TPA2** and **TPA5** respectively, the electron densities were extended to the auxiliary electron donor and also remain delocalized on the triphenylamine donor which exhibited the increased donating ability *2D*-D-π-A system over the D-π-A dye. While the LUMO plots of the dyes were quite similar when adding more electron donor, they revealed that adding more electron donors can tune up HOMO level and increase the donating ability.

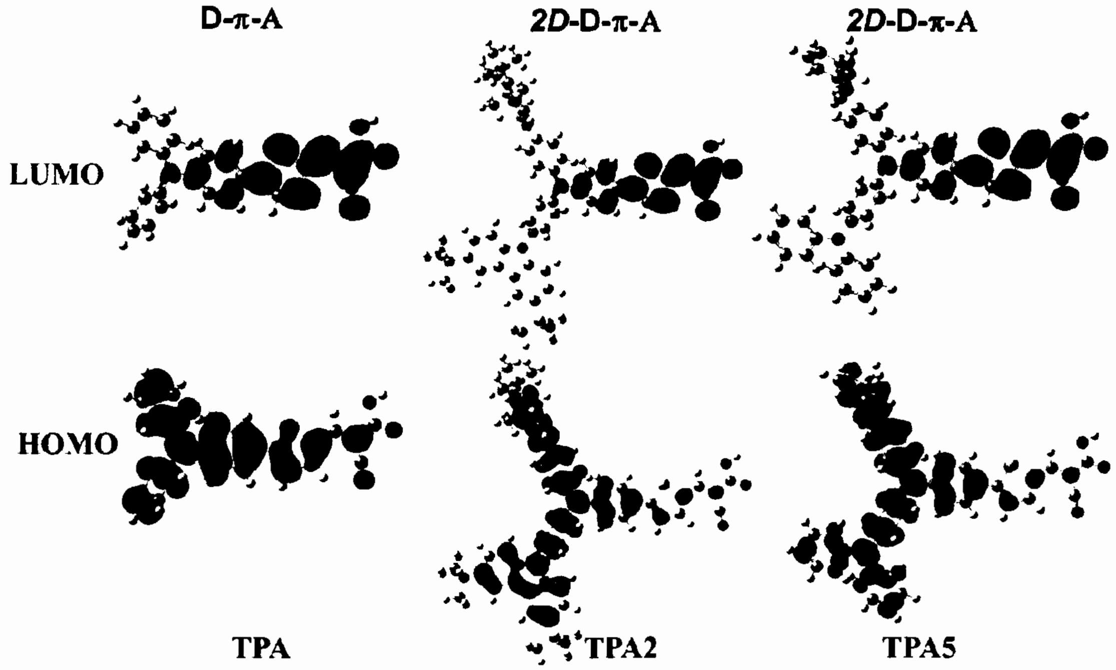

Figure 3.5 Isodensity plotted of HOMO and LUMO for the triphenylamine dyes (TPA, TPA2, TPA5) by B3LYP/6-31G(d,p) level

3.3.3 Absorption spectra and light harvesting properties

In order to understand electronic transitions, TD-DFT calculations in the C-PCM continuum salvation model [64] using dichloromethane solvent were performed with CAM-B3LYP functional. The calculated transition energies of **TPA1-TPA6** for the maximal absorption wavelength (λ_{max}), vertical excitation energy (E_g) and oscillator strength (f) together with the main excitation configuration are listed in Table 3.2.

As shown, the overall calculated absorption spectra observed peak into two regions around 270-330 and 430-450 nm. First is at higher absorption wavelength which was assigned to an intramolecular charge transfer (ICT) from the donor part in HOMO to the acceptor end group in LUMO. The second peak is at the lower absorption wavelength which was assigned as π-π* transition.

Table 3.2 Maximal absorption wavelength (λ_{max}), excitation energy (E_g), oscillator strength (f), electronic transition configurations of triphenylamine dyes obtained by TD-CAM-B3LYP/6-31G(d,p) level

Dye	λ_{max} (in nm), (εx10^{-4} M^{-1}cm^{-1})	E_g (in eV)	f	Transition Configuration
TPA	269, (4.25)	4.61	0.2970	0. 85(H→L+3) + 0.07(H-1→L+3)
	430, (10.37)	2.88	1.4305	0. 80(H→L) + 0.14(H-1→L)
TPA1	283, (5.83)	4.38	0.2973	0.65(H→L+4) + 0.07(H→L+1)
	429, (10.77)	2.89	1.4860	0.61(H→L) + 0.21(H-1→L)
TPA2	300, (8.27)	4.13	0.8585	0.29(H→L+2) + 0.26(H-1→L) +
	428, (11.16)	2.90	1.5399	0.23(H→L+4) 0.59(H→L) +
				0.25(H-2→L)
TPA3	327, (18.99)	3.79	2.3508	0.62(H→L+1) + 0.10(H-1→L+2)
	435, (12.27)	2.85	1.6931	0.61(H→L) + 0.14(H-2→L)
TPA4	300, (5.49)	4.13	0.5280	0.49(H→L+2) + 0.19(H→L+1) +
	441, (10.47)	2.81	1.4444	0.14(H→L+3) 0.60(H→L) +
				0.25(H-1→L)
TPA5	317, (6.95)	3.91	0.6495	0.45(H-1→L) + 0.29(H→L+2) +
	453, (10.58)	2.74	1.4596	0.12(H→L+3)0.65(H→L) +
				0.24(H-2→L)
TPA6	336, (21.15)	3.69	2.4086	0.54(H→L+1) + 0.21(H-1→L+2)
	438, (12.25)	2.83	1.6916	0.40(H-2→L) + 0.36(H→L) +
				0.14(H-3→L)

Comparing the absorption maxima of the dyes in aspect of three architectures (D-π-A, *D*-D-π-A and 2*D*-D-π-A), the calculated results show the 2*D*-D-π-A system to have a more broadening region. Furthermore, the presence of fluorene moiety between primary donor and auxiliary donor (carbazole and diphenylamine moieties) in order to extend the conjugation length was found. The calculated λ_{max} were 435 and 438 nm for **TPA3** and **TPA6**, respectively. The presence of fluorene moiety in carbazole end-capped molecule (**TPA3**) was slightly red-shifted around 7 nm compared to **TPA2** with no fluorene moiety, while the presence of fluorene moiety in diphenylamine end-capped molecule (**TPA6**) was blue-shifted about 15 nm compared to **TPA5**. We can conclude that the presence of fluorene moiety does not effect the extension of the conjugation length as expected. Therefore, in this section the details of *2D*-D-π-A absorption spectra with different electron donor groups compared to the D-π-A reference is discussed. The simulated UV–vis absorption spectra of **TPA**, **TPA2** and **TPA5** dyes are shown in Figure 3.6.

For carbazole auxiliary donor, the maximal absorption wavelengths of **TPA2** dye was calculated as 428 nm. Its electronic transition was assigned as mixed-transition in terms of linear combination between 0.59(HOMO→LUMO) and 0.25(HOMO-1→LUMO). In the case of the diphenylamine moiety, the UV-Visible spectra of **TPA5** dye exhibited at 453 nm. This absorption peak was assigned as combined transition of 0.65(HOMO→LUMO) and 0.24(HOMO-2 →LUMO). As mentioned above, this absorption region was assigned as intramolecular charge transfer (ICT) which was confirmed by the computed difference in electronic density between ground- and the first excited-state, for instance **TPA**, **TPA2** and **TPA5** dyes as depicted in Figure 3.7.

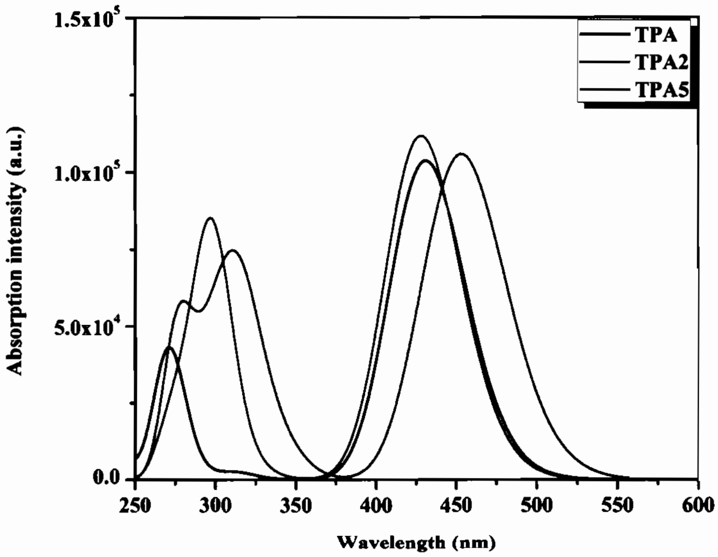

Figure 3.6 Simulated absorption spectra of the triphenylamine dyes (TPA, TPA2, TPA5) at the CAM-B3LYP/6-31g(d,p) level in dichloromethane solution

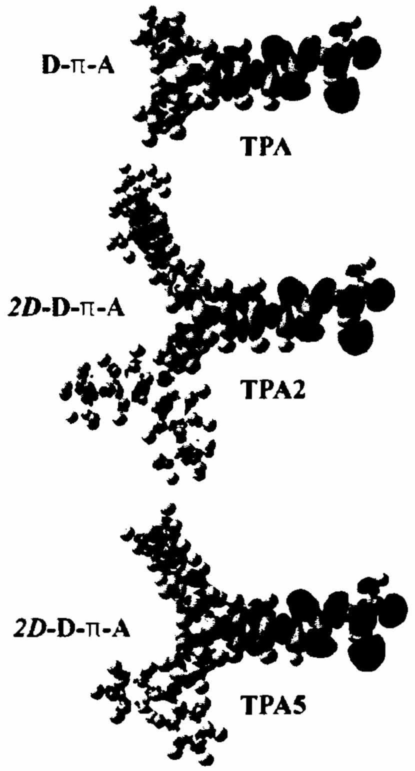

Figure 3.7 The charge density difference between the ground- and first excited-state of TPA, TPA2 and TPA5 dyes

The purple and yellow refer to an increase and a decrease of electronic density, respectively. As revealed, these three dyes show the decrease of electron density on the entire molecule and particularly on the carbazole- or diphenylamine-substituted auxiliary donor and TPA donor, while the increasing of electron density was mainly on the linker as well as acceptor group. The computed structures clearly show the strong charge-transfer character of the dyes as the electron densities were separated; depleted on the donor and auxiliary donor groups, while increased on the bridge and acceptor groups. These separated electron densities between donor and acceptor in part provided the driving force to push forward and control the direction of electron from donor and auxiliary donor directly to the acceptor part. We could conclude that adding more electron donating groups enhanced the donating ability of the triphenylamine dyes.

Generally, the dyes with broader absorption spectra and higher extinction coefficients are expected to have higher photo-to-current efficiency. When comparing

TPA2 and **TPA5** dyes with **TPA** dye, the results clearly show that the absorption wavelength of **TPA2** was negligibly blue-shifted (a.u. 2 nm) while the absorption wavelength of **TPA5** was large red-shifted by approximately 23 nm. This red-shift on calculated absorption results indicated that using the diphenylamine group as auxiliary donor instead of the carbazole unit can significantly improve the wide absorption wavelength in visible light to near infrared (IR) region as one of the key factors of a good dye sensitizer.

To understand the reason why adding the diphenylamine group can provide the red-shift on absorption spectra, the optimized structures of the dyes are discussed. When comparing the calculated absorption wavelength of the dyes with their optimized structures, the results show that the dyes, which have a lower EDA than the IDA, can exhibit the red-shift of absorption spectra because the conjugation length of those dyes can be extended. For instance, with **TPA5** dyes, the EDA is around 38 degrees and the IDA is around 49 degrees. This can enhance the extension of electron delocalization over the whole molecule indicating that **TPA5** dyes have the red-shift of absorption wavelength resulting in a good light harvesting ability.

3.3.4 Adsorption of dyes on $(TiO_2)_{38}$ cluster

In order to study the effect of different auxiliary electron donating groups on the adsorption property of triphenylamine-based dyes onto the titanium dioxide (TiO_2) surface, we carried out the **TPA2** and **TPA5** dyes adsorbed on $(TiO_2)_{38}$ surfaces as the complex structures of dye-TiO_2 for comparison of different electronic donating ability, the carbazole and diphenylamine as auxiliary electron donating groups were added as shown in **TPA2** and **TPA5**, respectively. These two dyes shared the same anchoring group of cyanoacrylic acid. It is well known that the most favorable adsorption configuration of cyanoacrylic acid is the bidentate bridging adsorption. [65,66] Therefore, we only modeled the bidentate bridging adsorption mode of **TPA2** and **TPA5** dyes in the complex structures of dye-TiO_2. The relaxed dye-TiO_2 structures were calculated using the PBE functional together with the Double-Numerical as implemented in the DMoL^3 program of the Material Studio software suite. The optimized structures of dye-$(TiO_2)_{38}$ structures are shown in Figure 3.8. Both of the two dyes showed the bond distances between 5c-Ti and O atom of dyes to be in the range of 2.06–2.18 Å. The adsorption energies (E_{ads}) of **TPA2** and **TPA5** dyes on

TiO_2 surface were calculated to be 21.98 and 22.19 kcal/mol respectively, indicating the strong interactions between the dyes and the TiO_2 surface.

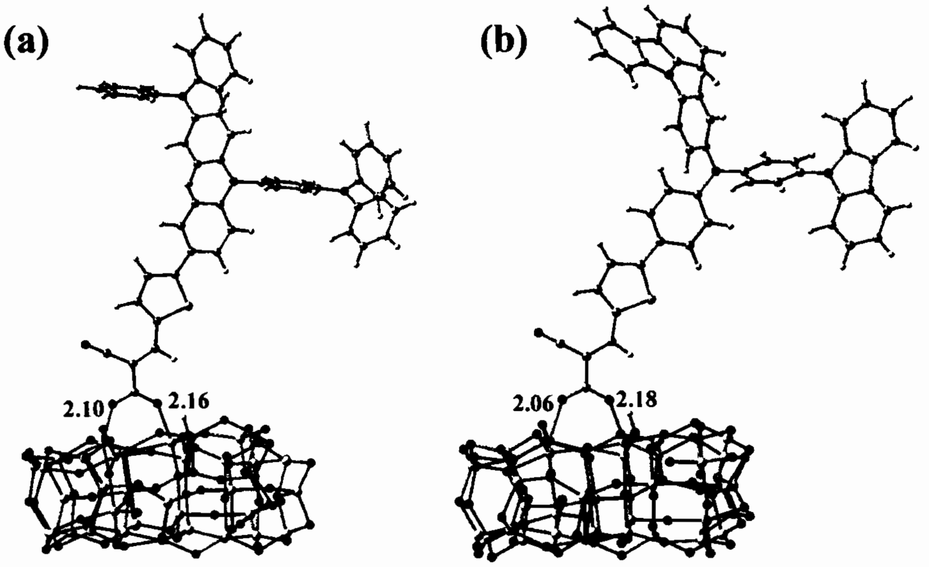
(a)
(b)
2.10
2.16
2.06
2.18

Figure 3.8 Relaxed structures of triphenylamine based dyes, (a) TPA2; (b) TPA5, adsorbed on $(TiO_2)_{38}$ surfaces by DMoL^3 calculation

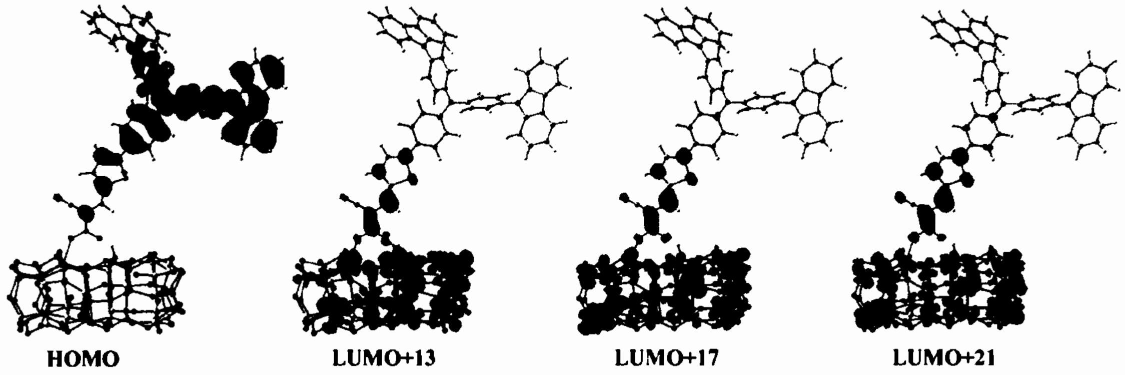
HOMO
LUMO+13
LUMO+17
LUMO+21

Figure 3.9 MOs of TPA5 adsorbed on $(TiO_2)_{38}$ surface related to the transitions calculated by TD-CAM-B3LYP/6-31G(d)

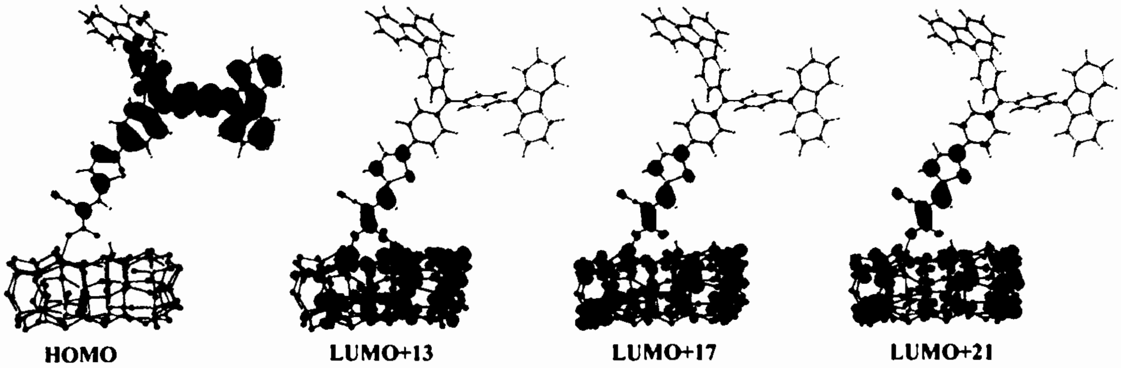

Figure 3.10 MOs of TPA2 adsorbed on $(TiO_2)_{38}$ surface related to the transitions calculated by TD-CAM-B3LYP/6-31G(d)

Besides, in order to investigate the mechanism of electron injection from dyes into TiO_2 surface using the DFT/TD-DFT calculations as implemented in the Gaussian09 program. The excitation energies and the electronic transitions were summarized in Table 3.3 and the frontier molecular orbitals of excited-state structures of dye-$(TiO_2)_{38}$ for **TPA5** were shown in Figure 3.9, and for **TPA2** see in Figure 3.10. There is a very similar trend between **TPA5** and **TPA2** dyes, therefore we only discuss the **TPA5** dye. The highest oscillator strength of 1.5539 for **TPA5** dye was assigned as the linear combination of 0.24(H→L+21) + 0.23(H→L+17) - 0.18 (H→L+12). The HOMO level for **TPA5** showed the electron density located on the triphenylamine group extend to carbazole and diphenylamine respectively, whereas the LOMO+12, LUMO+17 and LUMO+21 level for **TPA5** showed the electron density mainly located on TiO_2 surface and anchoring group of dyes. These compositions of three electronic transitions for two dyes, as shown in Figure 3.9 strongly indicated that when the intramolecular charge transfer was initially performed, electrons moved from auxiliary donor to the anchoring group via thiophene-bridging then jumped onto the TiO_2 surface. These calculated results, indicated that both of the auxiliary electron donor diphenylamine and carbazole groups can perform an excellent electron injection from triphenylamine dyes into the TiO_2 surface, which may improve the photo current as well as the conversion efficiency of the DSSCs cells.

Table 3.3 The excitation energies, oscillator strengths, and molecular compositions for the three lowest states of dyes adsorbed on $(TiO_2)_{38}$ surfaces calculated by TD-CAM-B3LYP/6-31(d) level of theory

Dyes	State	Excitation energy (eV, nm)	Oscillator strength (*f*)	Assignment
TPA2	$S_0 \rightarrow S_1$	2.82 (440)	1.8222	0.21(H→L+13) – 0.21(H→L+21) + 0.21(H→L+17)
	$S_0 \rightarrow S_2$	3.15 (393)	0.0000	0.70(H→L)
	$S_0 \rightarrow S_3$	3.37 (368)	0.0017	0.55(H→L+1) + 0.25(H→L+4)
TPA5	$S_0 \rightarrow S_1$	2.54 (488)	1.5539	0.24(H→L+21) + 0.23(H→L+17) – 0.18(H→L+12)
	$S_0 \rightarrow S_2$	2.64 (449)	0.0000	0.70(H→L)
	$S_0 \rightarrow S_3$	2.89 (429)	0.0030	0.64(H→L+1) + 0.19(H→L+4)

3.4. Conclusions

We have analyzed the effect of different auxiliary donor groups between carbazole and diphenylamine moieties and the insertion of fluorene moiety on the ground-state structure, electronic structure, the absorption spectra and the adsorption of the dye on TiO_2 cluster of triphenylamine based dye. Three organic dye systems D-π-A, *D*-D-π-A and *2D*-D-π-A were compared. According to the computational study of these architectures, *2D*-D-π-A system showed the most red-shift of absorption wavelength. Moreover, different auxiliary donor in the *2D*-D-π-A system provided a different effect. Diphenylamine auxiliary donor provided a small external dihedral angle (EDA) than an internal dihedral angle (IDA) resulting in the red-shift of absorption range due to extended conjugation length. According to the calculations, adding an auxiliary donor can significantly increase HOMO energy while slightly effecting LUMO energy. This study gave insight into the electronic transition of isolated dyes and dye-$(TiO_2)_{38}$ clusters. The electronic transitions of the isolated dyes were assigned as intramolecular charge transfer (ICT) character. The electronic transitions of dye-$(TiO_2)_{38}$ clusters revealed the delocalized electron from the dye directing to TiO_2 surface. According to our computational study, we suggested that the

TPA5 dye, which showed the most red-shift of absorption spectra, has the best potential to be employed as an efficient dye sensitizer in the DSSCs applications.

CHAPTER 4

MODIFICATION ON D-A-π-A CONFIGURATION TOWARD HIGH- PERFORMANCE STARBRURT TRIPHENYLAMINE-BASED SENSITIZER FOR DYE SENSITIZED SOLAR CELLS: A THEORETICAL INVESTIGATION

4.1 Introduction

Dye-sensitized solar cells (DSSCs) –the exciting work reported by O'Regan and Grätzel [4] in 1991– have attracted much attention as one of new opportunities to be the most promising renewable energy devices due to their potential advantages of easy fabrication, low cost and relatively high conversion efficiency. [67-69] These advantages are vital factors to endow DSSCs as a powerful competition to conventional silicon-based photovoltaic devices. Therefore, over a thousand articles on DSSCs were published just by the end of year 2010. [36] The typical components of DSSCs usually contain three important parts consisting of dye molecules adsorbed on nanocrystalline layers of oxide semiconductor (such as TiO_2), redox electrolyte (such as iodide/triiodide couple), and a counter electrode such as platinum. [69] As the key component of DSSCs, the sensitizers have the function of absorbing light to excited electrons into excited states and consequently injecting electron into the conduction band of semiconductor. Thus, the sensitizers have been attracted considerable attention, and a large number of the modification of new sensitizers have been designed and investigated. [70]

The modification on dye sensitizers is an effective way to tune the structural and absorption properties which are important to gain a promising photo-to-current conversion efficiency (η). Therefore, metal free organicsensitizerswith high molar extinction coefficients ($>5.0\times10^4$ $M^{-1}cm^{-1}$) have become more promising for DSSCs than traditional ruthenium complex dyes although the power conversion efficiency (η) of metal free organic dyes-based DSSCs –more than 10% up to now [71]– are still lower than that of ruthenium-based –the highest record exceeding 11%. [72] As a result, the most important issue is to improve the broader absorbance spectrum for metal free organic sensitizers. Recently, donor-π-acceptor (D-π-A) configuration for metal free organic sensitizers has been widely developed because of their high molar absorption coefficient, relatively simple synthetic procedure, and easily molecular modification and tailoring as well as tunable optical properties. [40, 73-74]

In the past decade, various functional groups have been arranged and combined to construct D-π-A structural organic sensitizers for DSSCs including triphenylamine, indoline, carbazole, phenothiazine, coumarine and porphyrin based dyes. Among them, triphenylamine (TPA), thiophene derivative and cyanoacrylic acid moieties are the most commonly employed subunits for the electron donor, π-linker and electron acceptor or anchoring group, respectively. Recently, Zhang et al. [75] designed and synthesized triphenylamine-based D-π-A sensitizers with combination of thiophene unit and cyanoacrylic acid that exhibiting a high power conversion efficiency of 9.8%. On the basis of this model, the sensitizers were further developed by introducing additional electron withdrawing between the donor and π-linker to construct a new configuration defined as D-A-π-A.

A series of high-performance organic dyes with D-A-π-A architecture used in DSSCs have been reported by Zhu et al. [76] These D-A-π-A dyes containing additional electron withdrawing exhibited better conversion efficiencies relatively to traditional D-π-A dyes. On the basis of the D-A-π-A configuration, indoline moiety is so far used as an electron donor with high performance. It had been proved that indoline moiety is stronger electron-donating ability than triphenylamine. However, introducing starburst TPA structure as a donor in D-A-π-A dyes is one of the common strategies to suppress the improper charge recombination. This bulky-starburst shape can prevent the electrolyte from approaching the surface of TiO_2 and also suppressing the undesirable molecular aggregation subsequently, enhancing J_{sc} and V_{oc} and providing better device performance. In recent years, it has been found that the triphenylamine (TPA) derivatives are desirable for organic sensitizers in D-π-A system. Therefore, it is quite interesting to develop triphenylamine-based dye by structural modification on triphenylamine donor moiety to higher efficiency used in D-A-π-A configuration.

In this article, we reported the molecular design of eight organic dyes **TPA1 - TPA8** shown in Figure 4.1 that contain triphenylamine derivatives as the electron donors (denoted as D), bithiophene units as the π-conjugated linker (denoted as π) and a cyanoacrylic acid as the electron acceptor or anchoring group (denoted as A). The electron donors and π-conjugated linker were bridged by an electron deficient benzothiadiazole fragment (denoted as A) to construct a novel specific donor-acceptor-π bridge-acceptor (D-A-π-A) configuration. A series of novel triphenylamine derivatives with additional auxiliary donor as well as with different linker bridge types have been developed as promising candidates to tune up the donating ability expected to broaden the absorption ability.

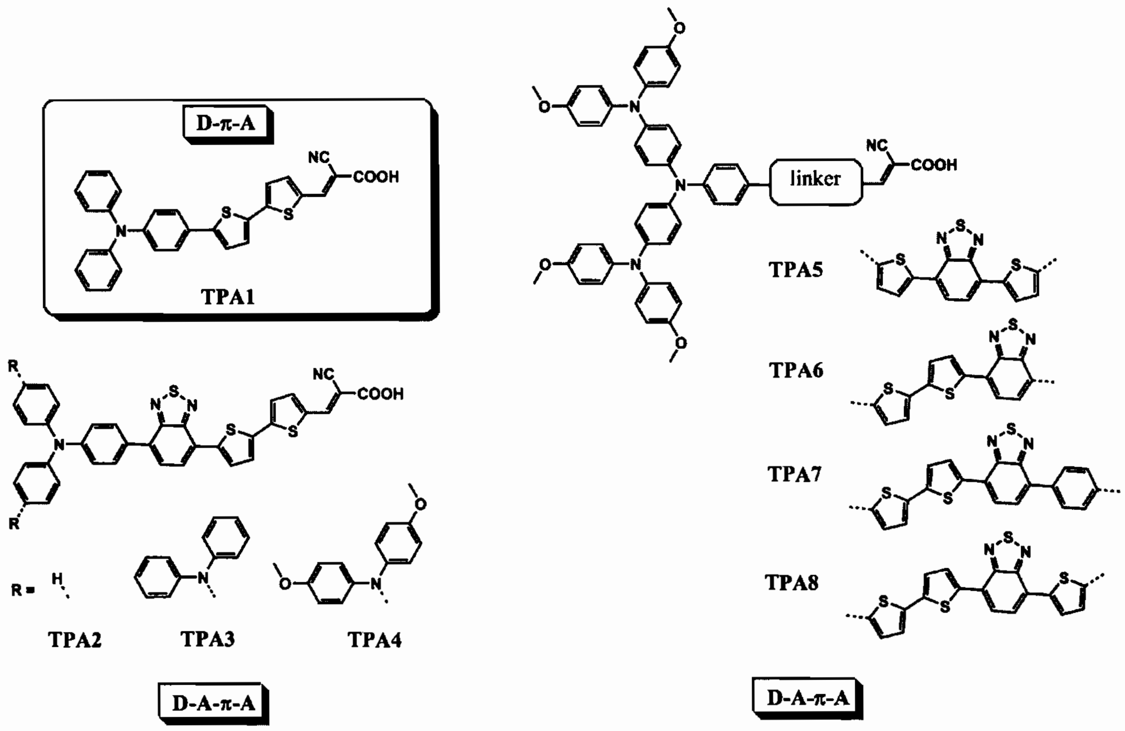

(a) (b)

Figure 4.1 Chemical structures of studied organic dyes: simple D-π-A and D-A-π-A dye architectures of (a) the triphenylamine-based dyes with different electron donating ability and (b) the dyes with different BTD unit positions

4.2 Computational details

We used the GAUSSIAN09 software suite for all of our calculations. The new modified triphenylamine-based dyes namely **TPA2-TPA8** represented to D-A-π-A dye architecture were computed in comparison with the **TPA1** represented to the simple D-π-A dye system. The ground-state geometries were fully optimized using the Density Functional Theory (DFT) method combined with Becke's three-parameter hybrid functional and Lee-Yang-Parr's gradient-corrected correlation functional (B3LYP) at 6-31G(d,p) level. All calculations were performed without symmetry constraints and only in gas phase. These optimized structures were calculated for the first excitation energy (E_g), maximal absorption wavelength (λ_{max}) and oscillator strengths (f) for the 10 states by using Time-Dependent Density Functional Theory (TD-DFT) with CAM-B3LYP at 6-31G(d,p) level in dichloromethane. Subsequently, the TD-DFT results were entered in to the SWizard program for the simulation of absorption spectra of these dyes.

Furthermore, electronic transition and its character related to the absorption wavelength are discussed in relation to the results. To gain insight into the electron injection capability of dyes, the adsorption of dyes on the $(TiO_2)_{38}$ cluster was performed with DFT calculations using DMol^3 program in Materials Studio version 5.5. The structure of $(TiO_2)_{38}$ was comprised of 38 TiO_2 units which modeled a TiO_2 nanoparticle, as discussed in a previous report. The $(TiO_2)_{38}$ configurations were fully optimized using the generalized gradient-corrected approximation (GGA) method. The Perdew–Burke–Ernzerhof (PBE) functional was used to account for exchange–correlation effects with the DNP basis set. The core electron was treated with DFT-semicore Pseudopotentials (DSPPs). After optimization, the adsorption energies (E_{ads}) of dyes on the $(TiO_2)_{38}$ cluster were obtained using the following equation:

$$E_{ads} = E_{dye} + E_{TiO_2} - E_{dye+TiO_2} \qquad (4.1)$$

where E_{dye} is the total energy of isolated dye, E_{TiO_2} is the total energy of $(TiO_2)_{38}$ cluster, and $E_{dye+TiO_2}$ is the total energy of dye-$(TiO_2)_{38}$ complexes. After applying the above expression equation, the results of the positive value of E_{ads} indicated a stable adsorption.

4.3 Results and discussion

4.3.1 Effect of incorporating benzothiadiazole (BTD) moiety

In the first part, we compared **TPA1** dye represented to a simple D-π-A system and **TPA2** dye which the BTD unit was introduced and considered as an additional electron accepting unit represented to the D–A–π–A configuration. The effect of incorporating BTD moiety on frontier molecular orbitals was analyzed. As shown in Figure 4.2, **TPA2** dye showed the calculated HOMO level of -4.88 eV slightly shifting up 0.26 eV compared to HOMO level of **TPA1** dye. Furthermore, it is worth to note that the BTD unit greatly influences to stabilize LUMO levels of -3.81 eV by dramatically shifting down 1.08 eV compared to LUMO level of **TPA1** dye. These indicate that the HOMO and LUMO levels are quite sensitive with BTD unit. According to these observations, the higher HOMO level of **TPA2** dye possibly leads to sufficient driving force for dye regeneration, whereas the lower LUMO level might be useful for electron injection. Moreover, the increased HOMO and decreased LUMO in **TPA2** dye incorporating of BDT resulting in the decreased HOMO–LUMO gap which may facilitate to red-shift and broad of the charge transfer (CT) band of absorption spectra.

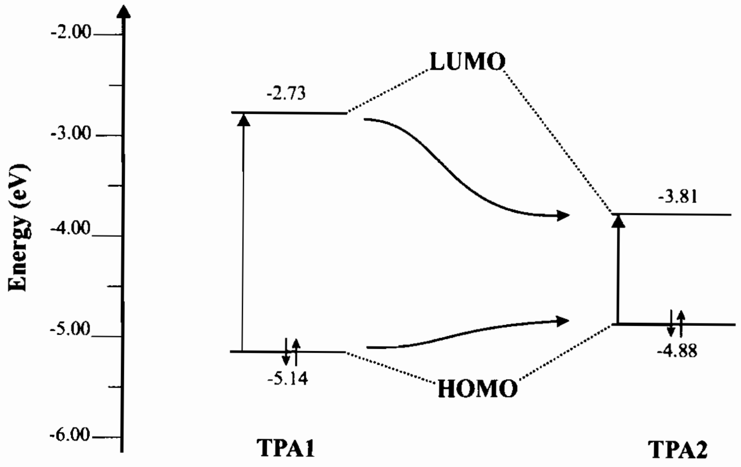

Figure 4.2 Calculated HOMO-LUMO levels of TPA1 and TPA2 dyes using B3LYP/6-31G(d,p) calculation

The effect of incorporating BTD moiety on UV-vis absorption spectra was subsequently analyzed. The excitation energies of **TPA1** and **TPA2** dyes were calculated by using time-dependent density functional theory (TDDFT) at CAM-B3LYP/6-31G(d,p) calculation. The calculated excitation energies and the corresponding transition assignments were listed in Table 4.1. As shown, our simulated results show that the CAM-B3LYP functionalgives the excitation energies of**TPA1** dye at 464 nm, excellently agree with experimental measurement of 473 nm from Justin Thomas and coworker.

The simulated adsorption spectra and the illustration of main electronic transition of **TPA1** and **TPA2** dyes were shown in Figure 4.3. The UV-Vis absorption spectra above 400 nm correspond to ICT transition. It has been observed that the presences of a BTD unit in **TPA2** dye significantly red-shifts its CT absorption band by 40 nm relative to **TPA1** dye. Moreover, the adding of BTD unit results in red-shift in 50 nm for absorption threshold indicating greatly enhances the sensitizer light-harvesting in the long wavelength region. The CT band of **TPA1** dye is a combination of (H→L), (H-1→L) and (H→L+1), similarly, the combination in **TPA2** dye are also (H→L), (H-1→L) and (H→L+1) as appear in **TPA1** except the additional transition of HOMO-2 to LUMO+1. Considering on schematic illustrations of the charge transfer transition as shown in Figure 4.3, the main transitions for two dyes are from HOMO to LUMO orbitals which are corresponding to electron transfer from donor to anchoring group. It has been observed that adding of BTD moiety, the transition from HOMO-2 to LUMO+1 which is corresponding to electron transfer from donor to BTD additional acceptor has been performed. These indicate that BTD moiety can facilitate the electron transfer from donor to BTD additional acceptor, and then go through anchoring group in the D-A-π-A configuration, Figure 4.3 shows red-shifted CT band and stronger CT character in **TPA2**.

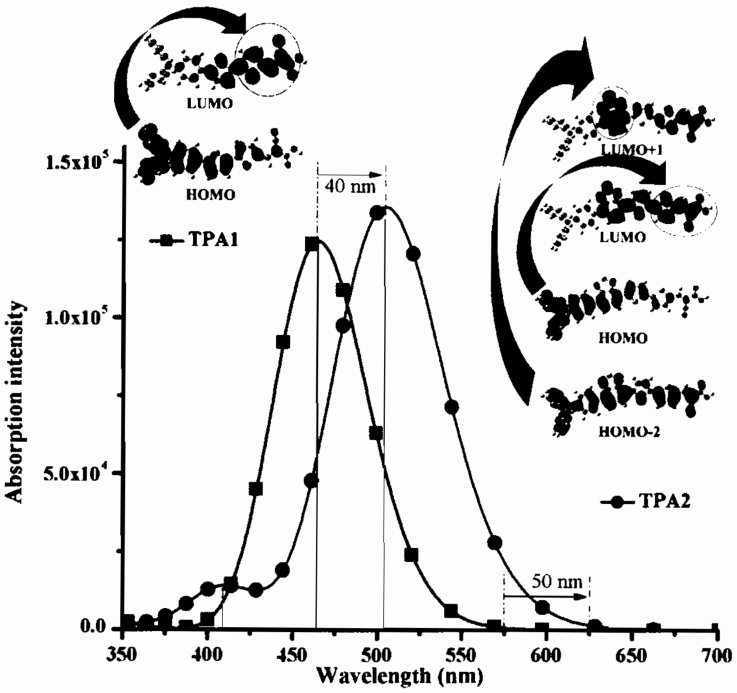

Figure 4.3 Simulated absorption spectra of TPA1 and TPA2 dyes containing with additional electron withdrawing group of benzothiadiazole (BTD) obtained by TD-CAM-B3LYP/6-31G(d,p) calculation in CH_2Cl_2

Table 4.1 Calculated excitation energies (*E*), oscillator strengths (*f*), and compositions in terms of molecular orbital contributions of TPA1-TPA8 dyes obtained under TD-CAM-B3LYP/6-31G(d,p) level in CH_2Cl_2

Dyes	state	*E* (eV, nm)	*f*	Main compositions
TPA1	$S_0 \rightarrow S_1$	2.67 (464.3) (473)[a]	1.7226	0.57 (H→L) -0.37 (H-1→L) -0.15 (H→L+1)
	$S_0 \rightarrow S_2$	3.62 (342.4)	0.0387	0.51 (H-1→L) -0.32 (H→L+1) +0.26 (H→L) -0.18 (H-2→L) -0.12 (H-4→L) +0.10 (H→L+3)
TPA2	$S_0 \rightarrow S_1$	2.46 (504.1)	1.8731	0.53 (H→L) +0.38 (H-1→L) +0.19 (H→L+1) -0.15 (H-2→L+1)
	$S_0 \rightarrow S_2$	3.03 (408.9)	0.1909	0.48 (H→L+1) -0.37 (H-1→L) +0.22 (H-2→L+1) -0.22 (H-3→L) +0.10 (H→L)
TPA3	$S_0 \rightarrow S_1$	2.40 (515.8)	1.8823	0.47 (H-2→L) -0.43 (H→L) -0.20 (H→L+1)+0.11 (H-6→L+1) +0.11 (H-3→L+1)
	$S_0 \rightarrow S_2$	2.94 (422.2)	0.2638	0.36 (H→L+1) +0.35 (H-2→L) +0.29 (H-3→L) +0.25 (H→L) -0.24 (H-2→L+1) -0.13 (H-6→L)
TPA4	$S_0 \rightarrow S_1$	2.36 (525.9)	1.7988	0.45 (H-2→L) +0.42 (H→L) +0.21 (H→L+1) -0.16 (H-3→L) +0.13 (H-2→L+1) +0.12 (H-6 →L+1)
	$S_0 \rightarrow S_2$	2.87 (432.0)	0.3428	0.35 (H-3→L) -0.33 (H-2→L) +0.31 (H→L+1) +0.31 (H→L) +0.18 (H-2→L+1) +0.13 (H-6→L)

Table 4.1 Calculated excitation energies (*E*), oscillator strengths (*f*), and compositions in terms of molecular orbital contributions of TPA1-TPA8 dyes obtained under TD-CAM-B3LYP/6-31G(d,p) level in CH_2Cl_2 (Continued)

TPA5	$S_0 \rightarrow S_1$	2.22 (558.3)	1.6965	0.47 (H-2→L) +0.44 (H→L) -0.21 (H-3→L)
	$S_0 \rightarrow S_2$	2.88 (430.6)	0.1424	0.50 (H→L) -0.33 (H-2→L) +0.32 (H-3→L) +0.12 (H-6→L)
TPA6	$S_0 \rightarrow S_1$	2.14 (580.2)	1.7109	0.48 (H-2→L) +0.42 (H→L) -0.24 (H-3→L) +0.11 (H→L+2)
	$S_0 \rightarrow S_2$	2.75 (451.4)	0.0506	0.54 (H→L) -0.32 (H-2→L) +0.27 (H-3→L) -0.14 (H-6→L)
TPA7	$S_0 \rightarrow S_1$	2.43 (510.5)	1.9413	0.48 (H-2→L) +0.35 (H→L) -0.24 (H-3→L) -0.16 (H-2→L+1) +0.12 (H→L+2) -0.11 (H→L+1)
	$S_0 \rightarrow S_2$	3.08 (402.0)	0.0143	0.50 (H→L) +0.27 (H-2→L) +0.26 (H-3→L) +0.20 (H→L+2) +0.17 (H-4→L)
TPA8	$S_0 \rightarrow S_1$	2.18 (568.1)	2.0692	0.51 (H-2→L) +0.34 (H→L) -0.25 (H-3→L) -0.11 (H-2→L+1)
	$S_0 \rightarrow S_2$	2.83 (438.3)	0.0261	0.55 (H→L) +0.28 (H-3→L) -0.24 (H-2→L) -0.18 (H-4→L) +0.13 (H→L+2)

[a] The absorption spectra were recorded in THF taken from ref [77]

In addition, a new absorption band is observed at around 420 nm for **TPA2** dye incorporating with BTD unit while it disappeared in **TPA1** dye. The details of the corresponding absorption data are listed in Table 4.1. The main transition is the excitation from HOMO to LUMO+1 which is corresponding to electron transfer from donor to additional acceptor BTD unit. It is clearly seen that the additional band in **TPA2** dye resulted from the dramatic decreasing of secondary excitation energy (from

3.62 eV for **TPA1** dye to only 3.03 eV for **TPA2** dye). In any way, a new absorption band improves the light-harvesting of **TPA2** dye which may benefit to higher efficiency in organic sensitizers.

In brief, it is interesting to note that the advantages of the BTD unit from above analysis confirms the designing of organic sensitizer in the novel specific D-A-π-A configuration is outstanding than the normal D-π-A system.

To further identify the effect of incorporating BTD moiety on the adsorption property and the mechanism of electron injection, the adsorption modeling of two configuration dyes –one is **TPA1** dye without BTD unit and another is **TPA2** dye incorporating with BTD unit– after binding to $(TiO_2)_{38}$ cluster were investigated under TD-CPCM-CAM-B3LYP/6-31G(d) that can accurately predict the electron injection of the dyes in the current study. The adsorption modeling of two configuration dyes was simulated by PBE/DNP in Dmol^3 program. The optimized structures of **TPA1-** and **TPA2-TiO$_2$** complex dyes are shown in Figure 4.4, and the adsorption energy (E_{ads}) are listed in Table 4.2. The adsorption energy (E_{ads}) of **TPA1-** and **TPA2-TiO$_2$** complex dyes was calculated to be 22.57 and 22.20 kcal/mol, respectively. It can be obviously seen that two configuration dyes could firmly absorb on the TiO_2 anatase (101) surface. Moreover, the calculated dipole moments of these complex dyes are listed in Table 4.2 and also shown in Figure 4.4. As shown, the calculated dipole moments of **TPA2-TiO$_2$** complex dye (40.21D) incorporating with BTD unit increases relative to **TPA1-TiO$_2$** complex dye (34.45D) without BTD unit. This indicates that adding of BTD unit can enhance the charge transfer property in term of dipole moments corresponding to the red-shifted of absorption property and electronic transitions of bare dyes shown in Figure 4.3.

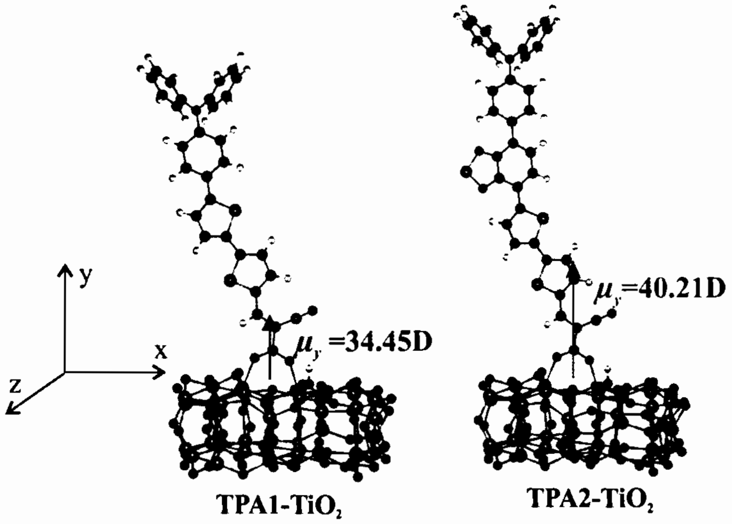

Figure 4.4 Optimized structures of TPA1- and TPA2-TiO$_2$ adsorption complexes calculated by PBE/DNP in DMoL^3

Table 4.2 The calculated adsorption energy (E_{ads}) and molecular dipole moment (Debye) in perpendical direction to the TiO$_2$ surface of TPA1-, TPA2-, TPA4- and TPA6-TiO$_2$ adsorption complexes by Dmol^3 calculation

Complexes	Ti-O (TiO'-O') distance (Å)	E_{ads} (Kcal/mol)	Dipole moment (D)			
			μ*	μ_x	μ_y	μ_z
TPA1- TiO$_2$	2.13(2.15)	22.57	35.52	3.80	34.45	-7.79
TPA2- TiO$_2$	2.12 (2.13)	22.20	42.18	10.81	40.21	-6.51
TPA4- TiO$_2$	2.12 (2.14)	26.87	73.55	17.79	72.43	-9.97
TPA6- TiO$_2$	2.13 (2.16)	25.13	75.69	9.67	74.93	-8.37

* μ = the molecular dipole moment

μ_x, μ_y and μ_z= dipole moment vectors in the x, y and z directions, respectively

μ_y is dipole moment in perpendicular direction to the TiO$_2$ surface

It is well-known that the mechanism of electron injection from the dye to the semiconductor can be theoretically elucidated by the study of the electronic structure of the dye adsorbed on the semiconductor, which can be classified into two types. The first mechanism, indirect injection, involves photoexcitation to a dye excited state, and then an electron is transferred to the semiconductor. The second is a direct mechanism, a one-step electron injection from the ground state of the dye to the conduction band of the semiconductor by photoexcitation.

The electronic transitions for **TPA1**- and **TPA2-TiO$_2$** complex dyes are listed in Table 4.3, and their electronic structures were shown in Figure 4.5. As shown, the strongest electronic transition with largest oscillator strength for these two dyes was assigned to $S_0 \rightarrow S_1$ corresponding to the linear combination of 0.35 (H→L+24) +0.20 (H-1→L+24) for **TPA1-TiO$_2$** and the linear combination of 0.38 (H→L+12) -0.24 (H→L+10) for **TPA2-TiO$_2$** complex dyes, respectively.

The HOMO-1 is delocalized over the dye, while the LUMO+12 and LUMO+21 are distributed at the dye-$(TiO_2)_{38}$ interface, indicating the strong coupling between the excited state of dye and the conduction band states of TiO_2. This result indicates that the direct injection mechanism is identified in the present dyes. These transition characters and MOs of the dye-$(TiO_2)_{38}$ model system show that the sensitization mechanism in the prototypes is an interfacial direct charge transfer process corresponding to electron injection from the excited dyes to the conduction band of the TiO_2 surface. This theoretical evidence altogether supports the direct injection mechanism.

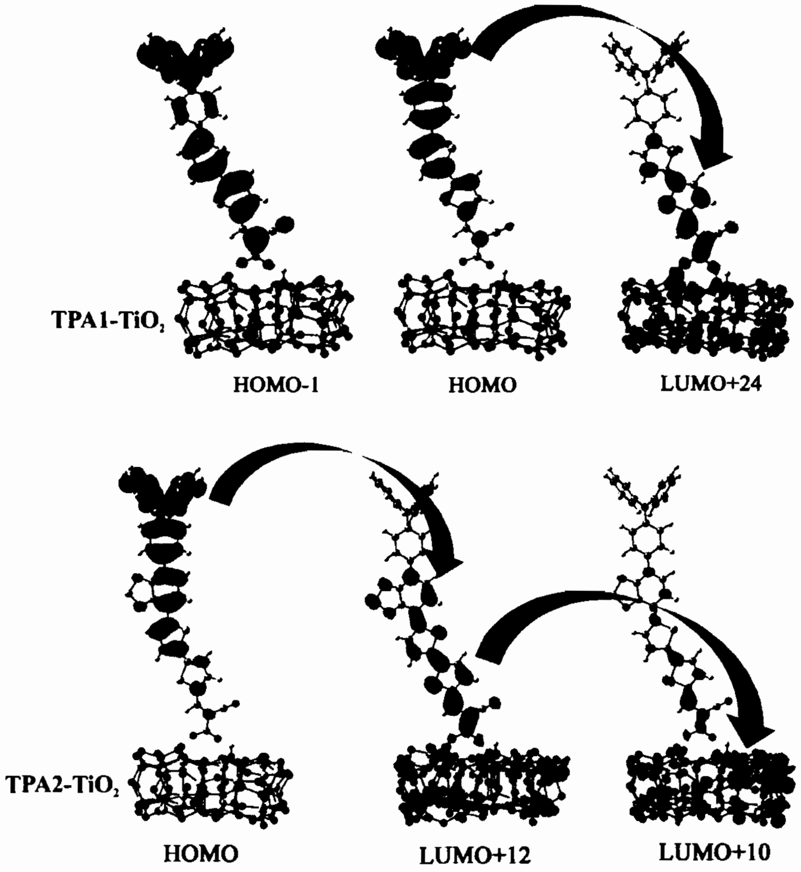
TPA1-TiO$_2$
HOMO-1
HOMO
LUMO+24
TPA2-TiO$_2$
HOMO
LUMO+12
LUMO+10

Figure 4.5 Electronic transitions of TPA1- and TPA2-TiO$_2$ adsorption complexes calculated by TD-CAM-B3LYP/6-31G(d,p) in CH$_2$Cl$_2$

Table 4.3 The calculated excitation energy (*E*), oscillator strengths (*f*) and corresponding transition natures of TPA1- and TPA2-TiO$_2$ adsorption complexes obtained under TD-CAM-B3LYP/6-31G(d,p) level in CH$_2$Cl$_2$

Dyes	state	*E* (eV, nm)	*f*	Main compositions
TPA1-TiO$_2$	$S_0 \rightarrow S_1$	2.60 (476)	2.1334	0.35 (H→L+24) +0.20 (H-1→L+24)
TPA2-TiO$_2$	$S_0 \rightarrow S_1$	2.24 (553)	2.1583	0.38 (H→L+12) -0.24 (H→L+10)

As shown in Figure 4.5, the HOMO and HOMO-1 plots for **TPA1-TiO$_2$** complex dyes showed the electrons delocalized predominantly on the whole dye molecule, while the LUMO+24 plots showed electrons mainly delocalized over the anchoring group and $(TiO_2)_{38}$ cluster. This represented to the mechanism of electron transfer from donor directly to TiO$_2$ via anchoring group. However, it is interesting to note that there is much difference between two dyes when pay attention to the unoccupied MOs. For the **TPA2-TiO$_2$** complex dye, the LUMO+12 plot showed electrons mainly delocalized over the anchoring group and $(TiO_2)_{38}$ cluster as well as the LUMO+10 showed most of electrons moved forward to the $(TiO_2)_{38}$ cluster. These two transition characters, (H→L+12) and (H→L+10) together with MOs of the dye-$(TiO_2)_{38}$ model system showed that the sensitization mechanism in the prototypes is also an interfacial direct charge transfer process corresponding to electron injection from the excited dyes to the conduction band of the TiO$_2$ surface, which indicate that **TPA2-TiO$_2$** performed more ability in electron injection process with stronger ICT character compared to **TPA1-TiO$_2$** complex. This revealed that the incorporating of additional electron acceptor BTD moiety is beneficial to facilitate the electron transfer as well as the electron injection mechanism into the $(TiO_2)_{38}$ surface.

4.3.2 Effect of tuning the electron donating ability of starburst triphenylamine (TPA) donor

The current sensitizers are triphenylamine (TPA) donor which is widely used in DSSCs due to its good electron donating ability as well as its special propeller starburst molecular structure. Therefore, many research groups have great interest of using triphenylamine as electron donor in the field of solar cells. Recently, our group reported the introduction of diphenylamine moiety at para position of TPA acting as auxiliary donor to improve the donating ability of TPA donor which significantly improved the absorption ability. For this reason, we aim to design more efficient dye sensitizers via adding different auxiliary donor into TPA donor for a novel specific D–A–π–A configuration. **TPA3** dye containing the diphenylamine moiety as auxiliary donor and **TPA4** dye containing a stronger donating group of bis(4-methoxyphenyl) amine as auxiliary donor introduced at para position of TPA donor were designed to compare with **TPA2**-based dye containing bared TPA donor.

The simulated UV-vis absorption spectra for **TPA2 – TPA4** dyes are plotted in Figure 4.6 and the data are summarized in Table 4.1. According to Figure 4.6, there are two strong absorption peaks in the UV-visible spectrum. The major absorption band at higher absorption wavelength is around 500-525 nm and is ascribed to the intramolecular charge transfer (ICT) from donor to anchoring part for all dyes, whereas the additional absorption band is around 400 nm corresponding to electron transfer from donor to additional acceptor BTD unit (see in Figure S2-S4 in supporting information). By tuning the electron donor group, the λ_{max} value of the charge transfer band for the dyes was systematically red-shifted in the order of 504 < 515 < 525 nm for **TPA2** < **TPA3** < **TPA4**, respectively. This phenomenon can be as ascribed mainly due to the electron donating effect of insertion of the diphenylamine and bis (4-methoxyphenyl) amine moieties of **TPA3** and **TPA4** dyes which benefit of some steric congestion and elongate the length of π-conjugation. Thus, when compare to a simple TPA donor (**TPA2** dye), a significant red shift of the absorption spectra was observed in **TPA3** and **TPA4** dyes. We found that the latter with strong donating ability of bis(4-methoxyphenyl)amine exhibits a bathochromic shift (10 nm) of the absorption wavelength compared to the former. Therefore, we choose our largest red shifted dye (**TPA4**) as initial conformation to further finding out the position of additional acceptor in dye molecules.

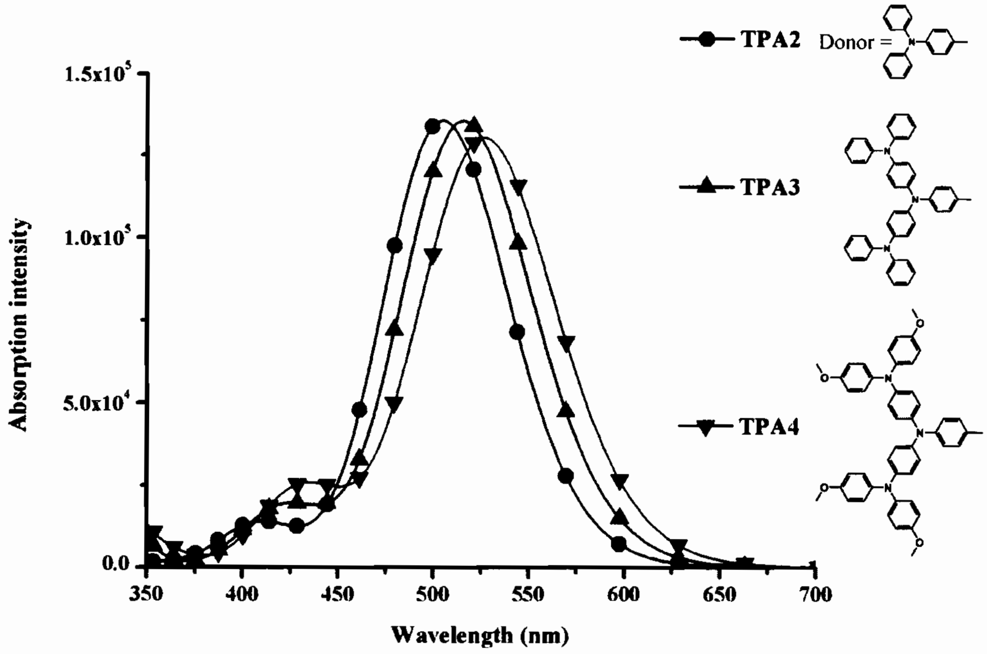

Figure 4.6 Simulated UV-vis absorption spectra of TPA2-TPA4 dyes calculated by TD-CAM-B3LYP/6-31G(d,p) calculation in CH_2Cl_2

4.3.3 Effect of different positions of BTD unit in π-conjugated bridge

Our continuous interest is to study a series of triphenylamine derivatives with an introduction of benzothiadiazole (BTD) unit by varying different positions of BTD into the molecular framework. The positions of BTD as an additional electron withdrawing group are between donor and π conjugated in **TPA4** dye denoted as Aππ linker , between π conjugated linker in **TPA5** dye denoted as πAπ linker, and between π-conjugated and anchoring group for **TPA6** dye denoted as ππA linker. Their absorption spectra were shown in Figure 4.7, as well as their electronic transitions were summarized in Table 4.1. As shown, we found that the systematically red-shifted of the major absorption band for these dyes were obviously increased in order from 526 < 558 < 580 nm for Aππ < πAπ < ππA linker, respectively. A significant red shift of the absorption spectra can be attributed to elongate the length of π-conjugation with planarity of dyes incorporating with BTD unit. As results, the red-shifted broadening of the absorption spectrum to near IR region of **TPA6** is desirable for harvesting the solar spectrum and leads to a higher photocurrent.

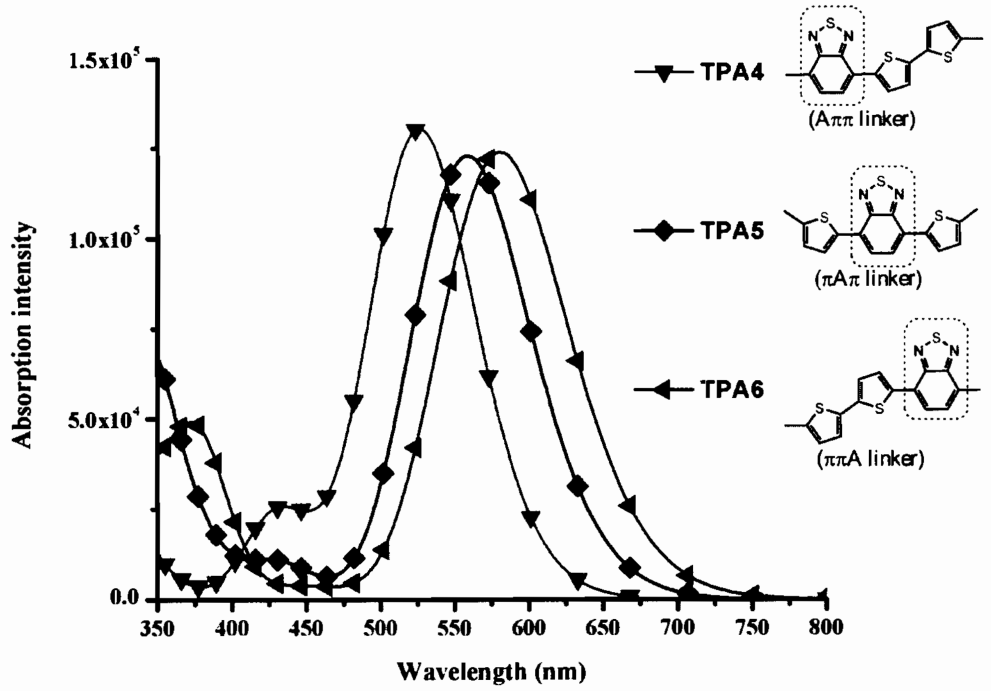

Figure 4.7 Simulated UV-vis absorption spectra of TPA4-TPA6 dyes calculated by TD-CAM-B3LYP/6-31G(d,p) calculation in CH_2Cl_2

As shown in Table 4.1, the main electronic transitions are the combination of 0.45 (H-2→L) +0.42 (H→L) for **TPA4** dye, the combination of 0.47 (H-2→L) +0.44 (H→L) for **TPA5** dye, and combination of 0.48 (H-2→L) +0.42 (H→L) for **TPA6** dye, respectively. The HOMO plot showed electron density mainly located on the triphenylamine and its auxiliary donor, while the HOMO-2 showed a slight higher electron density over π-linker. Meanwhile, electron density at the LUMO is mainly delocalized across the Aππ, πAπ or ππA linker of thiophene (π) and benzothiadiazole (A) units to anchoring group. These electronic transitions exhibited the electron-separated in D-A-π-A architecture which suggests that the HOMO→LUMO electronic transitions corresponding to intramolecular charge transfer (ICT) character, while HOMO-2→LUMO electronic transitions corresponding to mixed transitions between ICT and π-π* transitions.

As known from our results, the best BTD position is at the end of π-conjugated bridge (ππA linker) in **TPA6** dye with the largest red-shifted of the spectrum to absorb most of the sunlight. To further explore on how the different behaviors of BTD positions in linker affect to the anchoring group were questioned. **TPA4-TiO_2** and **TPA6-TiO_2** complexes dyes represented to AπA and πAA linker, respectively, were modeled and performed in $DMoL^3$ program. The adsorption property of **TPA4-TiO_2** and **TPA6-TiO_2** complexes dyes was calculated. The optimized structures of **TPA4-TiO_2** and **TPA6-TiO_2** adsorption complexes are shown in Figure 4.8, and the calculated adsorption energy (E_{ads}) are listed in Table 4.2. As shown, the calculated adsorption energy (E_{ads}) for **TPA4-TiO_2** and **TPA6-TiO_2** are 26.87 and 25.13 kcal/mol, respectively. These results indicated that πAA is slightly weaker in adsorption energy than AπA dye. The dipole moments of these complexes were also investigated, it is worth to note that the absorption spectra for **TPA6** (580 nm) is significantly red-shifted from **TPA4** dye (525 nm), therefore, we expected to see stronger dipole moment in **TPA6** as well. Unfortunately, the calculated dipole moment after binding to TiO_2 surface for **TPA6** (74.93D) is only slightly decreased compared to **TPA4** (72.43D), see **Table 4.2**. As can be seen from those values, this indicates that the strength of charge transfer property of **TPA6-TiO_2** complex dyes could be decreased. It is probably due to the designing of additional BTD unit was adjacently connected to the anchoring group (πAA) which is very close to TiO_2 surface, consequently, the injected electron on the surface might be pulled back by electron-deficient character of BTD unit. Moreover, Bauerle et al. [78] studied on experiments of transient photovoltage/photocurrent measurements, time correlated single photon counting technique, nanosecond laser photolysis, ultrafast transient absorption and electrochemical impedance spectroscopy. They reported that additional BTD unit which is placed close to the anchoring group (πAA) showed unusually fast recombination with injected electrons in semiconductor surface.

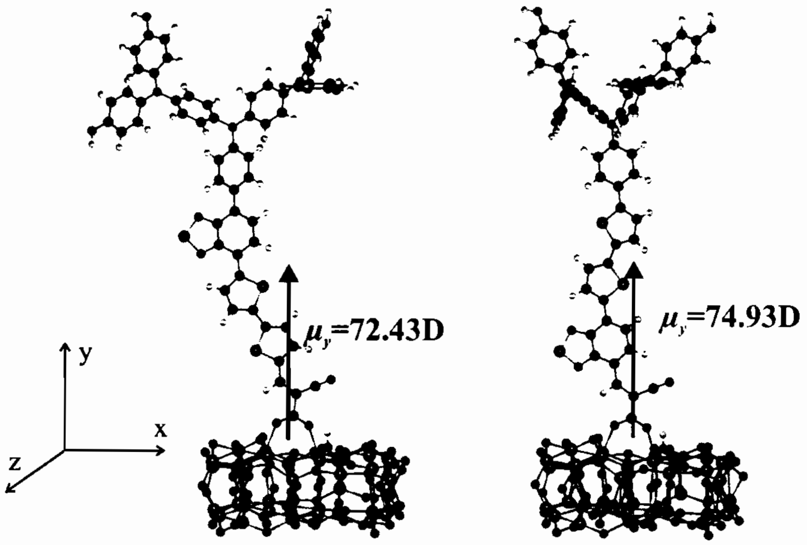

TPA4-TiO$_2$ TPA6-TiO$_2$

Figure 4.8 Optimized structures of TPA4- and TPA6-TiO$_2$ adsorption complexes calculated by PBE/DNP in DMoL^3

Therefore, we attempted to improve our best dye (**TPA6**) by placing away additional BTD unit from the anchoring group with a rigid linker to block the electron recombination between TiO$_2$ and oxidized dye. The BTD unit and anchoring group of cyanoacrylic are separated by phenyl for **TPA7** dye (denoted as A-π(P)-A) and thiophene for **TPA8** dyes (denoted as A-π(T)-A), respectively. Their absorption spectra were shown in Figure 4.9.

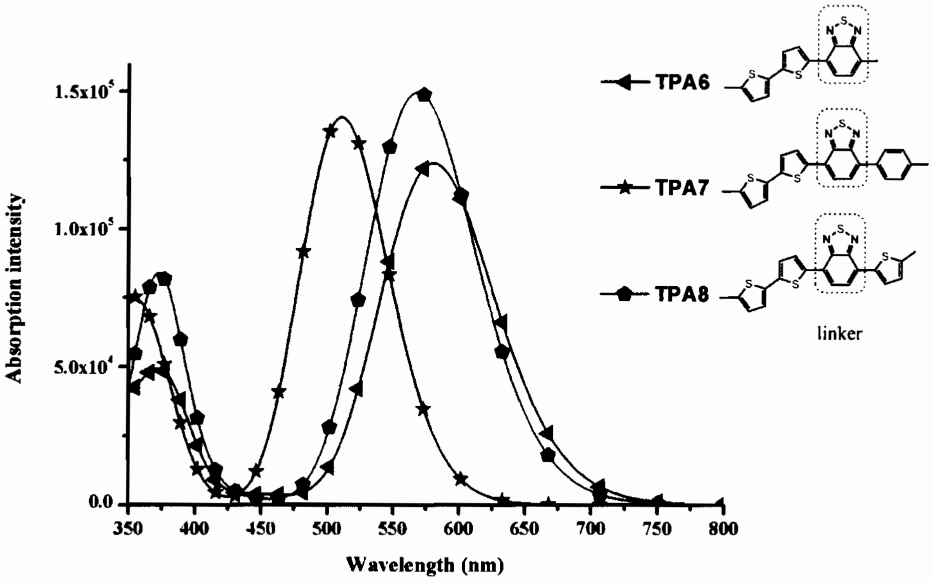

Figure 4.9 Simulated UV-vis absorption spectra of TPA6-TPA8 dyes calculated by TD-CAM-B3LYP/6-31G(d,p) calculation in CH_2Cl_2

As shown, the introduction of different rigid linker in between additional acceptor and anchoring group affected to different of absorption wavelength as in following order of 511 and 568 nm for the **TPA7** and **TPA8** dye with phenyl and thiophene moieties as π-bridge, respectively. Compared to **TPA6** dye, the absorption spectra of **TPA7** dye which adding of phenyl ring as rigid linker showed very large blue shift. When replacing of phenyl ring with thiophene moiety as rigid linker in **TPA8** dye, the absorption spectra of **TPA8** dye was significantly red-shifted of 58 nm. This is due to the more planar conformation of thiophene as π-bridge (0.27 degree) than phenyl (32.67 degree) as shown in Figure 4.10. However, these dyes with introduction rigid linker (phenyl and thiophene moieties) show a slightly blue-shifted from the dye without rigid linker corresponding to the HOMOs and LUMOs level as shown in Figure 4.11. The main electronic transitions are listed in Table 4.1 and are also corresponding to HOMO → LUMO and HOMO-2 → LUMO as assigned as ICT and π-π* transition.

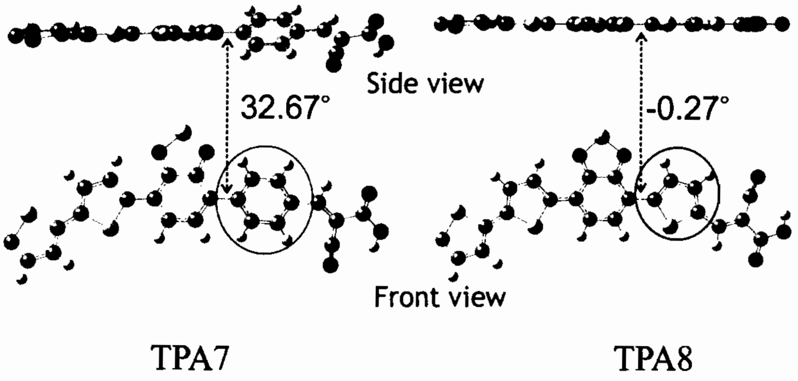
Side view
32.67°
-0.27°
Front view
TPA7
TPA8

Figure 4.10 Comparison of optimized ground-state structures of TPA7 and TPA8 dyes

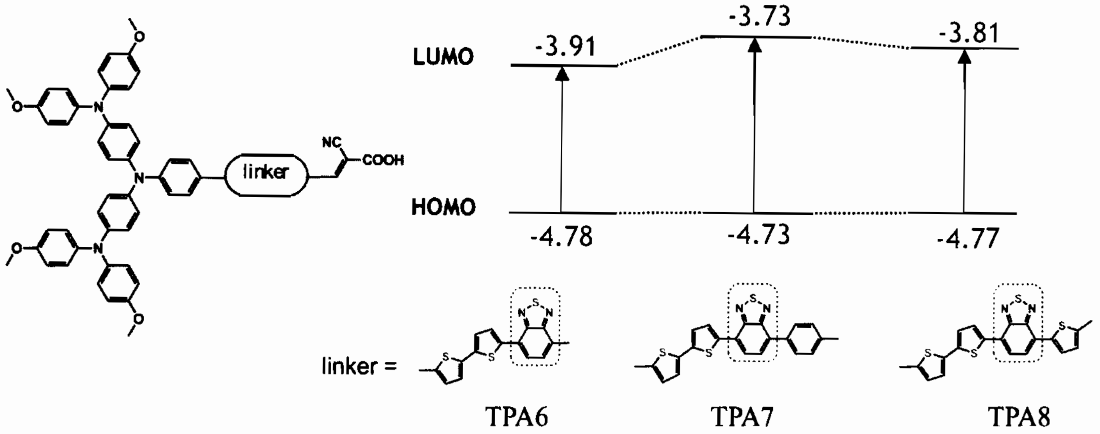
LUMO
HOMO
-3.91
-3.73
-3.81
-4.78
-4.73
-4.77
linker
NC
COOH
linker =
TPA6
TPA7
TPA8

Figure 4.11 Comparison of calculated energy level of HOMO and LUMO for TPA7 and TPA8 dyes compared with TPA6 dye

4.4 Conclusions

In conclusion, the triphenylamine-based dyes with D-A-π-A configuration featuring with benzothiadiazole (BTD) unit as additional electron acceptor group were designed and theoretically investigated. Interestingly, the incorporating BTD moiety significantly decreased LUMO level and energy gap, while increased HOMO level and dipole moment leading to the red shift of absorption spectra which could be helpful to facilitate the electron transfer as well as to greatly enhance the light harvesting ability. Consequently, the broader absorption region was achieved by the introducing of more auxiliary donor on starburst triphenylamine moiety in the D-A-π-A structure. Furthermore, the difference in the position of BTD moiety in

π-conjugation spacer can also broaden the absorption spectrum to near IR region. Although the absorption band of **TPA6** dye with the designing of additional BTD unit adjacently connected to the anchoring group was found to be red-shifted compared to others, the calculated dipole moment was not dramatically improved owing to its fast recombination process. However, the insertion of the planar rigid linker in between BTD moiety and anchoring group was effectively maintained the appearance of best character of the light absorption property as well as can be expected to block the unfavorable charge recombination due to the further BTD position away from anchoring group. According to our computational study, the successfully theoretical study should be able to use as first attempt to design and screen of new efficient organic dyes for the experimental synthesis, to save cost and time.

CHAPTER 5

TRIPLE BOND-MODIFIED ANTHRACENE SENSITIZERS FOR DYE-SENSITIZED SOLAR CELLS: A COMPUTATIONAL STUDY

5.1 Introduction

DSSCs have received extensive attention since the first report of high-efficiency dye-sensitized solar cells (DSSCs) by O'Regan and Grätzel in 1991, [4] DSSCs manufacture requires relatively low-cost, facile processes compared to traditional silicon-based solar cells. Thus, the conversion of sunlight to electricity using DSSCs is a promising source of affordable renewable energy. During recent decades, there have been numerous reports of DSSCs-based investigations, with over 1000 articles published by the end of the 20th century, [36] and this trend continues to grow. Metal-free organic-dye-based sensitizers show promise for DSSCs applications, and there is active experimental and theoretical research into the development of organic-dye-based DSSCs cells with high solar-to-electricity conversion efficiency.

The majority of research into metal-free organic dyes is concerned with the design of novel dye sensitizers, which are a key component in the DSSCs working principle to harvest solar irradiation for converting light to electricity. The metal-free dye based on a donor-π-conjugated-acceptor (D-π-A) architecture can provide high-efficient photovoltaic performance, the highest record exceeding 11%. [72] A variety of electron donating groups (D) have been reported, including triarylamine, coumarin, carbazole, fluorine, and phenothiazine. Three main electron acceptor groups (A) are used, namely, cyanoacrylic acid, carboxylic acid, and rhodanine-3-acetic acid.

The presence of a π-conjugated linker in an organic sensitizer broadens the visible region absorption band by extending the length of the π-conjugation system. Structural modification of the π-conjugated linker can greatly improve DSSCs performance. Researchers have varied π-conjugated bridges by using a series of acenes comprising polycyclic aromatic hydrocarbons with fused benzene rings in a rectilinear arrangement. In particular, an anthracene moiety, which consists of three fused benzene rings, shows promise as an acene-modified linker. In recent years, Fan et al. [77] reported a series of dye sensitizers with acene-modified linkers, from benzene to pentacene. Fan reported that the presence of an anthracene unit provided several advantages, including good light-harvesting efficiency (*LHE*) and improved electron injection properties. Thus, anthracene shows promising as a linker component to provide a highly efficient dye sensitizer for DSSCs applications. Additionally, the anthracene group outperforms other acene-modified linkers in the benzene to pentacene series, with an overall efficiency of approximately 5.44%.

Generally, there are two ways to derivatize anthracene as a π-conjugated linker; substituent groups can be introduced at either the 9,10- or the 2,6-positions on the anthracene unit to provide alternative conjugation pathways. However, substitution at the 2,6-positions on anthracene is less thermodynamically favorable compared to 9,10-disubstitution, and there are few reports on the incorporation of substituents at the 2,6-positions. Nonetheless, substitution at the 2,6-positions offers lower steric congestion than that seen for 9,10-disubstitution, and generally maintains better planarity with the rest of the conjugated system. A planar structure can provide a broader absorption spectrum, leading to better light harvesting performance. The majority of previous reports have focused on development of organic sensitizers containing 9,10-disubstituted anthracene moieties for DSSCs. For example, Thomas et al. [28] reported the preparation of dye sensitizers featuring 9,10-substituted anthracene linkers inserted between triarylamine-based donor and cyanoacrylic acid acceptor units via a conjugation pathway composed of thiophene and benzothiadiazole units. Teng et al. [30] designed and synthesized a series of metal-free organic dyes bridged by a π-conjugation system containing anthracene. One of the reported dyes showed excellent power conversion efficiency of up to 7.03% under simulated AM 1.5 irradiation (100 mW/cm^2). Heo et al. [29] reported the synthesis of various anthracene mediated π-conjugated dyes incorporating triple-bond and thiophene moieties for fine-tuning molecular configuration and for broadening the absorption spectrum. Li et al. [21] reported a series of organic sensitizers featuring a 9,10-diaryl-substituted anthracene unit that facilitated the construction of high conversion efficiency solar cells. However, all of the reported 9,10-anthracene-based sensitizers suffered severe steric congestion between the anthracene core and the substituent aromatic rings. Therefore, relieving the steric congestion introduced by substitution at the 9,10-positions on anthracene has the potential to improve the power conversion efficiency of these organic-dye-based DSSCs.

Recently, Yan et al. [79] had studied on the introduction of triple bond (TB) moiety between an electron donor and π-conjugate linker. However, the triple-bond insertion on this way brings to reduce open-circuit photovoltage (V_{oc}) owing to faster interfacial charge recombination. On the other hand, Yang et al. [80] had employed TB inserted between π-conjugate linker and an electron acceptor. The results showed that better electron injection from the excited state resulting in significantly improved a short circuit photo current (J_{sc}). Thus, we believed that the triple-bond modification is an important consideration in the future dyes design.

Theoretical studies investigating the relationships between structure, and the properties and performance of dye sensitizers offer shorter development times and significant cost savings over traditional synthetic approaches. Accurate first-principle density functional calculations using supercomputing facilities are now commonly available to research groups. Calculations are employed as a tool to design, study, and screen dye sensitizer candidates prior to synthesis. Computer-aided rational design of new dye sensitizers has recently seen reports from several groups, including our own group. In this study, we aimed to develop anthracene-based dyes that incorporate a triple bond (TB)-modified π-conjugated linker to alleviate steric congestion between the anthracene moiety and its neighboring aromatic rings. We introduced thiophene units at the 9- and 10- positions of an anthracene ring without TB-modification for dye **An1,** as a reference dye. For the **An2** dye, we introduced a TB connector between the 9-position on anthracene and the thiophene substituent. The **An3** dye incorporated a TB group at the 10-anthracene position, and the **An4** dye featured TB 9,10-disubstitution. The molecular structures of the **An1–An4** dyes are shown in Figure 5.1.

Structural, optical, and electronic properties were investigated to identify the effects of the different TB-substitutions on the light harvesting properties of the dyes.

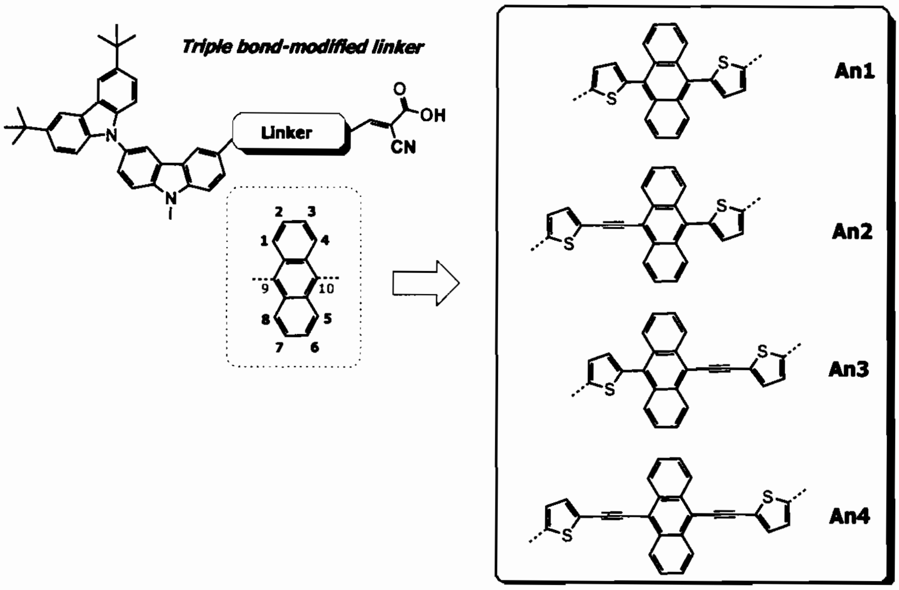

Figure 5.1 Sketch map of the studied dyes An1-An4

5.2 Computational details

All calculations on the structure and electronic properties of the isolated dyes have been performed with the GAUSSIAN 09 program. The ground state geometries of the modified **An1–An4** anthracene-based dyes were fully optimized using Density Functional Theory (DFT) with Becke's three-parameter hybrid function and Lee-Yang-Parr's gradient-corrected correlation function (B3LYP) at the 6–31G(d,p) level. All calculations were performed without symmetry constraints in the gas phase. Optimized structures were then be used to calculate excitation energy (E_g), maximum absorption wavelength (λ_{max}), and oscillator strength (f) for the 10 lowest energy states in dichloromethane solvent (CH_2Cl_2), by applying Time-Dependent Density Functional Theory (TD-DFT) with CAM-B3LYP at the 6-31G(d,p) level of theory. The TD-DFT results were entered into the SWizard program for simulation of the dye absorption spectra.

To gain insight into the electron injection properties, the TiO_2 film were modeled with a stoichiometric anatase (101) surface as the $(TiO_2)_{38}$ cluster, which is similar to that described by Nazeeruddin et al. [81] This model by DFT calculations using the DMoL^3 program in Materials Studio, version 5.5 has been wildly used to study dye@TiO_2 adsorption and represents a reasonable choice between accuracy and computational convenience, and nicely reproduces the main electronic characteristics of TiO_2 nanoparticles. The HOMO, LUMO and HOMO–LUMO energy gap of the this cluster are calculated to be 27.98, 23.52, and 24.46 eV, respectively, while the lowest excitation is obtained as 3.75 eV which is reasonably higher than typical band gaps of TiO_2 nanoparticles of a few nm size of 3.2–3.3 eV. The TiO_2 conduction band edge was calculated at ca. -4 eV vs. vacuum, in good agreement with experimental values. In addition, this cluster size has been comparatively tested with a relatively larger $(TiO_2)_{82}$ cluster and the both clusters shows a similar conduction band structure, within 0.1 eV, to the corresponding periodic model. Therefore, this work we use the $(TiO_2)_{38}$ cluster for representing the TiO_2 surface for dye adsorption.

The $(TiO_2)_{38}$ configurations were fully optimized using the generalized gradient-corrected approximation (GGA) method. The Perdew–Burke–Ernzerhof (PBE) function was applied with the DNP basis set to account for exchange-correlation effects. The core electron was subjected to a DFT-SemicorePseudo Potential (DSPP). The criteria for the optimization threshold are similar to those used in our previous reports. After optimization, adsorption energies (E_{ads}) of the dyes on $(TiO_2)_{38}$ clusters were obtained by Equation 5.1:

$$E_{ads} = E_{dye} + E_{TiO_2} - E_{dye+TiO_2} \tag{5.1}$$

where E_{dye} is the total energy of the isolated dye, E_{TiO_2} is the total energy of the $(TiO_2)_{38}$ cluster, and $E_{dye+TiO_2}$ is the total energy of the dye-$(TiO_2)_{38}$ complex. Following calculation, a positive E_{ads} value indicates stable adsorption of the dye onto TiO_2.

5.3 Results and discussion

5.3.1 Optimized ground-state geometries

To gain insight into the molecular structures of the studied dyes, the ground-state geometries of dyes **An1–An4** were optimized using DFT at the B3LYP level with the 6-31G(d,p) basis set. The dyes are grouped into three parts as shown in Figure 5.2 (a): (i) two carbazole groups (Cbz) acting as donor, (ii) different thiophene groups (Thi), an anthracene moiety (An), or a triple bond (TB) as linker, and (iii) cyanoacrylic acid (Cyn) as the acceptor. Figure 5.2 (b) shows optimized ground-state geometries for **An1–An4.** Table 5.1 summarizes the dye C-C bond lengths (r) and dihedral angles (ϕ). The calculated C-C bond lengths are identical for all dyes within the donor moiety (Cbz-Cbz) (1.42 Å), between the donor and linker (Cbz-Thi) (1.46 Å), and between the linker and acceptor (Thi-Cyn) (1.43 Å). The dihedral angles formed between the two donors (Cbz-Cbz) lie approximately 60° out-of-plane from each other, resulting in reduced dye-aggregation at the donor group. All of the calculated dihedral angles formed between the π-linker and the cyanoacrylic acid acceptor (Thi-Cyn) are close to zero and accordingly, these components are almost coplanar.

To investigate the relationships between the various π-conjugated linkers and the charge transfer properties, we examined the critical dihedral angles on the linker moiety. From the side view of the studied dyes in Figure 5.2 (b), the presence of an anthracene moiety as linker-bridge in the **An1** dye, produces a large dihedral angle, with the anthracene and thiophene groups almost perpendicular at the 9,10-anthracene positions, providing significant steric effects and loss of planarity. Insertion of TB at position 9 on anthracene in **An2**, at position 10 in **An3**, and at both 9,10-positions in **An4**, significantly decreases the dihedral angles compared to the **An1** dye. These observations reveal that the presence of a triple bond decreases the dihedral angles at the 9,10-funtionalized positions on anthracene, which in turn reduces steric hindrance, and increases planarity within the anthracene dye.

Furthermore, to describe the length of the conjugated bridge in the dye, we define "L" as the distance of coplanarity formed between π-conjugated linker and the cyanoacrylic acid acceptor. The side view in Figure 5.2 (b) shows that distance *L* for the **An1** dye is approximately 8.18 Å. Substitution with TB at 9-position in the **An2** dye has little effect on *L*; the distance is similar to that seen for dye **An1**. Insertion of TB at position-10 in dye **An3** produces a significant increase in *L*, to 10.72 Å. This suggests that the presence of TB at the 10-functionalized position on anthracene extends the π-conjugation system. Position 10 is closer to the cyanoacrylic anchor than is the 9-position, which is positioned opposite to the acceptor group. Finally, the presence of TB groups at both the 9- and 10-positions in **An4** results in coplanarity between the anthracene moiety and the core molecule, and provides the longest *L* distance of 17.53 Å. The distance *L* is a key parameter for optimizing these anthracene based sensitizers.

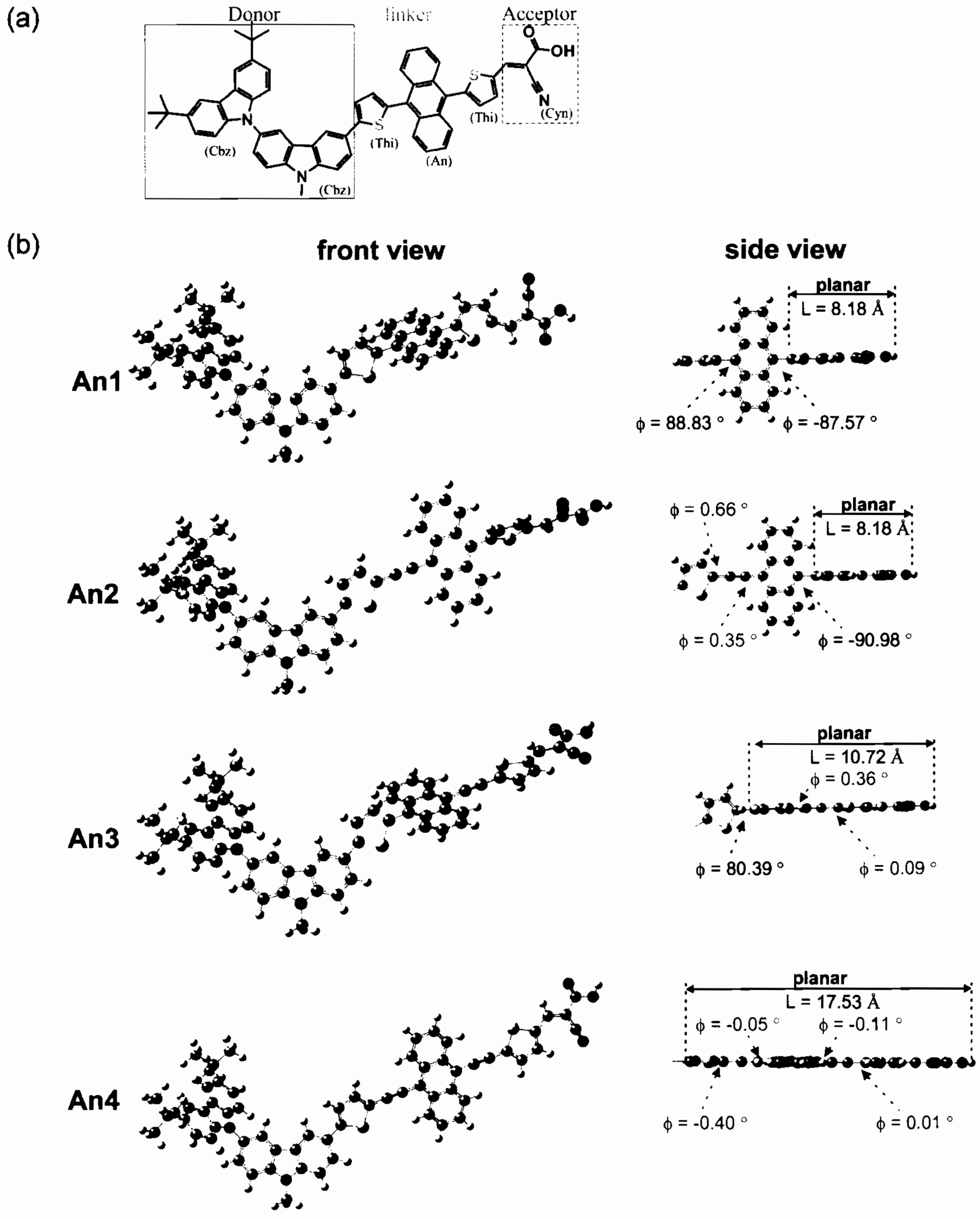
(a)
Donor
linker
Acceptor
O
OH
N
S
(Cbz)
(Cbz)
(Thi)
(Thi)
(An)
(Cyn)
(b)
front view
side view
An1
planar
L = 8.18 Å
ϕ = 88.83 °
ϕ = -87.57 °
An2
ϕ = 0.66 °
planar
L = 8.18 Å
ϕ = 0.35 °
ϕ = -90.98 °
An3
planar
L = 10.72 Å
ϕ = 0.36 °
ϕ = 80.39 °
ϕ = 0.09 °
An4
planar
L = 17.53 Å
ϕ = -0.05 °
ϕ = -0.11 °
ϕ = -0.40 °
ϕ = 0.01 °

Figure 5.2 (a) The molecular structures were categorized into three parts of donor, linker, and acceptor, (b) Optimized structures of the studied dyes An1 – An4 calculated by B3LYP/6-31G(d,p) level of theory

Table 5.1 **Selected bond lengths (*r*, Å) and dihedral angles (*ϕ*, degree) for optimized structures of dyes An1–An4 calculated at the B3LYP/6-31G(d,p) level of theory.**

Dyes	**Donor**	**Donor-Linker**	**Linker**						**Linker-Acceptor**
	Cbz-Cbz	Cbz-Thi	Thi-An	Thi-TB	TB-An	An-TB	TB-Thi	An-Thi	Thi-Cyn
Bond length *(r)*									
An1	1.42	1.46	1.48					1.48	1.43
An2	1.42	1.46		1.40	1.42			1.48	1.43
An3	1.42	1.46	1.48			1.41	1.40		1.43
An4	1.42	1.46		1.40	1.41	1.41	1.40		1.43
Dihedral angle *(ϕ)*									
An1	59.21	29.20	88.83					-87.57	0.19
An2	59.98	-27.92		0.66	0.35			-90.98	-0.13
An3	58.72	-29.68	80.39			0.36	0.09		-0.15
An4	58.26	-37.36		0.40	0.05	0.11	-0.01		-0.08

Cbz = Carbazole, Thi = Thiophene, An = Anthracene, TB = Triple bond, Cyn = Cyanoacrylic acid

5.3.2 Frontier molecular orbitals (FMOs)

To further explore the effects of different π-conjugated linkers on intramolecular charge transfer (ICT), we plotted the electron distributions in two frontier molecular orbitals: the highest occupied molecular orbitals (HOMO) and the lowest unoccupied molecular orbitals (LUMO). Figure 5.3 illustrates the HOMO and LUMO frontier molecular orbitals, and the charge density differences (Δρ) between ground and the excited states. An important characteristic of electron density in the frontier molecular orbitals is the overlap between the HOMO and LUMO. At LUMO of **An1** and **An2**, there are no electron distributions on anthracene unit indicating that the HOMO and LUMO do not overlap. This suggests that ICT would not occur across the anthracene unit for these dyes. From the **An3** and **An4** in Figure 5.3, the well-overlapped HOMO and LUMO orbitals extend across the anthracene π-linker, suggesting good induction and electron-withdrawing properties for the donor and acceptor, respectively. Thus, we anticipate that this strong-overlapping character will facilitate ICT between the donor and acceptor, subsequently toward to conduction band of TiO_2.

Furthermore, we performed the Δρ plots revealing electron density differences between the ground- and excited-states to provide further evidence for ICT. The decreased (purple) mainly localized on the donor and linker parts, while the increased (yellow) electron densities localized on the anchoring group. In regards to the electron density delocalized throughout the entire molecular backbone, the ICT as well as the injection mechanism are possible when transition occurs for all dyes. The ICT property was generally accepted that is related to the dipole moment (μ) of the individual dye perpendicular to the surface of semiconductor. It is reasonable that the larger μ of the adsorbed dyes, the larger V_{oc}. Therefore, we performed dipole moment calculation under B3LYP/6-31G(d,p) level at the geometry of isolated dyes. The calculated total dipole moments (μ) are listed in Table 5.2. The total μ of dyes increases in the order of **An1** (6.30) < **An2** (7.25) < **An3** (7.47) < **An4** (9.52) as the planarity changes. The largest vertical dipole moment of **An4** dye is considered to provide the great ICT property.

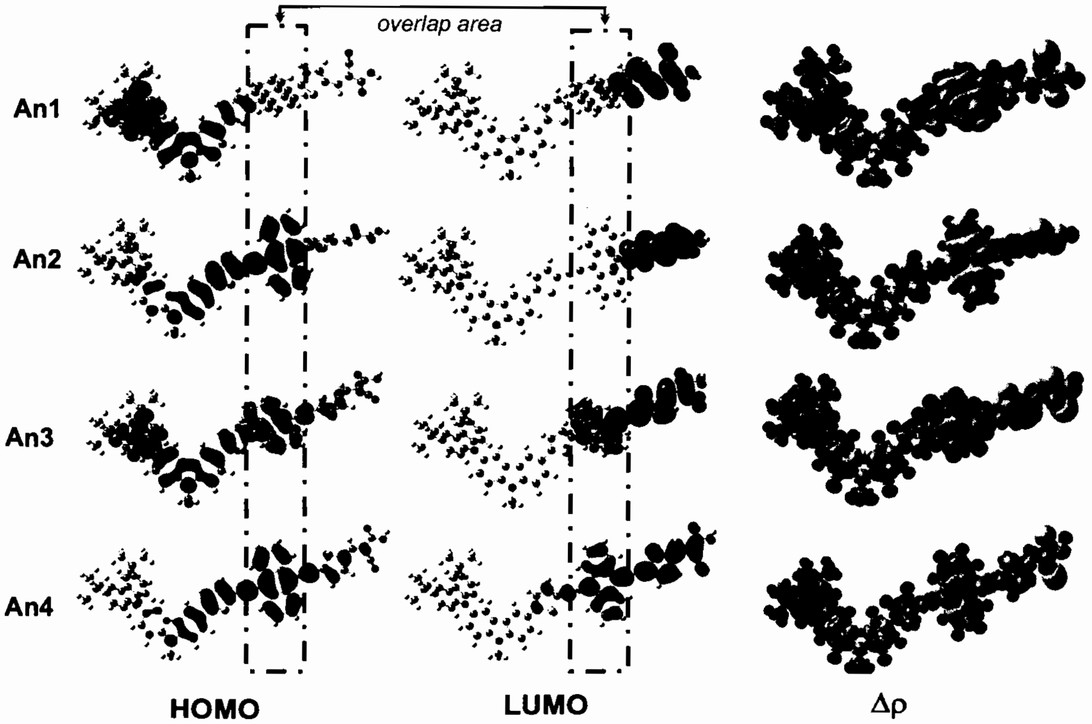
overlap area
An1
An2
An3
An4
HOMO
LUMO
Δρ

Figure 5.3 **The frontier molecular orbitals of HOMO (left) and LUMO (middle), and the charge density difference between the ground- and excited-state (right) of the studied dyes calculated under TD-CAM-B3LYP/ 6-31G(d,p). The purple represents where the electrons are decreased and the yellow represents where the electrons are increased**

Table 5.2 **The maximum absorption wavelength (λ_{abs}), oscillator strength (*f*), light harvesting efficiency (*LHE*), electron injection driving force (ΔG^{inject}) and transition compositions of An1- An4 dyes, calculated by TD-CAM-B3LYP/6-31G(d,p) in CH_2Cl_2 solution (C-PCM model).**

Dyes	μ_y [a] (Debye)	λ_{abs}, nm(eV)	*f*	*LHE* [b]	[c] E_{ox}*	[d] ΔG^{inject}	Transition compositions
An1	6.30	374 (3.31)	0.8596	0.86	2.01	-1.99	(+0.62) H-1→L+1 (–0.21) H-2→L+1
An2	7.25	450 (2.75)	1.6038	0.97	2.39	-1.61	(+0.63) H→L+1 (+0.22) H-1→L+1
An3	7.47	490 (2.53)	1.6325	0.98	2.71	-1.29	(+0.51) H-1→L+1 (–0.40) H→L
An4	9.52	562 (2.21)	2.2861	0.99	2.92	-1.08	(+0.63) H→L (–0.17) H→L+1

[a] μ_y is dipole moment in the direction perpendicular to the TiO_2 surface

[b] $LHE = 1 - 10^{-A} = 1 - 10^{-f}$

[c] $E_{ox}^* = E_{ox} - \lambda_{abs}$

[d] $\Delta G^{inject} = E_{ox}^* - E_{CB}$

5.3.3 Energy diagram

Figure 5.4 shows calculated HOMO and LUMO energy levels for dyes **An1–An4**. Importantly, the HOMO energy level is required to match with the redox potential of the iodine/triiodide (I^-/I_3^-) electrolyte system for suitable charge recombination back to the oxidized dyes, whereas the LUMO level is required to match with the TiO_2 conduction band (CB) edge for efficient injection of excited electrons. For LUMO levels, the criterion for an efficient electron injection process requires that the energy gap between the LUMO and the CB edge of TiO_2 is greater than approximately 0.2 eV. As shown in Figure 4, the simulated LUMO levels are -2.89, -3.14, -2.96, and -3.12 eV for **An1-An4,** respectively, which are greater magnitude than the CB of $(TiO_2)_{38}$ cluster of -4.00 eV in the experiment. The energy gaps between the acceptor LUMO and TiO_2 CB calculated to be 0.61, 0.36, 0.54, and 0.38 eV for the **An1-An4** dyes, respectively, indicating that injection of excited electrons from the dye excited-state into the TiO_2 conduction band edge should be thermodynamically favorable.

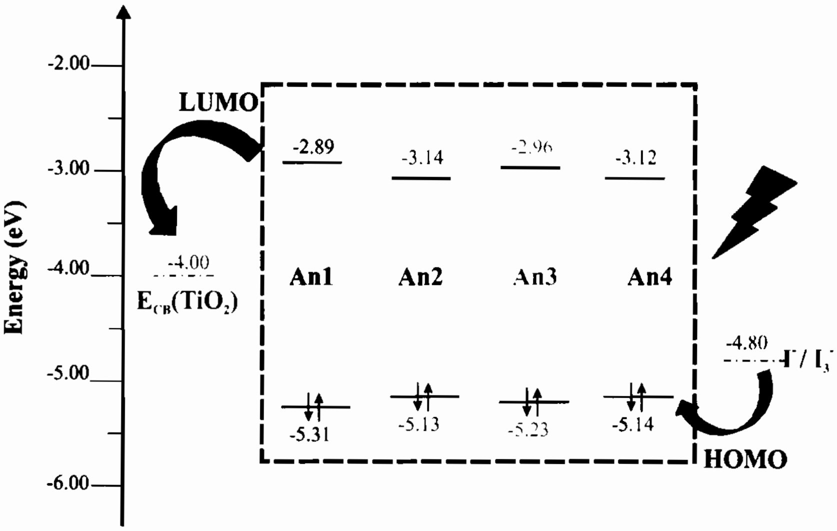

Figure 5.4 Computed HOMO-LUMO energy levels for the studied dyes An-An4 at the TD-CAM-B3LYP/6-31G(d,p), together with the TiO_2 conduction band edge and theI^-/I_3^- redox potential.

For HOMO level, HOMO energy levels must lie below the I^-/I_3^- redox couple (-4.80 eV) for efficient electron regeneration. Figure 5.4 shows that the HOMO energies of the studied dyes are -5.31, -5.13, -5.23, and -5.14 eV for **An1–An4**, respectively. Thus, there is a sufficient driving force for fast and efficient regeneration of the oxidized dye. Relatively large energy gaps between the LUMO energies of these dyes and the semiconductor CB together with the low lying HOMO of the I^-/I_3^- redox couple would be beneficial to photovoltaic conversion.

5.3.4 Absorption spectra and light harvesting properties

To determine the dye optical absorption characteristics and electronic transitions in CH_2Cl_2 solvent, we performed TD-DFT calculations using the CAM-B3LYP function under the C-PCM continuum salvation model. The calculated maximum absorption wavelengths (λ_{abs}), oscillator strengths (f), electronic transitions, and light harvesting efficiencies (*LHE*) are listed in Table 5.2. Simulated absorption spectra for the **An1–An4** dyes are shown in Figure 5.5.

The dyes exhibit two major absorption regions at roughly 292–374 and 450–562 nm. We ascribe the absorption bands below 400 nm to π-π^* transitions of the conjugated molecules. Bands in the longer wavelength region greater than 400 nm commonly arise from to ICT transitions, which are an important band for DSSCs applications. Figure 5.5 shows that **An1** exhibits λ_{abs} at 374 nm, which is below 400 nm, and thus ICT is probably absent due to the large dihedral angles measured at the position 9 and 10 of anthracene for **An1**, as discussed in **Section 5.3.1**.

It is interesting to compare the optical properties of the **An1** dye without TB, and the **An2–An4** dyes, which incorporate TB as a π linker. The dye λ_{abs} values fall in the order **An4** (562 nm) > **An3** (490 nm) > **An2** (450 nm) > **An1** (374 nm). The inclusion of TB in the π-conjugation chain causes red shift of the dye λ_{abs} values. Compared to λ_{abs} of **An1** dye at 374 nm, the red shifts of the λ_{abs} are calculated to be 76, 116, and 188 nm for **An2**, **An3**, and **An4**, respectively. These results clearly indicate that TB significantly extends the π-conjugation length, resulting in emergence of strongly favorable ICT. The extension of the linker conjugation length is further confirmed by the L distance, which increases in the order **An2** (8.18 Å) <

An3 (10.72 Å) < **An4** (17.53 Å). **An4** exhibits the broadest and most intense absorption spectrum. Therefore, **An4** is expected to be the most suitable dye for DSSCs applications.

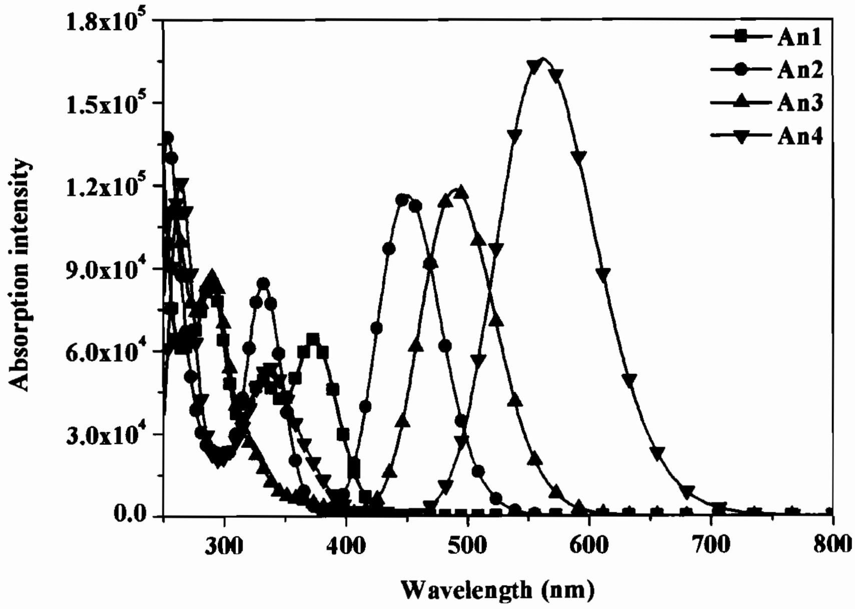

Figure 5.5 The simulated UV-Vis spectra of An1-An4 dyes using TD-CAM-B3LYP/6-31G(d,p) model in CH_2Cl_2 solution

We also calculated the light harvesting efficiency (*LHE*) to determine the extent of light absorption and J_{sc} values for the dyes. The *LHE* can be approximated by **Equation 5.2.**

$$\mathrm{LHE} = 1 - 10^{-A} = 1 - 10^{-f} \tag{5.2}$$

where, *A(f)* is the absorption intensity (oscillator strength) of the dye, associated with λ_{abs}, Φ_{inject} is the quantum yield of electron injection, and $\eta_{collect}$ represents electron collection efficiency. The *LHE* against absorption wavelength are plotted in Figure 5.6, while the calculated *LHE* values at maximum wavelengths are listed in Table 5.2. **An2–An4** dyes with triple bond-modified linkers show greater *LHE* values than the **An1** dye without TB. These results show that TB-modification can greatly improve the light harvesting efficiency. LHE curves obviously show high efficiency of **An4** which is superior to others, and is expected to be potential sensitizers for harvesting light in near infrared region than the other compounds. Because the *LHE* is proportional to J_{sc}, as shown in Equation 5.3, we expect that the **An4** dye will also have the greatest J_{sc} value, and thus, use of **An4** would provide the greatest efficiency DSSCs.

$$J_{sc} = \int \mathrm{LHE}(\lambda)\ \Phi_{inject}\,\eta_{collect}\,\mathrm{d}\lambda \tag{5.3}$$

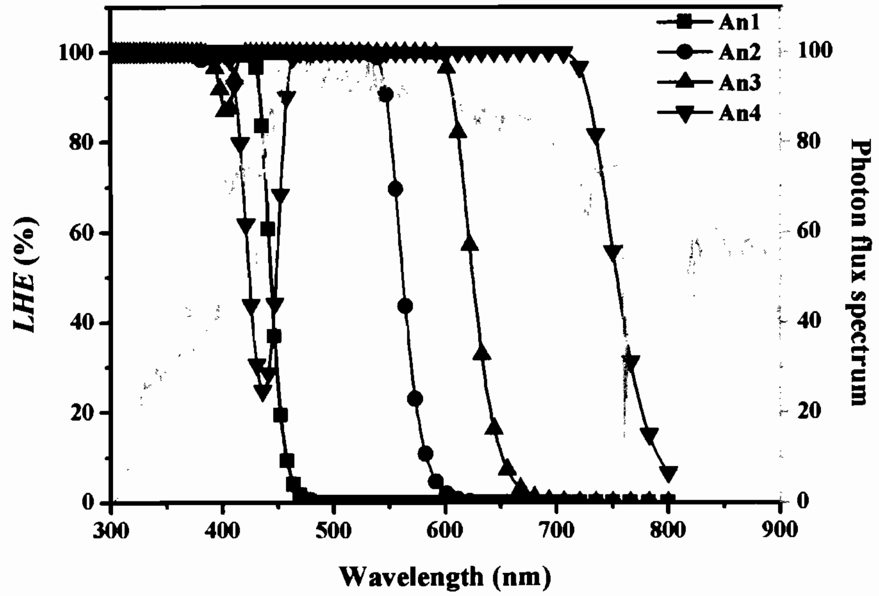

Figure 5.6 LHE curve of An21-An4 dyes along with photon flux spectrum at ASTM-G173 AM1.5

5.3.5 Driving force ($\Delta G^{\mathrm{inject}}$) and the electron injections process

For electron injection processes in DSSCs, the free energy change ($\Delta G^{\mathrm{inject}}$) is an important parameter for characterizing the rate and efficiency of the reaction. Figure 5.7 schematically shows the free energy change ($\Delta G^{\mathrm{inject}}$) that occurs as a result of electron injection in a DSSCs. The initial state of the reaction is the excited state of dye adsorbed on TiO_2 particles, and the final state corresponds to the injection of an electron into the conduction band of the TiO_2 particle. The $\Delta G^{\mathrm{inject}}$ can be obtained from Equation 5.4, representing the energy difference between these initial and final states, where $E_{ox}*$ representing to the photo-induced excited states of the organic dyes and E_{CB} representing to reduction potential of the TiO_2 semiconductor. The $E_{ox}*$ can be computed from Equation 5.5, where E_{ox} is the redox potential of the dye in the ground state and λ_{abs} is the absorption energy.

$$\Delta G^{inject} = E_{ox}* - E_{CB} \tag{5.4}$$

$$E_{ox}* = E_{ox} - \lambda_{abs} \tag{5.5}$$

Taking into account the ΔG^{inject} listed in Table 5.2, we found that all ΔG^{inject} values are negative with sufficiently high ΔG^{inject} values (>0.2 eV) to obtain a high efficiency of electron injection in DSSCs, the electron injection process thermodynamically possible (i.e., ΔG^{inject} <0), confirming that the LUMO level of the dye must lie above the TiO_2 CB edge. Therefore, photo-excitation should be capable of producing sufficiently excited electrons for injection into the TiO_2 conduction bands. To enable sufficient driving force for electron injection, a good overlap of the excited states of the dye and the potential of the TiO_2 is crucial.

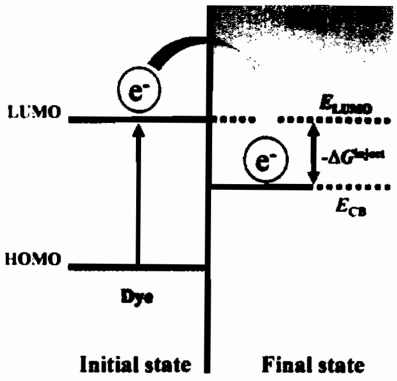

Figure 5.7 Schematic of free energy change (ΔG^{inject}) producing from the energy difference between E_{LUMO} and E_{CB}

5.3.6 Adsorption of dyes onto a $(TiO_2)_{38}$ cluster

To further study the structure of the dye sensitizer-semiconductor interface and the process of electron transfer from the dye sensitizer to semiconductor surface, we modeled the **An1-**, **An2-**, **An3-**, and **An4-TiO$_2$** adsorption complexes (**Dyes-TiO$_2$**) using the Dmol^3 computer program. Figure 5.8 shows the optimized structures, and Table 5.3 lists the adsorption energies (E_{ads}). As shown, the optimized adsorbed-dye structures are positioned almost perpendicular to the TiO_2 surface, linked by two O-Ti bonds in a bidentate-bridging adsorption mode. The calculated E_{ads} values for **Dyes-TiO$_2$** are in the range 19–21 kcal/mol, indicating strong interactions between the dyes and the TiO_2 surface. In addition, to consider to dipole moment of the dyes adsorbed onto $(TiO_2)_{38}$ cluster, we made the C2 axis of the carboxylate in the dye parallel to the y-axis, and the semiconductor surface is parallel to the xz plane as shown in Figure 5.8. As shown, the calculated dipole moments along y-axis (μ_y) were also shown in Figure 5.8. The μ_y of dyes increased in the order of **An1** (21.730) <**An2** (24.52) < **An3** (25.04) <**An4** (26.02), respectively. This calculated result confirms the strong intramolecular charge transfer (ICT) property of TB modified-linker dyes (**An2**, **An3**, **An4**) over the anthracene linker dye **An1**.

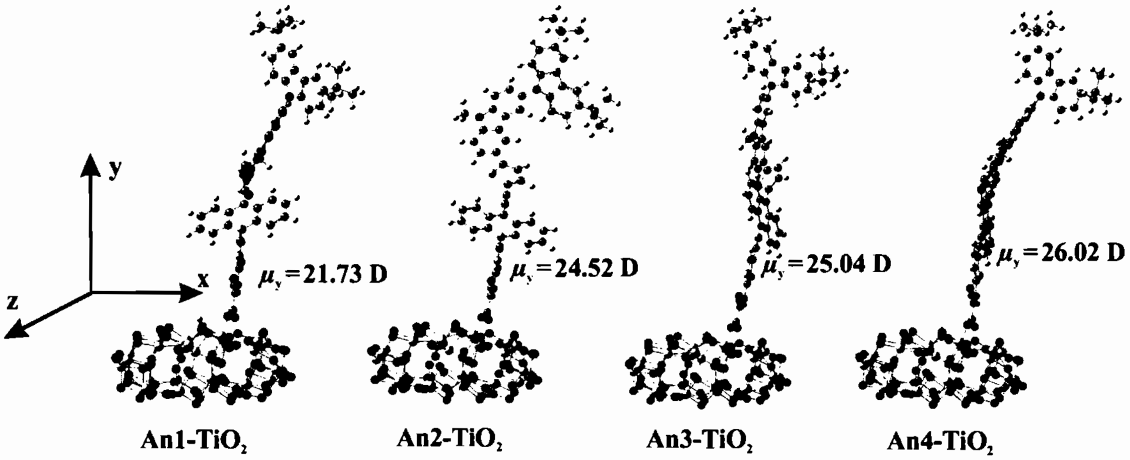

Figure 5.8 Optimized structures of An1-, An2-, An3- and An4-TiO$_2$ adsorption complexes calculated by PBE/DNP in the DMoL^3

Table 5.3 The calculated adsorption energy (E_{ads}) obtained using the DMoL^3 computer program. Excitation energies (E_{ex}), oscillator strengths (*f*), and the transition compositions for An1-, An2-, An3-, and An4-TiO$_2$ adsorption complexes, calculated by the TD-CAM-B3LYP/3-21G (d,p) level of theory

Complexes	E_{ads} (kcal/mol)	E_{ex}, eV(nm)	*f*	Transition compositions
An1-TiO$_2$	20.72	3.07 (404)	0.5570	(+0.90) H→L
An2-TiO$_2$	19.58	3.76 (449)	1.6644	(+0.24)H→L+60(+0.24) H→L+59
An3-TiO$_2$	19.88	2.50 (495)	2.0339	(+0.26) H-1→L+21(+0.21) H-1→L+12
An4-TiO$_2$	20.80	2.19 (566)	2.6740	(+0.26) H→L+9 (+0.26) H→L+20

Upon excitation, electronic coupling and electron transfer take place between the LUMO on the dye and the CB on TiO$_2$. Thus, it is important to analyze the frontier molecular orbitals of the **Dyes-TiO$_2$** complexes, and for the LUMO in particular. A schematic description of the electronic structure for the free dyes, bare TiO$_2$ and dye@TiO$_2$ system is depicted in Figure 5.9. In order to see which dye has the electron coupling between the dye's LUMO and the conduction band of TiO$_2$, there are two points of view to discuss. First is the position of electronic transition from the ground to the excited state. Second is their electronic character before and after excitation for confirming the electron injection mechanism. To get more insights into the orbital charge densities for frontier molecular orbitals of the **Dyes-TiO$_2$** complexes, the optimized geometries of the **Dyes-TiO$_2$** complexes from DMoL^3 were further calculated the electronic transition energies with TD-DFT calculations using CAM-B3LYP functional with the 3-21G(d) basis as implemented in the GAUSSIAN09 program. The results are shown in Table 5.3. Figure 5.10 shows selected isosurface frontier molecular orbitals, including HOMO, LUMO, and other interacting orbitals of the **Dyes-TiO$_2$** complexes. For the **An1-TiO$_2$** adsorption complex in Figure 5.10 (a), the electronic transition corresponds to a HOMO→LUMO interaction. The HOMO electron density localizes on the Cbz-Cbz donor group, while electron density in the LUMO is located on the TiO_2 surface. However, this transition does not represent the direction of electron transfer, because there is no electron density located at the cyanoacrylic acid anchoring group for the LUMO of the dye acceptor. This calculated result probably arises because of the twisted anthracene geometry in **An1**, with dihedral angles at the 9- and 10-positions that are almost perpendicular to the cyanoacrylic acid anchoring plane (Section 5.3.1), and which result in suppression of electron transfer.

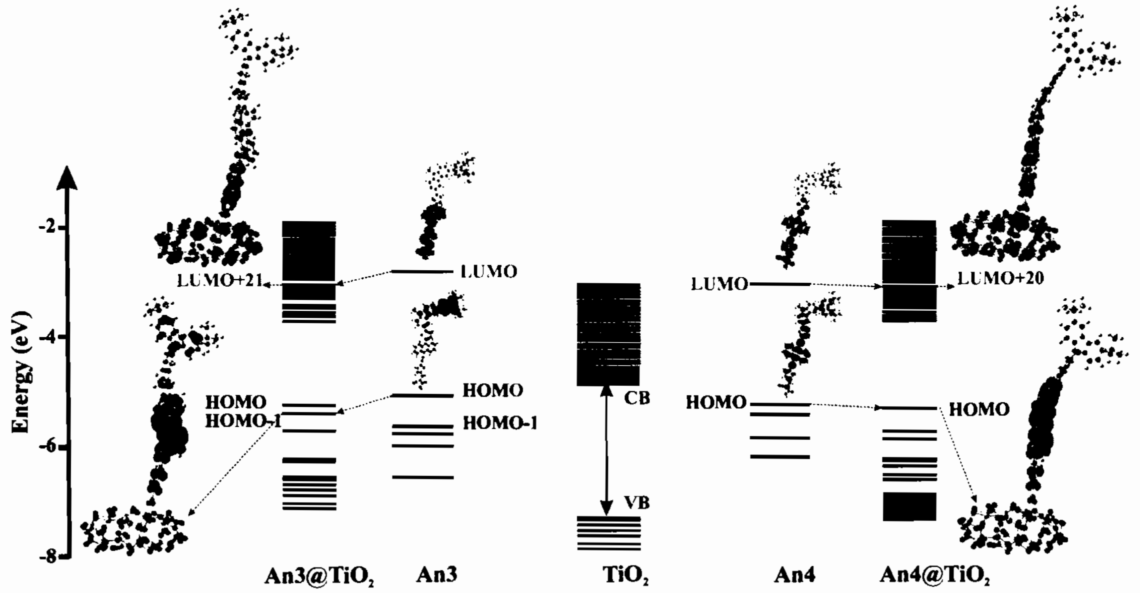

Figure 5.9 Schematic energy diagram of isolated An3 and An4 dyes, isolated TiO_2, and interacting An3@TiO_2 and An4@TiO_2

For the **An2-TiO_2** adsorption complex in Figure 5.10 (b), the electronic transition corresponds to the linear combination of HOMO→LUMO+59 and HOMO→LUMO+60. The electron distribution of the HOMO mainly localizes on the anthracene moiety and the adjacent carbazole unit. This calculated result is consistent with the incorporation of TB between 9-anthracene and the carbazole donor, which results in a significantly decreased dihedral angle between anthracene and the adjacent carbazole group, and consequently improved electron transfer from the carbazole donor onto anthracene. However, electron density cannot extend past the 10-position because of the large dihedral angle, and consequently, there is no electron density located on the cyanoacrylic acid anchoring group for LUMO+59 or LUMO+60. Thus, this transition also could not represent a route for electron transfer from the dye to the TiO_2 surface.

In contrast, **An3-TiO_2** and **An4-TiO_2** adsorption complexes in Figure 5.10 (c) and 5.10 (d) with TB at positions 10 and 9,10 on anthracene, respectively, have much smaller dihedral angles at the 10-position and are essentially planar. Consequently, electron transfer to the TiO_2 surface via the cyanoacrylic-anchoring group can occur. As shown, the HOMO-1 electron distribution for **An3-TiO_2** and HOMO for **An4-TiO_2** are mainly localized on the anthracene moiety, with slight delocalization to the anchoring group, while the patterns of LUMO+12 and LUMO+21 for **An3-TiO_2,** and LUMO+9 and LUMO+20 for **An4-TiO_2,** show that the electron distribution is delocalized across both the TiO_2 surface and the cyanoacrylic-anchoring group. These distributions represent electron transfer from the dye via the anchoring group to the TiO_2 surface as a consequence of direct electron injection. The effects of connecting the anchoring group to anthracene at different positions for **An3-TiO_2** (9-position) and **An4-TiO_2** (9,10-positions) adsorption complexes are similar. The reason is that electron density can transfer from anthracene to the TiO_2 surface through the small dihedral angle between anthracene and thiophene at the 10-position10-position. Thus, the presence of **TB** plays a key role in electron transfer and in the injection mechanism at the $(TiO_2)_{38}$ surface.

5.4 Conclusions

In summary, we used computational methods to design and investigate a series of three anthracene-based dyes, **An2–An4**, with a TB-modified π-conjugated linker and compared these to the **An1** dye without TB substitution. Interestingly, all three anthracene-based sensitizers **An2–An4** showed significant decreases in the dihedral angle between the anthracene unit and its substituents at the 9,10-positions, resulting in a nearly planar molecular geometry for each dye. The presence of a planar structure

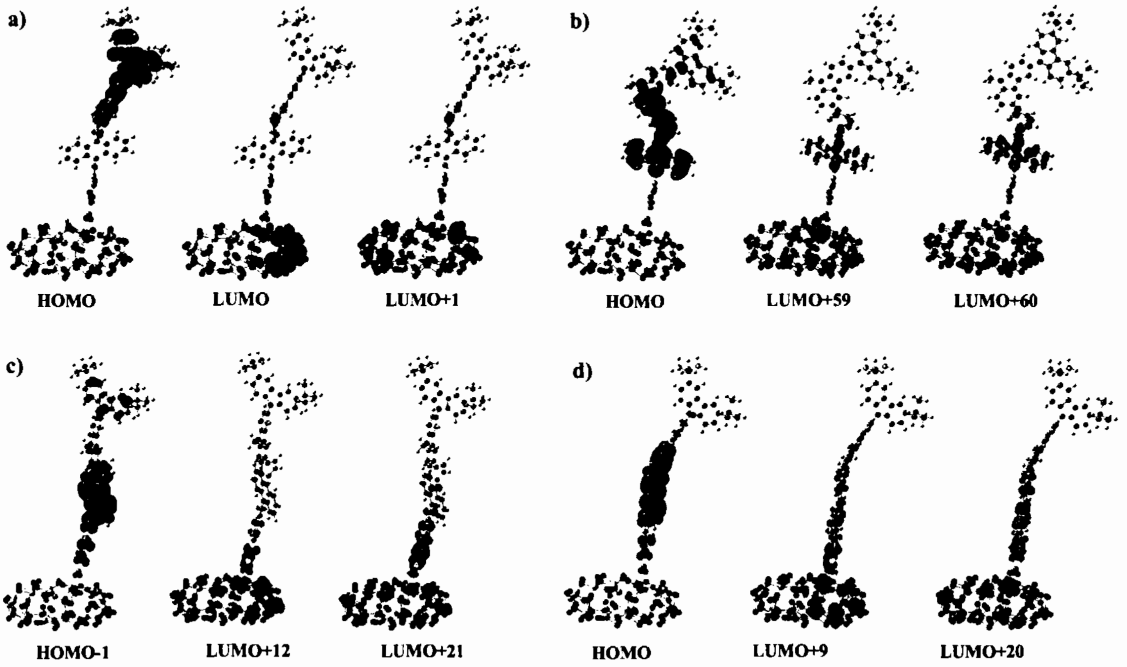

Figure 5.10 Electronic transitions of a) An1-, b) An2-, c) An3- and d) An4-TiO_2 adsorption complexes calculated by TD-CAM-B3LYP/6-31G(d,p).

greatly affects the absorption spectra, which broadens with increasing coplanarity distance (*L*). Furthermore, molecular coplanarity of with the π-conjugated linker has a significant effect on electron distribution overlap on anthracene, which facilitates ICT. According to calculated absorption spectra, the **An4** dye exhibits a prominent red-shift in its absorption peak, which is beneficial to its light-harvesting efficiency. The calculated electronic transitions for the dye-$(TiO_2)_{38}$ clusters revealed that dyes bearing a TB moiety directly linked between anthracene and the anchoring group, exhibit electron injection from the dye to the TiO_2 surface. These results indicate that inclusion of a triple bond-modified π-conjugated linker in these dyes during synthesis is necessary for the construction of high-efficiency organic sensitizers.

CHAPTER 6

THEORETICAL INVESTIGATION ON INFLUENCE OF DIFFERENT ELECTRON DONORS AND CONJUGATE BRIEGES IN ORGANIC DYES FOR DYE-SENSITIZED SOLAR CELLS

6.1 Introduction

Dye-sensitized solar cells (DSSCs), first presented by O'Regan and Gratzel in 1991, are the low-cost photovoltaic device to convert sunlight to electricity due to using the low-cost materials of titanium dioxide nanoparticles compared to an expensive material of pure silicon in traditional silicon-based solar cells. Moreover, DSSCs are also presented the advantages of high sunlight-to-electricity conversion efficiency as well as easy manufacturing procedures. These lead to considerable increasing attention in scientific research resulting in numerous publications on DSSCs investigations over 1000 articles by the end of 21st century. The challenge for DSSCs study is to develop high solar-to-electricity conversion efficiency which the highest record was limited at about 12% for ruthenium (Ru) complex dye sensitizer so far discontinued increasing for two decades. In the past decade, metal-free organic dyes were developed and the conversion efficiency records are around 9%. At present, the study on metal-free organic dyes considered promising sensitizer in DSSCs have been greatly high attended both of an experimental synthesis and testing as well as theoretical calculations.

The majority of development on metal-free organic dyes is devoted to design novel dye sensitizer which is the key component in DSSCs working principle to harvest of solar irradiation for converting light to electricity. Recently, a widely used approach to modify the dye structure is to design in the donor- π conjugated -acceptor (D-π-A) architecture which can achieve high efficient photovoltaic performance. In D-π-A system, a variety of electron donating groups (D) such as triarylamine, coumarin, carbazole, fluorene, and phenothiazine, etc. have been widely employed. On the other side, basically three types of electron acceptor groups (A) namely cyanoacrylic acid, carboxylic acid and rhodanine-3-acetic acid were widely used.

The electron donors in organic sensitizers play a vital role in determining the overall conversion efficiency studied by many research teams. Wan and coworkers reported the effect of different electron donor groups affecting to a significant distinction for the overall conversion efficiencies of the dye-sensitized solar cells. In order to fine tune donating ability for a good electron transfer from donor to acceptor, the double electron donor groups were presented called as D–D–π–A type organic dyes. Namuangruk and coworkers reported that double electron donor groups can enhance the electron-donating ability as well as can provide a direct electron injection from the dyes to TiO_2 in one step. Interestingly, Khanasa and coworkers suggested that further improvements could be made by introducing an additional donor moiety into the organic dyes to form a 2D–D–π–A structure. Based on this type, the organic dyes have a beneficial influence to enhanced energy conversion efficiency as a promising candidate for improved performance DSSCs. Because the electron donors in organic sensitizers play a crucial role in determining the overall conversion efficiency, thus, it is interesting to study the influence of the electron donor. However, to the best of our knowledge, there were only a few reports studied on the different electron donors in D–D–π–A and 2D–D–π–A types organic dyes. Therefore, this study interested in the design of new sensitizers based on D–D–π–A system with different electron donor groups.

As in the case of new dye sensitizer development, the theoretical investigations are very important to understand the relationship between the structure, properties, and performance of dye sensitizer by worthy less time and cost consuming compared to synthetic approach. Today, accurate first principle density functional calculations are available on supercomputing facilities used by more research groups. The calculations are employed as a tool to design, study, and screen the new dye sensitizer before synthesis. Computer-aided rational design of new dye sensitizers has recently attracted a considerable for several groups, including ours.

In this work, we reported on the development of new dye sensitizers based on D–D–π–A system with different electron donor groups as well as π-conjugate bridges in order to compare their effects on the dye structure and light absorption. The studied organic dyes as influence of different electron donor are showed in Figure 6.1. These dyes are designed in Donor-Donor-π conjugate-Acceptor (D-D-π-A) architecture where carbazole acting as primary donor group (denoted as D) and cyanoacrylic acid acting as acceptor group (denoted as A). We decide to only change the secondary donor group (denoted as D) based on fluorene, carbazole and phenothiazine moieties in an attempt to improve absorption ability. In addition, to improve the phenothiazine-based dye, we decide to change only on the linker bridges to red shift (bathochromic shift) the absorption spectrum. Therefore, the new dyes can be rationally designed by increasing conjugation lengths from 1 to 3 units of two different linker bridges between thiophenephenyl and thiophene linkers. The new designed dye structures in the present study consist of "carbazole" and "phenothiazine" moieties acting as electron donors, "thiophenephenyl"and "thiophene" acting as linker bridges, and "cyanoacrylic acid" acting as an electron acceptor. The chemical structure of new designed dyes is shown in Figure 6.1.

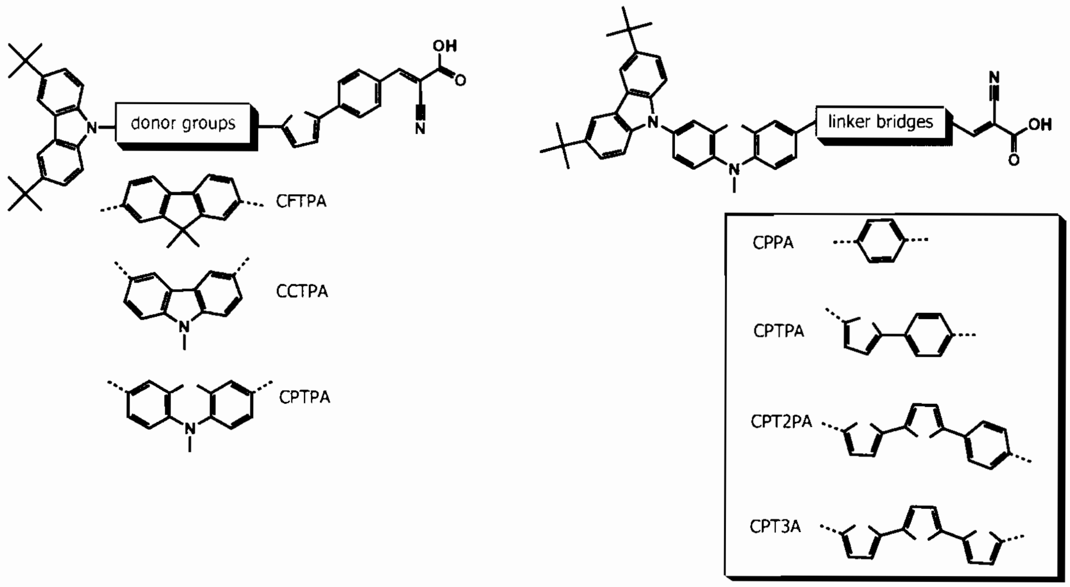

Figure 6.1 Chemical structure of newly designed dyes

6.2 Computational details

At the ground-state-optimized geometries, the Gaussian09 package software suite was carried out for all *ab initio* calculations. The calculations were done respectively in following 2 steps: first step, the geometry optimized structures and frontier orbital energy levels were calculated using the density functional theory (DFT) with hybrid functional of Becke's three parameter gradient-corrected exchange potential and the Lee-Yang-Parr gradient-corrected correlation potential (B3LYP) combined with 6-31G(d,p) level of theory. The HOMO/LUMO orbital distributions were also calculated in this step. Second step, the excited-state energies, absorption wavelengths and theirs oscillator strengths of all optimized structures were computed using time dependent density functional theory (TD-DFT) method. The solar cells work in solvent phase, thus, UV/Vis calculated data for these dyes were reported in solvent. The Conductor-like Polarizable Continuum Model (CPCM) was used to evaluate solvation effects. The UV/Vis absorption calculations were carried out in dichloromethane (DCM) according to the experimental set up at C-PCM/TD-CAMB3LYP/6-31G(d,p) level of theory. Calculation of the lowest 25 singlet–singlet excitations at the ground-state-optimized geometries allowed us to simulate a large portion of the absorption spectrum. The simulation of the absorption spectra was performed by using the SWizard program with using the Gaussian model.

6.3. Results and discussion

6.3.1 Ground-state structures

The ground-state geometries of the dyes were fully optimized using popular method of density functional theory (DFT) combined with the hybrid functional of B3LYP at 6-31G(d,p) level of theory. The calculated conformations on ground-state of the new designed phenothiazine-based are shown in Figure 6.2 and 6.3. Their selected dihedral angle parameters (in degree) are summarized in Table 6.1 and 6.2.

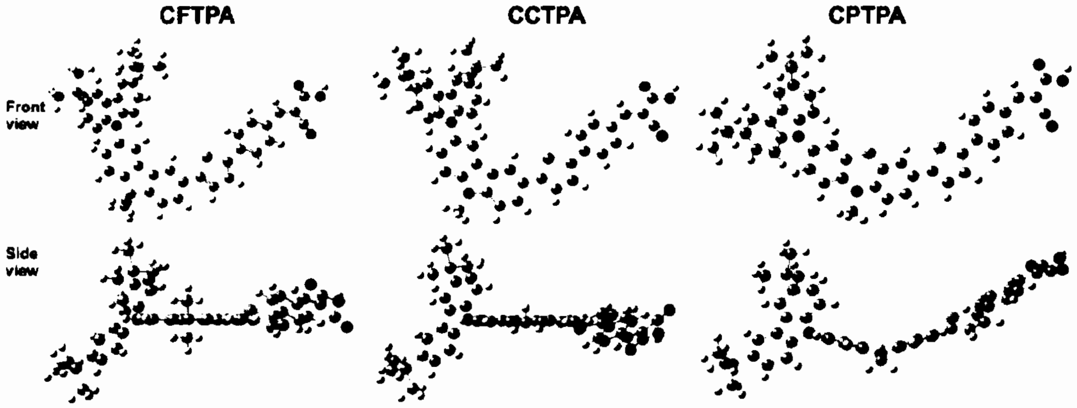

Figure 6.2 Optimized ground-state geometries of CFTPA, CCTPA and CPTPA dyes by B3LYP/6-31G(d,p) calculation

To get further insight into the effect of different electron donors on molecular conformation, we have scanned the dihedral angel for the optimized structures. They are composed of five moieties on the dye molecules; (i) "carbazole" group acting as secondary electron donor (C-section), (ii) different primary electron donor groups of "fluorene", "carbazole" and "phenothiazine" (F/C/P-section) for **CFTPA**, **CCTPA** and **CPTPA** dyes, respectively, (iii) group acting as linker (T-section), (iv) "phenyl" group acting as linker (P-section), and (v) "cyanoacylic acid" acting as electron acceptor (A-section).

Table 6.1 The optimized geometrical parameters, dihedral angle (in degree), of the studied organic dyesby using B3LYP/6-31G(d,p) method

Dyes	Dihedral angle (°) / intergroup				in F/C/P group
	C-(F/C/P)	(F/C/P)-T	T-P	P-A	P-P
CFTPA	-54.3798	26.2205	13.5076	-0.1143	0.1054
CCTPA	-57.7809	-25.9635	-12.8374	0.4249	-0.1841
CPTPA	-55.4947	25.4326	-18.3203	0.1902	35.8452

The results showed that the dihedral angels between intergroup of whole molecules are the same trend. The dihedral angel between secondary and primary electron donor groups exhibit large dihedral angle calculated to be of 54.3798, 57.7809 and 55.4947 degree for **CFTPA**, **CCTPA** and **CPTPA** dyes, respectively. These twisted conformations should beneficial to minimize the dye aggregation. However, all of the studied organic dyes exhibit nearly coplanar conformations between the π-conjugated linker system (calculated dihedral angle to be in the rage of 12-18 degree) and planar conformations between the π-conjugated and cyanoacrylic acid group (calculated dihedral angle close to 0 degree). We believe that these planar molecular structures should improve the intramolecular electron transfer (ICT) from the electron-donor to the electron-acceptor groups in these dyes.

It is interesting to note that the dihedral angels between the phenyl groups (P-P column) of primary electron donor group (F/C/P groups) are different. For both **CFTPA** and **CCTPA** optimized structures, we observed that fluorene and carbazole moieties exhibit coplanar conformations between the phenyl groups of electron-donor calculated to be close to 0 degree. On the other hand, **CPTPA** optimized structure showed non-planar structures with butterfly conformations (calculated dihedral angle to be around 35 degree) that could suppress dye aggregation. These findings are quite similar to the previous studies. Therefore, these calculated results indicate that the effect of different primary electron donor group is to facilitate potentially to inhibit aggregation by using phenothiazine moiety as electron donor group

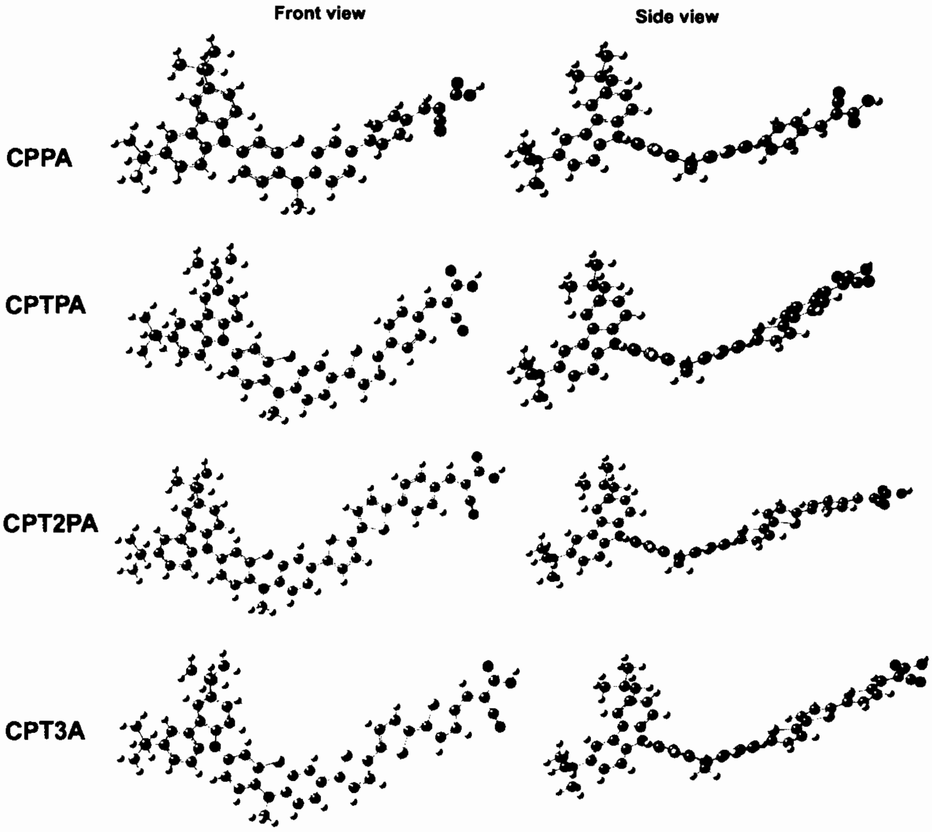

Figure 6.3 Optimized ground-state geometries of CPPA, CPTPA, CPT2PA, and CPT3A dyes by B3LYP/6-31G(d,p) calculation

For the effect of conjugate bridge, the results showed that the dihedral angles for thiophenephenyl and thiophene linkers are the same trend (i.e., large dihedral angles between carbazole-phenothiazine plane around 55 degree, while small dihedral angles between linker bridge and acceptor group around 0 degree), except the dihedral angles between intergroup of each linker. The dihedral angles between adjacent thiophene units of thiophenelinker (calculated to be 22.57, 7.40 and 3.57 degree for **CPTA**, **CPT2A** and **CPT3A** dyes, respectively) are smaller than that of thiophenephenyl linker (calculated to be 33.51, 18.32 and 16.62 degree for **CPPA**, **CPTPA** and **CPT2PA** dyes, respectively). These optimized structures of the dyes in the ground state indicate that the π-conjugate thiophene linker bridge is more suitable to electron transfer from the donor to acceptor part.

Table 6.2 The optimized geometrical parameters, dihedral angle (in degree), of the new designed phenothiazine-based dyesby using B3LYP/6-31G (d,p) method

Dyes	Dihedral angle (°) / intergroup						in P group
	C-P	P-P	T1-T2	T-P		P-A	P-P
CPPA	-54.03	-33.51				0.27	35.57
CPTPA	-55.49	25.43		-18.32		0.19	35.85
CPT2PA	-55.56	24.86	8.38	-16.62		-0.67	35.84
		P-T			T2-T3	T-A	
CPT3A	-55.32	25.56	-11.53		3.57	-0.10	35.73

6.3.2 Intramolecular charge transfer (ICT)

In DSSCs, one of the most important features for organic dye sensitizer is intramolecular charge transfer (ICT) from electron donating part to the electron accepting part. In order to study the effect of different electron donor groups on intramolecular charge transfer, the distribution patterns of the frontier molecular orbitals (FMO); highest occupied molecular orbitals (HOMOs) and lowest unoccupied molecular orbitals (LUMOs) of the studied dyes at ground-states were calculated. The plotted of electronic structures for HOMO and LUMO were shown in Figure 6.4 and 6.6. The contribution portions of their density of state were summarized in Table 6.3 and 6.4.

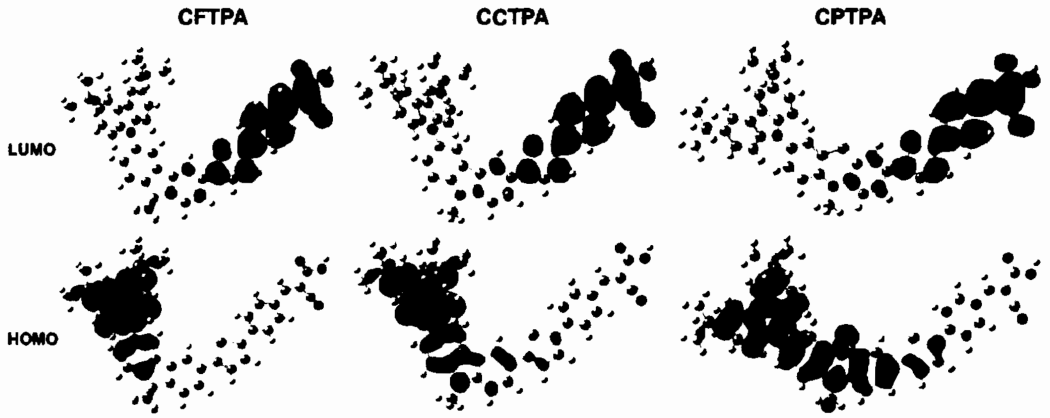

Figure 6.4 The frontier molecular orbitals of CFTPA, CCTPA and CPTPA dyes

Table 6.3 Calculated charge distribution oneach group of the donor, π-spacer and acceptor of the studied organic dyesunder B3LYP/6-31G(d,p) method.

Dyes	Electronic levels	The percent contribution (%)			
		D (Carbazole)	D (F/C/P)	π (Thiophenephenyl)	A (Acceptor)
CFTPA	LUMO	0	4	46	50
	HOMO	88	12	0	0
CCTPA	LUMO	0	4	46	50
	HOMO	77	20	3	0
CPTPA	LUMO	0	4	46	50
	HOMO	51	43	5	1

It can be clearly seen that charge distributions on HOMOs are mainly delocalized on the carbazole donor unit and some on the F/C/P units. The calculated percent contributions are increased from 12% to 20% and 43% when secondary electron donor groups were changed from fluorine (**CFTPA** dye) to carbazole (**CCTPA** dye) and phenothiazine (**CPTPA**dye), respectively.

On the other hand, for LUMO, the contributions of electron density are delocalized on the linkers (thiophenephenyl or bithiophen) and cyanoacrylic acid acceptor group. The portion of electron density is the same (calculated to be 4%, 46% and 50% for primary donor, linker and acceptor parts, respectively, for all **CFTPA, CCTPA, CPTPA** dyes) when electron donor groups were changed among fluorene, carbazole and phenothiazine moieties.

These results indicate that the charge separate between the HOMO and LUMO levels can provide the ability to control unidirectional of electron flow from the donor to acceptor part. This different spatial orientation of HOMO and LUMO is favorable for intramolecular charge transfer (ICT) phenomena.

In order to visualize the charge transfer features of these dyes, we examined the changes of the total electron densities between the ground- and the first excited-states as shown in Figure 6.5, where the yellow and purple color refers to an increase and a decrease of electron density, respectively. As the density difference map reveals, the electron density of the studied organic dyes exhibits a decrease at the electron donor group and π-linker while an increase mainly at the cyanoacrylic acid acceptor group. This indicates that these dyes have a larger intramolecular charge transfer (ICT) phenomena occurred throughout the whole backbone of the molecules. This charge transfer character of the lowest excited state is expected as one of the key factors influencing the injection efficiency of the photoexcited electron into the TiO_2 conduction band.

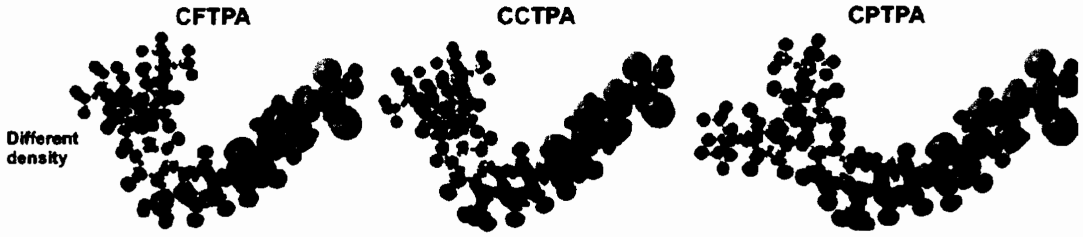

Figure 6.5 **The different density between ground- and the first excited-state of CFTPA, CCTPA and CPTPA dyes**

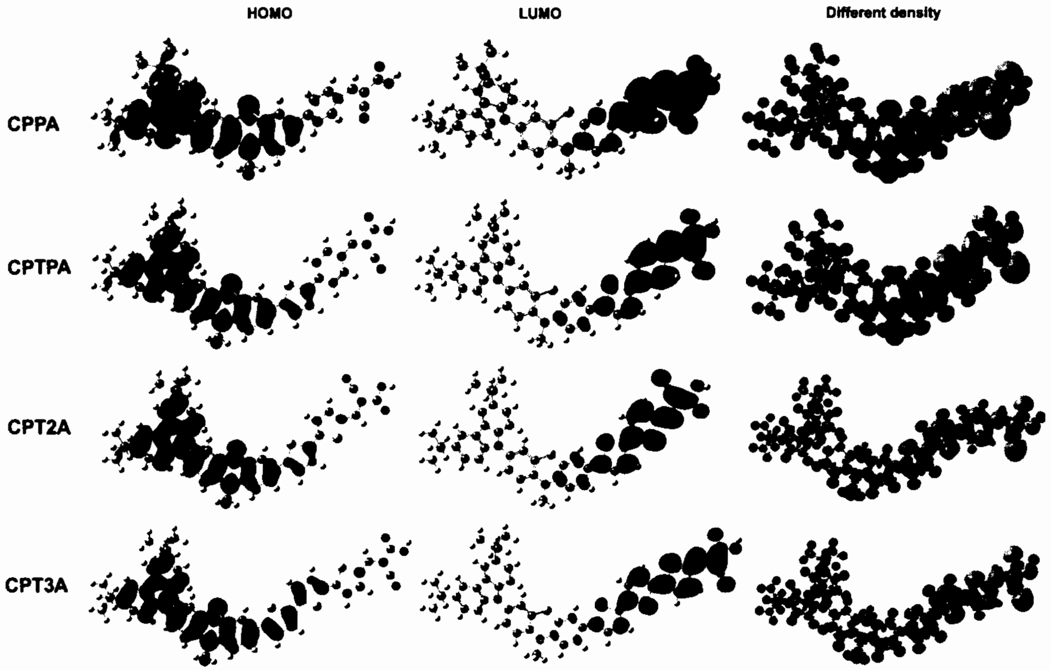

Figure 6.6 **The frontier molecular orbitals of CPPA, CPTPA, CPT2PA, and CPT3A dyes, and the different density between ground- and the first excited-state of CPPA, CPTPA, CPT2PA, and CPT3A dyes**

Table 6.4 Calculated charge distribution on each group of the donor, π spacer and acceptor of the new designed phenothiazine-based dyes under B3LYP/ 6-31G(d,p) method.

Dyes	Electronic levels	The percent contribution (%)			
		D (Carbazole)	D (Phenothiazine)	π (Thiophenephenyl)	A (Acceptor)
CPPA	LUMO	0	8	33	59
	HOMO	61	37	1	1
CPTPA	LUMO	0	4	46	50
	HOMO	51	43	5	1
CPT2PA	LUMO	0	2	53	46
	HOMO	36	48	16	1
				(Thiophene)	
CPT3A	LUMO	0	2	59	38
	HOMO	38	45	16	1

For the effect of conjugate bridge, the charge distributions on HOMO are still localized on the donor part, but the calculated percent contributions are decreasing when thiophene units were increased in both of thiophenephenyl and thiophene linkers. On the other hand, the electron density of LUMO is mainly localizedon the bridge and acceptor units. Obviously, the results exhibited that this different spatial orientation of HOMO and LUMO is favorable for intramolecular charge transfer (ICT). We also examined the different of the total electron densities between the ground- and excited-state as shown in Figure 6.6, and we observed that a larger intramolecular charge transfer (ICT) phenomena was occurred throughout the whole backbone of the molecule. This result indicates that these new designed phenothiazine-based dyes are suitable to use for efficient dyes with high ICT character.

6.3.3 Energy level

The energy levels of the molecular orbital from the HOMO-3 to the LUMO+2 of the studied organic dyes obtained at the B3LYP/6-31G(d,p) level of theory are shown in Figure 6.7 and 6.8. For HOMO level, the effect of different electron donor groups (fluorene, carbazole and phenothiazine) is energetically favorable affect to randomly stabilize and destabilize the HOMO for both of thiophenephenyl and bithiophene linkers. For LUMO level, all the LOMO levels of the studied organic dyes are higher than the conduction band of TiO_2 providing enough driving force for electron injection.

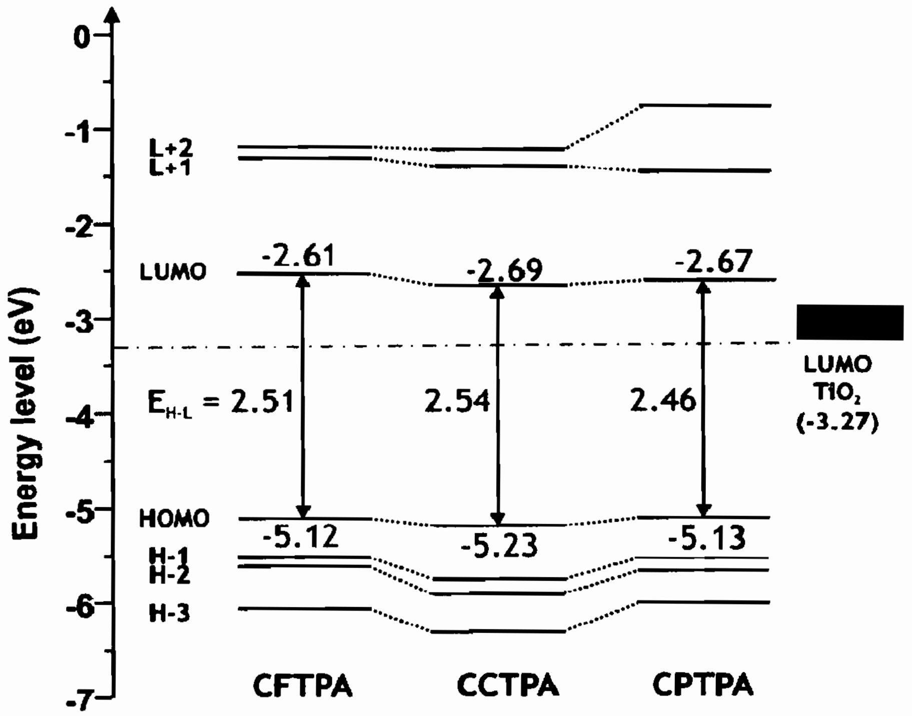

Figure 6.7 LUMO and HOMO energy level diagram of CFTPA, CCTPA, and CPTPA dyes

Furthermore, the effect of conjugate bridge, the increasing of conjugated linker lengths (both of thiophenephenyl and thiophene linkers) up to 3 units can affect on both of HOMO and LUMO levels. The calculated HOMO levels are systematically destabilized when the number of thiophene go up to 3 units, whereas the calculated LUMO levels are systematically stabilized. As a result, the HOMO–LUMO gaps (E_{H-L}) are narrowed in order of 2.55 > 2.46 > 2.36 eV for **CPPA**, **CPTPA**, **CPT2PA** dyes and 2.50 > 2.35 > 2.26 eV for **CPPA**, **CPTPA**, **CPT2PA** dyes, respectively. Furthermore, the LUMO levels of all dyes are located above the TiO_2 LUMO level. Therefore, these dye sensitizers have sufficient driving force for electron injection to TiO_2.

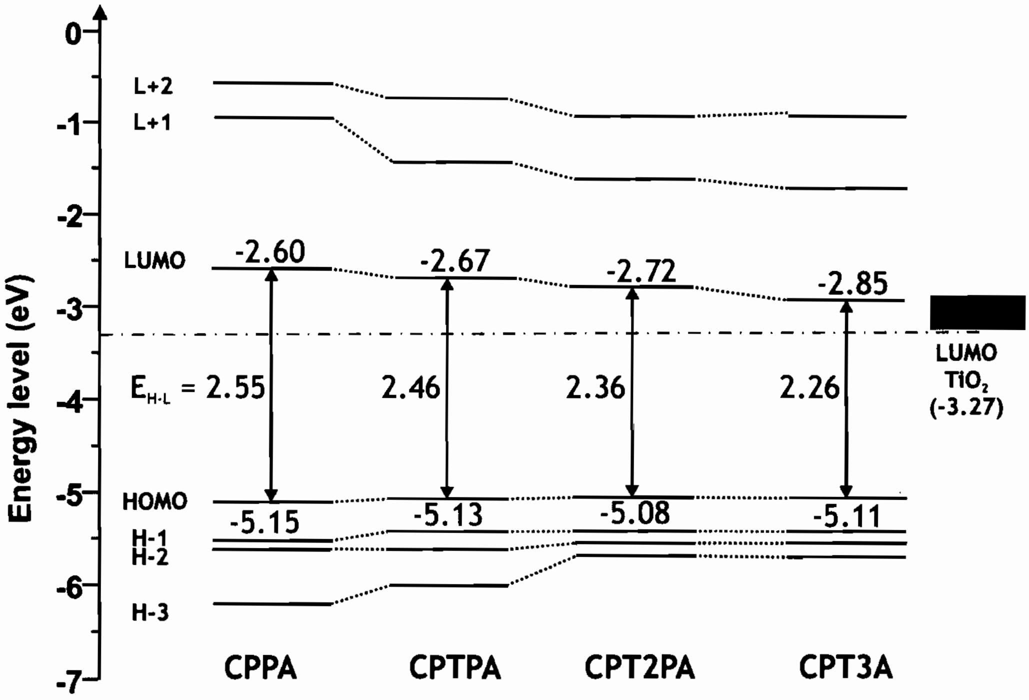
Energy level (eV)
0
-1
-2
-3
-4
-5
-6
-7
L+2
L+1
LUMO
HOMO
H-1
H-2
H-3
-2.60
-2.67
-2.72
-2.85
E_{H-L} = 2.55
2.46
2.36
2.26
-5.15
-5.13
-5.08
-5.11
LUMO
TiO₂
(-3.27)
CPPA
CPTPA
CPT2PA
CPT3A

Figure 6.8 LUMO and HOMO energy level diagram of CPPA, CPTPA, CPT2PA and CPT3A dyes

6.3.4 UV-Vis Absorption spectra

To gain insight into the effect of different electron donor groups on the optical property, TD-DFT method has been used to calculate and simulate the absorption spectra with the hybrid functional CAM-B3LYP at 6-31G(d,p) level in dichloromethane. The calculated results obtained through these calculations are summarized in Table 6.5 and 6.6, and their simulated absorption spectra are shown in Figure 6.9 and 6.10.

These dyes showed two absorption bands around 250 and 400 nm for thiophenephenyl linker (**CFTPA**, **CCTPA**, and **CPTPA** dyes). The absorption peak around 250 nm is assigned as π-π* electronic transitions while the absorption peak around 400 nm are assigned as intramolecular charge transfer between the donor and acceptor moieties. The calculated maximum absorption wavelengths (λ_{max}) for **CFTPA**, **CCTPA**, and **CPTPA** dyes are in order of 391 < 406 ≅ 404 nm, respectively. It is clearly seen that the dyes with carbazole and phenothiazine moieties showed a red shift in absorption maxima than that of the dyes with fluorene moiety. These results exhibit that the absorption ability of carbazole and phenothiazine moieties are better than that of fluorene moiety.

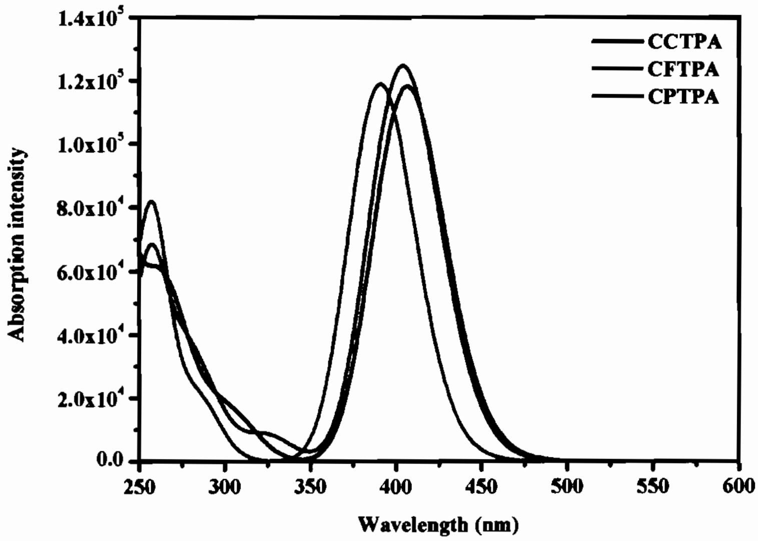

Figure 6.9 Simulated absorption spectra of CFTPA, CCTPA, and CPTPA dyes

Table 6.5 Maximal absorption wavelength (λ_{max}), excitation energy (E_g), oscillator strength (f), and electronic transition configurations of the studied organic dyes obtained by TD-CAM-B3LYP/6-31G(d,p) level indichloromethane

Dye	λ_{max} (in nm), (εx10^{-4} $M^{-1}cm^{-1}$)	E_g (in eV)	f	Transition Configuration
CFTPA	391 (118,939)	3.17	1.6422	0.64(HOMO-1→LUMO), -0.16(HOMO-3→LUMO), 0.13(HOMO-1→LUMO+1), -0.13(HOMO-5→LUMO)
CCTPA	406 (118,293)	3.05	1.6324	0.45(HOMO-1→LUMO), 0.42(HOMO→LUMO), 0.21(HOMO-4→LUMO), -0.13(HOMO-3→LUMO),
CPTPA	404 (124,787)	3.07	1.7288	0.46(HOMO→LUMO), 0.34(HOMO-1→LUMO), 0.31(HOMO-3→LUMO), 0.17(HOMO→LUMO+1)

We notice that the trend of the calculated oscillator strengths for **CFTPA, CCTPA,** and **CPTPA** dyes are in order of around $1.64 \cong 1.63 < 1.73$, respectively. These indicate that the computed oscillator strengths of the dyes with phenothiazine unit slightly increase compared to the dyes with fluorene and carbazole moieties. Thus, the dyes with phenothiazine-based moiety should be better absorbance efficiency than the dyes with fluorene and carbazole moieties.

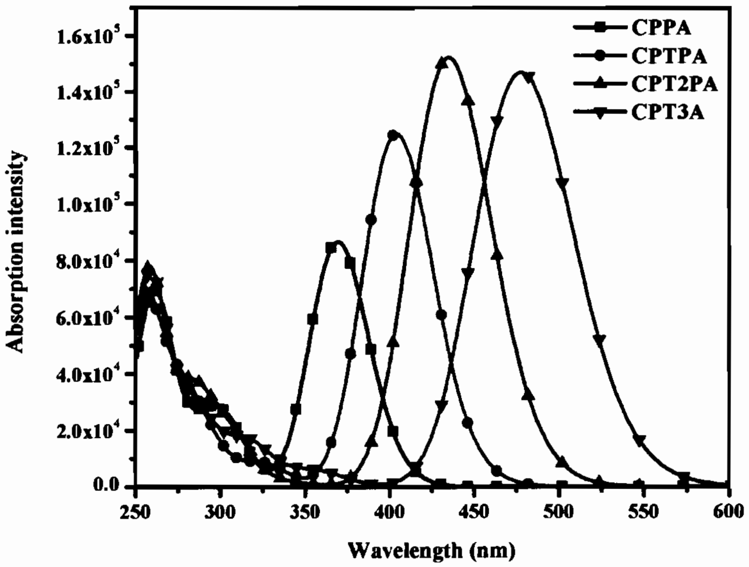

Figure 6.10 Simulated absorption spectra of CPPA, CPTPA, CPT2PA, and CPT3A using the hybrid functional CAM-B3LYP at 6-31G(d,p) level in dichloromethane

The visible absorption spectra of the new designed phenothiazine-based dyes were shown in Figure 6.10, exhibiting two absorption bands around 260 and 350-500 nm. The first peak is consistent with π-π* electronic transitions, while the second peaks for each dyes are consistent with an intramolecular charge transfer (ICT) character. As can be seen from Figure 6.10, the ICT peaks were red-shifted when the number of conjugation length was increased from 1 to 3 units which consistent with an increase in conjugation linker length of the dyes.

The calculated maximum absorption spectra (λ_{max}) are in order of 369, 404, 435 nm for **CPPA, CPTPA, CPT2PA** dyes, respectively, and 414, 450 477 nm for **CPTA, CPT2A, CPT3A** dyes, respectively. This indicates that the **CPT3A** dye which is the broadest of absorption wavelength shows the best absorption property to harvest the more sunlight. Also, the calculated absorption intensities (molar extinction coefficient; ε) are increased in order of 8.6, 12.4, 15.2x10^{-4} M^{-1}cm^{-1} for **CPPA, CPTPA, CPT2PA** dyes, respectively, and 9.2, 11.9, 14.6x10^{-4} M^{-1}cm^{-1} for **CPTA, CPT2A, CPT3A** dyes, respectively. These results are similar to the calculated oscillator strength (f) are in order of 1.1949, 1.7288, 2.1018 for **CPPA, CPTPA, CPT2PA** dyes, respectively, and 1.2735, 1.6424, 2.0269 for **CPTA, CPT2A, CPT3A** dyes, respectively. These indicate that **CPT2PA** and **CPT3A** dyes are high absorption ability which are suitable to use for the efficient dye sensitizers.

Comparing between thiophenephenyl and thiophene linkers, these results clearly indicate that the λ_{max} of dyes with thiophene linkers (i.e., λ_{max} = 477 nm for **CPT3A** dye) is more red-shifted than that of dyes with thiophenephenyl linker (i.e., λ_{max} = 435 nm for **CPT2PA** dye). The longer absorption wavelength is probably due to the more planar structure on bithiophene linker than that on thiophenephenyl linker (see in Table 6.6). Thus, we expect that **CPT3A** dye is the promising dye for using in DSSCs application.

Table 6.6 Maximal absorption wavelength (λ_{max}), excitation energy (E_g), oscillator strength (f), and electronic transition configurations of the new designed phenothiazine-based dyes obtained by TD-CAM- B3LYP/ 6-31G(d,p) level in dichloromethane

Dye	λ_{max} (in nm), (εx10^{-4} $M^{-1}cm^{-1}$)	E_g (in eV)	f	Transition Configuration
CPPA	369 (8.6)	3.36	1.1949	0.50(HOMO→LUMO), -0.35(HOMO-1→LUMO), -0.22(HOMO-3→LUMO), 0.16(HOMO-5→LUMO), -0.13(HOMO→LUMO+2)
CPTPA	404 (12.4)	3.07	1.7288	0.46(HOMO→LUMO), 0.34(HOMO-1→LUMO), 0.31(HOMO-3→LUMO), 0.17(HOMO→LUMO+1)

Table 6.6 Maximal absorption wavelength (λ_{max}), excitation energy (E_g), oscillator strength (f), and electronic transition configurations of the new designed phenothiazine-based dyes obtained by TD-CAM- B3LYP/ 6-31G(d,p) level in dichloromethane (Continued)

Dye	λ_{max} (in nm), (εx10^{-4} $M^{-1}cm^{-1}$)	E_g (in eV)	f	Transition Configuration
CPT2PA	435 (15.2)	2.85	2.1018	0.47(HOMO→LUMO), 0.34(HOMO-1→LUMO), 0.25(HOMO-2→LUMO), 0.22(HOMO→LUMO+1)
CPT3A	477 (14.6)	2.60	2.0269	0.49(HOMO→LUMO), 0.36(HOMO-1→LUMO), 0.25(HOMO-2→LUMO), 0.15(HOMO→LUMO+1)

6.4 Methods validation with the Performance of DSSCs

In general, there are two ways to approach the computational calculations: (1) to have a deeper understanding of the observed results and (2) to screen predicting the properties of newly designed molecules. For the first approach, we are attempting to disclose the relationship between the DSSCs performance tested by experimentalist and the dye structures calculated by computational method, for example, the number density of dye, the dye aggregations, and other properties corresponding to cell parameters. In the commonly accepted method, such as DFT calculation, if methods are a validated quantitative analytical procedure that can provide accurate trend similar to experimental results, it is considered as a suitable tool for predicting the properties of newly designed dyes in the second approach. [50-59, 66, 83-84]

Nowadays, DFT is probably the most widely used method in computational chemistry, yielding an accurate prediction of several ground- and excited-state properties. Its success is mainly related to the recent development of a wide variety of increasingly complex and accurate exchange-correlation functionals. In order to set up an approach to screen novel candidate dyes, the calculation approach is need to be validated.

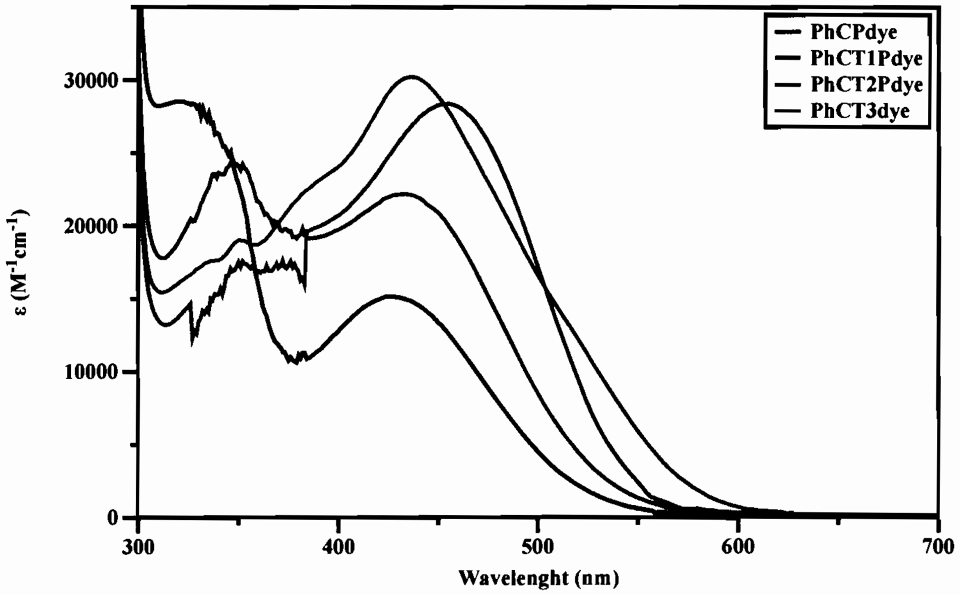

Figure 6.11 The absorption spectra of PhCPdye, PhCT1Pdye, PhCT2Pdye, and PhCT3dye

In this work, we use TD-CAM-B3LYP/6-31G(d,p) method for all calculations. We should compare our calculated results based on TD-CAM-B3LYP/6-31G(d,p) method and the available experimental observation. The absorption spectra of dyes recorded in dichloromethane are shown in Figure 6.11 taken from ref. 82. Compared to the calculated absorption spectra shown in Figure 6.10, the **PhCT3dye** shows the highest molar extinction coefficient and the most absorption broad peak which are agree with the calculated results. From our calculated results, we expect that **CPT3A** (or **PhCT3dye**) is the promising dye for using in DSSCs application.

To this end, we confirm the predicting dye efficiency by comparison with the available power conversion efficiency taken from ref. 82. The photovoltaic performance of DSSCs based on phenothaiazine dyes were listed in Table 6.7. As shown, **PhCT3dye** shows the highest photovoltaic performance of 4.02% which are agree with as observed in the DFT calculations. Thus, we believe that our approach allows for an accurate the methods validation.

According to their appealing performance to accuracy, our calculation methods are finally aimed to be used to qualitatively screen the suitable candidates for efficient dye sensitizers.

Table 6.7 Photovoltaic performance of DSSCs based on phenothaiazine dyes

Sample	J_{sc} (mA·cm^2)	V_{oc} (V)	ff	η
N719	12.68	0.71	0.71	6.34
PhCPdye	8.00	0.71	0.63	3.60
PhCT1Pdye	9.12	0.66	0.65	3.90
PhCT2Pdye	9.21	0.68	0.64	4.02
PhCT3dye	9.58	0.64	0.70	4.33

The experimental data were taken from ref [82]

6.5 Conclusions

In summary, we have employed DFT and TD-DFT to investigate the effect of different electron donors and conjugate bridges on the structural, optical, and electron transfer properties of new designed dyes. The different electron donor of fluorene, carbazole, and phenothiazine showed different structural conformation. The planar conformation was found by using fluorene and carbazole acting as electron donors, while the butterfly conformation was found by phenothiazine as electron donor. However, these two different conformations are not significantly effect on energy level, intramolecular charge transfer property as well as optical property.

For the effect of conjugate bridge, the LUMO energy level can be significantly decreased when increased the thiophene units. In addition, the red shifted of absorption spectra was found when the conjugated bridge was extended. Therefore, the increasing of conjugation length is one of the ways to develop new designed dye sensitizers for high efficiency.

CHAPTER 7
SUMMARY

Computational calculations based on DFT and TDDFT methods were used to design and investigate the properties of organic materials for using as dye sensitizers in dye-sensitized solar cells. Organic materials such as carbazole and diphenylamine moieties were designed as auxiliary donor groups connected between carbazole and diphenylamine donors. These dyes were designed in different three dye systems, D-π-A, D-D-π-A and 2D-D-π-A, and they were compared. According to the computational study of these architectures, 2D-D-π-A system showed the most red-shift of absorption wavelength. Moreover, different auxiliary donor in the 2D-D-π-A system provided a different effect. Diphenylamine auxiliary donor provided small external dihedral angle (EDA) than internal dihedral angle (IDA) resulting in the red-shift of absorption range due to extended conjugation length. Adding an auxiliary donor can significantly increase HOMO energy while slightly effecting LUMO energy. Therefore, we summarized that designing of dye architecture in 2D-D-π-A system with different auxiliary donor groups (2D) is one way to develop the dye's efficiency.

New organic dyes were designed in new dye system called as D-A-π-A by featuring a BTD unit as an additional electron acceptor group, and they were computationally investigated. Interestingly, an incorporated BTD moiety significantly decreased the LUMO level and energy gap, whereas it led to an increase in the HOMO level and dipole moment, leading to a redshift of absorption spectra, which could help facilitate electron transfer as well as greatly enhance the light-harvesting ability. Furthermore, the difference in the position of the BTD moiety in the π-conjugation spacer can also affect the absorption spectrum and lead to a broadening to the near IR region. However, the insertion of a planar rigid linker between the BTD moiety and the anchoring group effectively maintained the best character of the light absorption property and blocked the unfavorable charge recombination, because the BTD is positioned further away from the anchoring group. According to our computational study, the successful theoretical results show that computational models can be used to aid the design of efficient organic dyes for experimental synthesis, thus saving cost and time.

The conjugated linker is also important part in D-π-A dye's system. We used a triple bond (TB) to modify π-conjugated linker of antracene based dyes and compared these to the dye without TB substitution. Interestingly, all TB-modified sensitizers showed significant decreases in the dihedral angle between the anthracene unit and its substituents at the 9,10-positions, resulting in a nearly planar molecular geometry for each dye. The presence of a planar structure greatly affects the absorption spectracoplanarity of with the p-conjugated linker has a significant effect on electron distribution overlap on anthracene, which facilitates ICT. These results indicate that inclusion of a triple bond-modified π-conjugated linker in these dyes during synthesis is necessary for the construction of high-efficiency organic sensitizers.

Finally, the different electron donor of fluorene, carbazole, and phenothiazine as well as different conjugate bridges on the structural, optical, and electron transfer properties of new designed dyes were calculated. The different electron donor of fluorene, carbazole, and phenothiazine showed different structural conformation. The planar conformation was found by using fluorene and carbazole acting as electron donors, while the butterfly conformation was found by phenothiazine as electron donor. However, these two different conformations are not significantly effect on energy level, intramolecular charge transfer property as well as optical property. For the effect of conjugate bridge, the LUMO energy level can be significantly decreased when increased the thiophene units. In addition, the red shifted of absorption spectra was found when the conjugated bridge was extended. Therefore, the increasing of conjugation length is one of the ways to develop new designed dye sensitizers for high efficiency.

REFERENCES

REFERENCES

[1] H. Tsubomura and et al. “Dye sensitized zinc oxide: aqueous electrolyte: platinum photocell”, **Nature**. 261: 402-403, 1976.

[2] J. Gong and et al. “Review on dye-sensitized solar cells (DSSCs): Fundamental concepts and” , **Renewable and Sustainable Energy Reviews**. 16: 5848–5860, 2012.

[3] M. Grätzel and et al. “Solar energy conversion by dye-sensitized photovoltaic cells”, **Inorganica Chimica Acta**. 44: 6841-6851, 2005.

[4] B. Oregan and M. Grätzel. “A low-cost, high-efficiency solar cell based on dye-sensitized colloidal titanium dioxide films”, **Nature**. 353: 737-740, 1991.

[5] A. Hagfeldt and M. Grätzel, “Molecular Photovoltaics”, **Acc. Chem. Res**. 33: 269-277, 2000.

[6] Calculations in AS / A Level Chemistry site. “Promotion of electrons “, **UV-Visible absorption spectra**. http://www.chemguide.co.uk/analysis/ uvvisible/theory.html. May, 2015.

[7] Wikipedia the free encyclopedia. “fluorescence emission spectra”, **Fluorescence spectroscopy**. http://en.wikipedia.org/wiki/Emission_spectrum.html. May, 2015.

[8] Advanced imaging laboratory site, university of Victoria. “fluorescence”, **fluorescence with the microscope**. http://web.uvic.ca/ail/techniques/epi-fluorescence.html. May, 2015.

[9] Dana Riddle. “stokes shift”, **Feature Article: Coral Coloration: Fluorescence: Part 1**. http://www.advancedaquarist.com/2006/9/aafeature. May, 2015.

[10] F. Jensen. **Introduction to computational chemistry**. England: John Wiley & Sons Ltd, 1999.

[11] R. N. Barnett and U. Landman. “Born-Oppenheimer molecular dynamics simulations of finite systems: Structure and dynamics of $(H_2O)_2$”, **Physical review B**. 48(4): 1993, 1993.

[12] R.M. Dreizler and E.K.U. Gross. **Density Functional Theory: An Approach to the Quantum Many–Body Problem**. English: Springer, 1990.

[13] W. Kohn, A.D. Becke, and R.G. Parr, “Density functional theory of electronic structure,” **J. Phys. Chem**. 100(12): 974–980, 1996.

REFERENCES (CONTINUED)

[14] J. P. Perdew and K. Burke, “Generalized gradient approximation made simple”, **Phys. Rev. Lett.** 77: 3865-3868, 1996.

[15] T. H. Dunning and P. J. Hay, **Modern Theoretical Chemistry; Schefer III: Gaussian basis sets for molecular calculations**. New York: H.F. Ed. Plenum, 1977.

[16] R. G.Parr and W. Yang, Density Functional Theory of Atoms and Molecules, Oxford University Press, 1989.

[17] C. J. Cramer, **Essentials of computational chemistry. 2nd Ed. Theories and models**. England: John Wiley & Sons Ltd, 2004.

[18] P. Atkins and R. Friedman, **Molecular quantum mechanics. 4th Ed**. English: Oxford university press, 2005.

[19] A. Szabo and N.S. OStlund. **Modern quantum chemistry: Introduction to advanced electronic structure theory**. New York: Dover publications, inc., 1996.

[20] J. Xu and et al. “Conjugate spacer effect on molecular structures and absorption spectra of triphenylamine dyes for sensitized solar cells: Density functional theory calculations”, **Spectrochimica Acta Part A: Molecular and Biomolecular Spectroscopy.** 78(1): 287-293, 2011.

[21] W. Li and et al. “Theoretical investigation of triphenylamine-based sensitizers with different π-spacers for DSSC”, **Spectrochimica Acta Part A: Molecular and Biomolecular Spectroscopy**. 118: 1144-1151, 2014.

[22] Z. Ning and et al. “Starburst Triarylamine Based Dyes for Efficient Dye-Sensitized Solar Cells”, **The Journal of Organic Chemistry**. 73(10): 3791-3797, 2008.

[23] C. Jia and et al. “Theoretical study of carbazole–triphenylamine-based dyes for dye-sensitized solar cells”, **Spectrochimica Acta Part A: Molecular and Biomolecular Spectroscopy**. 86: 387-391, 2012.

[24] Z. Wan and et al. “Effects of different acceptors in phenothiazine-triphenylamine dyes on the optical, electrochemical, and photovoltaic properties”, **Dyes and Pigments**. 94(1): 150-155, 2012.

REFERENCES (CONTINUED)

[25] Z. Wan and et al. “Triphenylamine-based starburst dyes with carbazole and phenothiazine antennas for dye-sensitized solar cells”, **Journal of Power Sources**. 199: 426-431, 2012.

[26] Y. Wu and et al. “High-conversion-efficiency organic dye-sensitized solar cells: molecular engineering on D-A-[small π]-A featured organic indoline dyes”, **Energy & Environmental Science**. 5(8): 8261-8272, 2012.

[27] Y. Zhu and et al. “Organic D-A-π-A Solar Cell Sensitizers with Improved Stability and Spectral Response”, **Advanced Functional Materials**. 21(4): 756-763, 2011.

[28] K.R. Justin Thomas and et al. “Electro-optical properties of new anthracene based organic dyes for dye-sensitized solar cells”, **Dyes and Pigments**. 91(1): 33-43, 2011.

[29] D.U.K. Heo and et al. “Donor-π-Acceptor Type Diphenylaminothiophenyl Anthracene-mediated Organic Photosensitizers for Dye-sensitized Solar Cells”, **Bulletin of the Korean Chemical Society**. 34(4): 1081-1088, 2013.

[30] C. Teng and et al. “Molecular Design of Anthracene-Bridged Metal-Free Organic Dyes for Efficient Dye-Sensitized Solar Cells”, **The Journal of Physical Chemistry C**. 114(19): 9101-9110, 2010.

[31] Y. Hua and et al. “Significant Improvement of Dye-Sensitized Solar Cell Performance Using Simple Phenothiazine-Based Dyes”, **Chemistry of Materials**. 25(10): 2146-2153, 2013.

[32] S. Agrawal and et al. “Optical Properties and Aggregation of Phenothiazine-Based Dye-Sensitizers for Solar Cells Applications: A Combined Experimental and Computational Investigation”, **The Journal of Physical Chemistry C**, 117(19): 9613-9622, 2013.

[33] F. De Angelis and et al. “Time-Dependent DFT Study of [Fe(CN)6]4- Sensitization of TiO2 Nanoparticles”, **Journal of the American Chemical Society**. 126(46): 15024-15025, 2014.

[34] F. De Angelis and et al. “Direct vs. indirect injection mechanisms in perylene dye-sensitized solar cells: A DFT/TDDFT investigation”, **Chemical Physics Letters**. 493(4–6): 323-327, 2010.

REFERENCES (CONTINUED)

[35] S. Agrawal and et al. “First-principles study of the excited-state properties of coumarin-derived dyes in dye-sensitized solar cells”, **Journal of Materials Chemistry**. 21(30): 11101-11108, 2011.

[36] L.M. Peter and et al. “The Grätzel cell: where next?”, **Journal of Physical Chemistry Letters**. 2: 1861-1867, 2013.

[37] M. Grätzel “Photoelectrochemical cells,” **Nature**. 414: 338-344, 2001.

[38] Q. Yu and et al. “High-efficiency dyesensitized solar cells: the influence of lithium ions on exciton dissociation charge recombination, and surface states”, **ACS Nano**. 4: 6032-6038, 2010.

[39] W. Zeng and et al. “Efficient dye-sensitized solar cells with an organic photosensitizer featuring orderly conjugated ethylenedioxythiophene and dithienosilole blocks”, **Chemistry of Materials**. 22: 1915-1925, 2010.

[40] Z. Chen and et al. “Organic D-π-A dyes for dye-sensitized solar cell”, **Current Organic Chemistry**. 11: 1241-1258, 2007.

[41] M.K.R. Fischer and et al. “D-π-A sensitizers for dye-sensitized solar cells: linear vs branched oligothiophenes”, **Chemistry of Materials**. 22: 1836-1845, 2010.

[42] S.-L. Chen and et al. “How to design more efficient organic dyes for dye-sensitized solar cells? Adding more sp2-hybridized nitrogen in the triphenylamine donor”, **Journal of Power Sources**. 223: 86-93, 2013.

[43] S.H. Kim and et al. “The effect of N-substitution and ethylthio substitution on the performance of phenothiazine donors in dye-sensitized solar cells”, **Dyes and Pigments**. 97: 262-271, 2013.

[44] T. Duan and et al. “A new class of organic dyes containing β-substituted 2, 2’-bithiophenene unit as a π-linker for dye-sensitized solar cells: structural modification for understanding relationship of structure and photovoltaic performances”, **Journal of Power Sources**. 234: 23-30, 2013.

[45] J. Feng and et al. “First principles design of dye molecules with ullazine donor for dye sensitized solar cells”, **Journal of Physical Chemistry C**. 117: 3772-3778, 2013.

REFERENCES (CONTINUED)

[46] N. Mohammadi and et al. “Toward rational design of organic dye sensitized solar cells (DSSCs): an application to the TA-St-CA dye”, **Journal of Molecular Graphics and Modelling**. 40: 64-71, 2013.

[47] F. Ambrosio and et al. “Effect of the anchoring group on electron injection: theoretical study of phosphonated dyes for dye-sensitized solar cells”, **Journal of Physical Chemistry C**. 116: 2622-2629, 2011.

[48] M. Katono and et al. “Influence of the anchoring modes on the electronic and photovoltaic properties of D-π-A dyes”, **Journal of Physical Chemistry C**. 116: 16876-16884, 2012.

[49] J. Xu and et al. “Improvement of dye-sensitized solar cells: what we know and what we need to know”, **Energy & Environmental Science**. 3: 1170-1181, 2011.

[50] J. Xu and et al. “Conjugate spacer effect on molecular structures and absorption spectra of triphenylamine dyes for sensitized solar cells: density functional theory calculations”. **Spectrochimica Acta A: Molecular and Biomolecular Spectroscopy**. 78: 287-293, 2011.

[51] J. Zhang and et al. “Density functional theory characterization and design of high-performance diarylamine-fluorene dyes with different π spacers for dye-sensitized solar cells”, **Journal of Materials Chemistry**. 22: 568-576, 2012.

[52] C.-R. Zhang and et al. “Electronic structures and optical properties of organic dye sensitizer NKX derivatives for solar cells: a theoretical approach”, **Journal of Molecular Graphics and Modelling**. 38: 419-429, 2012.

[53] C.-K. Tai and et al. “DFT and TD-DFT investigations of metal-free dye sensitizers for solar cells: effects of electron donors and π-conjugated linke”, **Computational and Theoretical Chemistry**. 971: 42-50, 2011.

[54] P. Surawatanawong and et al. “Density functional study of monobranched and di-branched di-anchoring triphenylamine cyanoacrylic dyes for dye-sensitized solar cells”, **Journal of Photochemistry and Photobiology A: Chemistry**. 253: 62-71, 2013.

REFERENCES (CONTINUED)

[55] W.-L. Ding and et al. "Density functional theory characterization and verification of high-performance indoline dyes with D-A-π-A-A architecture for dye-sensitized solar cells", **Dyes and Pigments**. 98: 125-135, 2013.

[56] J. Zhang and et al. "Modification on C219 by coumarin donor toward efficient sensitizer for dye sensitized solar cells: a theoretical study", **Dyes and Pigments**. 99: 127-135, 2013.

[57] J. Tang and et al. "New starburst sensitizer with carbazole antennas for efficient and stable dye-sensitized solar cells", **Energy & Environmental Science**. 3: 1736-1745, 2010.

[58] T. Khanasa and et al. "Synthesis and characterization of 2D-D-π-A-type organic dyes bearing bis(36-di-tert-butylcarbazol-9-ylphenyl)aniline as donor moiety for dyesensitized solar cells", **European Journal of Organic Chemistry**. 2013: 2608-2602, 2013.

[59] S. Namuangruk and et al. "D-D-π-A-type organic dyes for dye-sensitized solar cells with a potential for direct electron injection and a high extinction coefficient: synthesis, characterization, and theoretical investigation", **Journal of Physical Chemistry C**. 116: 25653-25663, 2012.

[60] A.D. Becke "A new mixing of Hartree–Fock and local density-functional theories", **Journal of Chemical Physics**. 98: 1372-1377, 1993.

[61] M. Pastore and et al. "A computational investigation of organic dyes for dye-sensitized solar cells: benchmark, strategies, and open issues", **Journal of Physical Chemistry C**. 114: 7205-7212, 2010.

[63] S.I. Gorelsky and et al. "Electronic structure and spectra of ruthenium diimine complexes by density functional theory and INDO/S. Comparison of the two methods", **Journal of Organometallic Chemistry**. 635: 187-196, 2001.

[64] V. Barone and M. Cossi "Quantum calculation of molecular energies and energy gradients in solution by a conductor solvent model", **Journal of Physical Chemistry A**. 102: 1995-2001, 1998.

REFERENCES (CONTINUED)

[65] M.K. Mazeeruddin and et al. "Investigation of sensitizer adsorption and the influence of protons on current and voltage of a dye-sensitized nanocrystalline TiO_2 solar cell", **Journal of Physical Chemistry B**. 107: 8981-8987, 2003.

[66] T. Yakhanthip and et al. "Theoretical investigation of novel carbazole-fluorene based D-π-A conjugated organic dyes as dye-sensitizer in dye-sensitized solar cells (DSCs)", **Journal of Computational Chemistry**. 32: 1568-1576, 2012.

[67] M. Grätzel "Dye-sensitized solar cells", **Journal of Photochemistry and Photobiology C: Photochemistry Reviews**. 4: 145-153, 2003.

[68] M. Grätzel "Conversion of sunlight to electric power by nanocrystalline dye-sensitized solar cells", **Journal of Photochemistry and Photobiology A: Chemistry**. 164: 3-14, 2004.

[69] M.K. Nazeeruddin and et al. "Dye-sensitized solar cells: A brief overview", **Solar Energy**. 85: 1172-1178, 2011.

[70] A. Mishra and et al. "Metal-free organic dyes for dye-sensitized solar cells: from structure: property relationships to design rules" **Angew. Chem. Int. Ed.** 48: 2474-2499, 2009.

[71] A. Yella and et al. "Porphyrin-sensitized solar cells with cobalt (II/III)–based redox electrolyte exceed 12 percent efficiency" **Science**. 334: 629-634, 2011.

[72] M. Grätzel, "Solar energy conversion by dye-sensitized photovoltaic cells" **Inorg. Chem.** 44: 6841-6851, 2005.

[73] A. Dualeh and et al. "Influence of donor groups of organic D-π-A dyes on open-circuit voltage in solid-state dye-sensitized solar cells" **J. Phys. Chem. C**, 116: 1572-1578, 2012.

[74] Y. Ooyama and et al. "Control of molecular arrangement and/or orientation of D-π-A fluorescent dyes for dye-sensitized solar cells" **Chem. Lett**. 41: 1384-1396, 2012.

REFERENCES (CONTINUED)

[75] G. Zhang and et al. "High efficiency and stable dye-sensitized solar cells with an organic chromophore featuring a binary π-conjugated spacer" **Chem. Commun.** 2198-2200, 2009.

[76] W. Zhu and et al. "Organic D-A-π-A solar cell sensitizers with improved stability and spectral response" **Adv. Funct. Mater.** 21: 756-763, 2011.

[77] W. Fan and et al. "Acene-modified triphenylamine dyes for dye-sensitized solar cells: a computational study" **Chem. Phys. Chem.** 13: 2051-2060, 2012.

[78] S. Haid and et al. "Significant improvement of dye-sensitized solar cell performance by small structural modification in π-conjugated donor–acceptor dyes" **Adv. Funct. Mater.** 22: 1291-1302, 2012.

[79] C. Yan and et al. "Efficient triarylamine–perylene dye-Sensitized solar cells: influence of triple-bond insertion on charge recombination" **ACS Appl. Mater. Interfaces.** 7: 801–809, 2015.

[80] L. Yang and et al. "Electron-acceptor-dependent light absorption and charge-transfer dynamics in N-annulated perylene dye-sensitized solar cells" **J. Phys. Chem. C.** 119: 980–988, 2015.

[81] M. K. Nazeeruddin and et al. "Combined experimental and DFT-TDDFT computa-tional study of photoelectrochemical cell ruthenium sensitizers" **J. Am. Chem. Soc.** 127: 16835–16847, 2005.

[82] D. Muenmart. "Synthesis and characterization of novel organic material" Doctor's Thesis: Ubon Ratchathani University, 2013.

[83] Y. Surakhot and et al. "The number density effect of N-substituted dyes on the TiO_2 surface in dye sensitized solar cells: a theoretical study" **RSC Advances.** 5: 11549-11557, 2015.

[84] K. Sirithip and et al. "Zinc-porphyrin dyes with different meso-aryl substituents for dye-sensitized solar cells: experimental and theoretical studies" **Chem. Asian. J.** 10(4):882-93, 2014.

APPENDIX

LISTS OF PUBLICATIONS

1. R. Tarsang, V. Promarak, T. Sudyoadsuk, S. Namuangruk, and S. Jungsuttiwong "Tuning the electron donating ability in the triphenylamine-based D-π-A architecture for highly efficient dye-sensitized solar cells" **Journal of Photochemistry and Photobiology A: Chemistry**. 273: 8-16, 2014.
2. R. Tarsang, V. Promarak, T. Sudyoadsuk, S. Namuangruk, N. Kungwan and S. Jungsuttiwong "Modification of D–A–π–A Configuration toward a High-Performance Triphenylamine-Based Sensitizer for Dye-Sensitized Solar Cells: A Theoretical Investigation" **ChemPhysChem**. 15: 3809–818, 2014.
3. R. Tarsang, V. Promarak, T. Sudyoadsuk, S. Namuangruk, N. Kungwan, P. Khongpracha and S. Jungsuttiwong "Triple bond-modified anthracene sensitizers for dye-sensitized solar cells: a computational study" **RSC Advances**. 5: 38130–38140, 2015.

CURRICULUM VITAE

NAME	Mr. Ruangchai Tarsang
BORN	01 March 1986 in Ubon Ratchathani, Thailand
EDUCATION	2005-2008, B.Sc. (Chemistry, with 1st honor), Ubon Ratchathani University 2009-2011, M.Sc. (Chemistry), Ubon Ratchathani University
SCHOLARSHIPS	2006-2008, Scholarship from The American Chamber of Commerce in Thailand (AMCHAM), 2009-2014, Human Resource Development in Science Project (Science Achievement Scholarship of Thailand, SAST) program

Office of Academic Resources
Ubon Ratchathani University